DRA

SEPTEMBER, 1983

LIDS-TH-1328

Research Supported By:

General Electric Corporate Research and Development Center

NASA Ames and Langley Research Centers Grant NGL-22-009-124

Robust Multivariable Control for the F100 Engine

Efthimios Kappos

Laboratory for Information and Decision Systems

MASSACHUSETTS INSTITUTE OF TECHNOLOGY, CAMBRIDGE, MASSACHUSETTS 02139

September, 1983

LIDS-TH-1328

ROBUST MULTIVARIABLE CONTROL FOR THE F100 ENGINE

by

Efthimios Kappos

This report is based on the unaltered thesis of Efthimios Kappos, submitted in partial fulfillment of the requirements for the degree of Master of Science and Electrical Engineer at the Massachusetts Institute of Technology in August, 1983. The research was conducted at the M.I.T. Laboratory for Information and Decision Systems, with support provided by the General Electric Corporate Research and Development Center and NASA Ames and Langley Research Centers under grant NGL-22-009-124.

Laboratory for Information and Decision Systems
Massachusetts Institute of Technology
Cambridge, MA 02139

ROBUST MULTIVARIABLE CONTROL FOR THE F100 ENGINE

by

Efthimios Kappos
B.A., Oxford University (1980)

SUBMITTED IN PARTIAL FULFILLMENT OF THE
REQUIREMENTS FOR THE
DEGREE OF

MASTER OF SCIENCE

and

ELECTRICAL ENGINEER

at the

MASSACHUSETTS INSTITUTE OF TECHNOLOGY

Signature of the Author .....
Department of Electrical Engineering and Computer Science, August 6, 1983

Certified by .....
Professor M. Athans,
Thesis Supervisor

Certified by .....
Professor H.A. Spang
Thesis Co-Supervisor

Accepted by .....
Professor A.C. Smith
Chairman, Departmental Graduate Committee

ROBUST MULTIVARIABLE CONTROL FOR THE F100 ENGINE

by

Efthimios Kappos

Submitted to the Department of Electrical Engineering and Computer Science on August 1983 in partial fulfillment of the requirements for the Degrees of Master of Science and Electrical Engineer.

ABSTRACT

Robust local control of the Pratt & Whitney F100 turbofan engine is done using the LQG procedure. A linear model of the engine is augmented by important sensor and actuator dynamics. A novel model reduction method is developed based on the modal decomposition of the system transfer function. LQG control is accomplished in two steps: first, a Kalman filter transfer function is designed using some tools for loop-shaping. Then, a loop transfer recovery method is used to get an LQG controller that is robust with the full linear model replacing the reduced model on which the design was based. The resulting controller satisfies the control specifications of zero steady-state error to steps and fast response times.

THESIS SUPERVISORS: Dr. M. Athans, Professor of Systems Science and Engineering
Dr. H.A. Spang, Adjunct Professor of Electrical Engineering

ACKNOWLEDGEMENTS

I would like to thank my supervisors, Profs. M. Athans and H.A. Spang for their help in shaping the ideas of this thesis and for their patience in seeing it through.

This thesis benefitted considerably from discussions with Prof. G. Verghese and my fellow student and friend Marc Bodson.

I also thank Fifa Monserrate for the excellent job she did of typing this thesis.

This research was carried out at the MIT Laboratory for Information and Decision Systems. Primary financial support was provided by the General Electric Corporate Research and Development Center. The initial phases of this research were funded under NASA grant NGL-22-009-124.

TO MY PARENTS

TABLE OF CONTENTS

LIST OF FIGURES

CHAPTER 2:

CHAPTER 3:

CHAPTER 4:

(CONT. LIST OF FIGURES)

LIST OF TABLES

1. INTRODUCTION AND SUMMARY

1.1 Background

There is a very definite need for multivariable control design examples. Available methodologies (state-space and frequency-domain) can at best propose alternative controller design methods, but only through sufficiently complex examples can control engineers discover how the methods actually work and in what directions they need to be extended.

Especially since multi-input, multi-output, (MIMO) methodologies are by necessity more involved mathematically than their single-input, single-output (SISO) counterparts, the only way to see how these methodologies work is by applying them to some practical examples; this way also point to any shortcoming they might have. The above points will be demonstrated in this thesis.

At present, examples of MIMO control using the LQG procedure (used in this work) that are fairly nontrivial are few: they are mainly for low-order systems and a small number of inputs and outputs (a recent example is [6]).

Prior designs for the F100 jet engine, although numerous, do not include one based on the full LQG procedure which yields a dynamic controller. The reason for this was on one hand that there are no significant noise sources to justify a Kalman filter state estimator and also because some state measurements are possible so that state feedback can be implemented. The reasons for using an LQG approach here are first, that it yields a dynamic (non-constant) feedback controller which adds more flexibility to the design and second that not all state variables are measured or, at least, cannot be included as outputs.

A significant part of the thesis is dedicated to model reduction, the approximation of a large-order linear system by one of lower order. A subject of considerable interest lately, model reduction has however failed to make its connections with control. The fact that an aggregated model will be used in a feedback control loop has not been investigated thoroughly and most methods tend to be open-loop in their philosophy. This existence of model aggregation procedures in vacuo can lead to misleading or bad designs; a robustness viewpoint is needed to relate errors of approximation with allowable controls. This viewpoint is taken up in our work.

1.2 Contributions of the Thesis

The main contribution of this thesis is to provide an example of a control design sequence for a multivariable system, the F100 engine.

A basic first stage is that of model reduction. By controlling the order of a reduced model, one controls the order of the dynamic compensator. This freedom in the order of the dynamic controller is a desirable feature and an advantage over the algebraic design methods [23], where the order of the controller cannot be easily specified.

The reduction method developed in this thesis has a number of novel features:

Although basically a state aggregation method, it uses the residue analysis perspective for approximation. This results in a better understanding of the trade-offs involved in the approximation. It also makes the procedure complete, since it gives a way of selecting the poles of the system that are to be included in the reduced model.

Most importantly, the reduction procedure yields an approximate system that can be used in a feedback loop. The error involved in the approximation is kept under control and the robustness requirement translates into a bandwidth requirement for the plant-controller loop.

The controller design methodology is based on the LQG formulation and largely follows the work of Stein, Doyle and others (see e.g. [20],[21] and [19]). The design is done on the reduced model.

The emphasis is on the frequency-domain properties of the state-space based LQG designs. Simple and efficient tools for loop-shaping are employed that lead to satisfactory designs. These tools accomplish singular value "pinching" in selected frequency ranges using approximations derived from the Kalman Frequency Domain Equalities.

Finally, for the first time, a set of Inverse Kalman Frequency Domain equalities are derived. They are used to rederive the robustness properties of the LQ regulator and Kalman filter inverse return difference.

1.3 Outline of the Thesis

In Chapter 2 a description is given of the F100 engine. Its dynamic characteristics, as captured in the linear model at one operating point, are discussed. The performance specifications are given insofar as they are taken into account in our design.

Chapter 3 contains a comprehensive discussion of model reduction issues. The steps of our procedure are detailed and the F100 example is given as an application.

Chapter 4 is the design chapter. The LQG controller synthesis methodology is presented and applied to the engine example. A full presentation of the fine tuning of the controller is also included.

Chapter 5 contains a summary and some proposed directions for further research.

2. THE F100 ENGINE MODEL

2.1 Introduction

A linear model of the Pratt & Whitney F100 afterburning turbofan jet engine is used as the design example in this thesis ([1],[3],[16],[22]). It is the same model as that used in the National Engineering Consortium's Alternatives for Linear Multivariable Control (ALMC) conference, in 1976-77 [1]. It is a linearization of a nonlinear simulation of the F-100 engine at the operating point of 83° Power Lever Angle (PLA), sea-level static.

The purpose of this thesis is to provide local control of the engine using this model. Still, insofar as the linear model represents a real system, it is desirable to know some things about the engine itself. They can help a designer considerably in doing sensible control. They also provide the basis on which to interpret the dynamic characteristics of the engine that are captured in the linear model.

The present chapter starts with a brief discussion of the thermodynamic and fluidmechanic aspects of jet engines in general and of the F100 engine in particular.

The limitations arising from the real engine control problem are then given. The way these are taken into account in the more narrow context of local design is examined.

Next, the dynamic characteristics of the linear model are detailed. The multivariable pole-zero structure is given and the important dynamics are isolated using modal analysis.

Finally, the control requirements are stated. This sets the stage for Chapter 3, where an adequate reduced model for doing satisfactory control is derived.

2.2 The F100 Engine

2.2.1 A brief description of the F100 turbofan engine

Pratt & Whitney's F100 engine (Fig. 2.1) is an advanced, afterburning turbofan engine. Insofar as we shall try and derive guidance in doing multivariable control from a knowledge of the real engine characteristics, a brief thermodynamic and fluid mechanic description of the engine is desirable [8]. This will also help delineate the extent to which our control is realistic: there can be many acceptable designs for the available linear model but not all of them will make sense when applied to the real engine.

Our description will be with reference to Figs. 2.2, 2.3 and 2.4. A jet engine is a system that converts thermal energy into mechanical energy; the thermal energy is provided by the combustion of the fuel; the mechanical energy output is manifested as a net thrust due to the higher speed of the airflow at the exit of the engine. Thus a jet engine can be viewed as a high-velocity gas generator.

Except for the fuel combustion process, almost all turbomachinery flow processes are very nearly adiabatic. The naming of the various stages of the engine is standarized: they are called the station numbers and the most important of them are shown in Fig. 2.2. Additional ones for the F100 engine are shown in Fig. 2.4. The first stage of a turbojet engine, the inlet for the airflow, functions as a diffuser; it helps decelerate the flow, at the same time raising its temperature and pressure. In a temperature entropy diagram (Fig. 2.3)this corresponds to moving from point 0 to point 2 along a constant-entropy line.

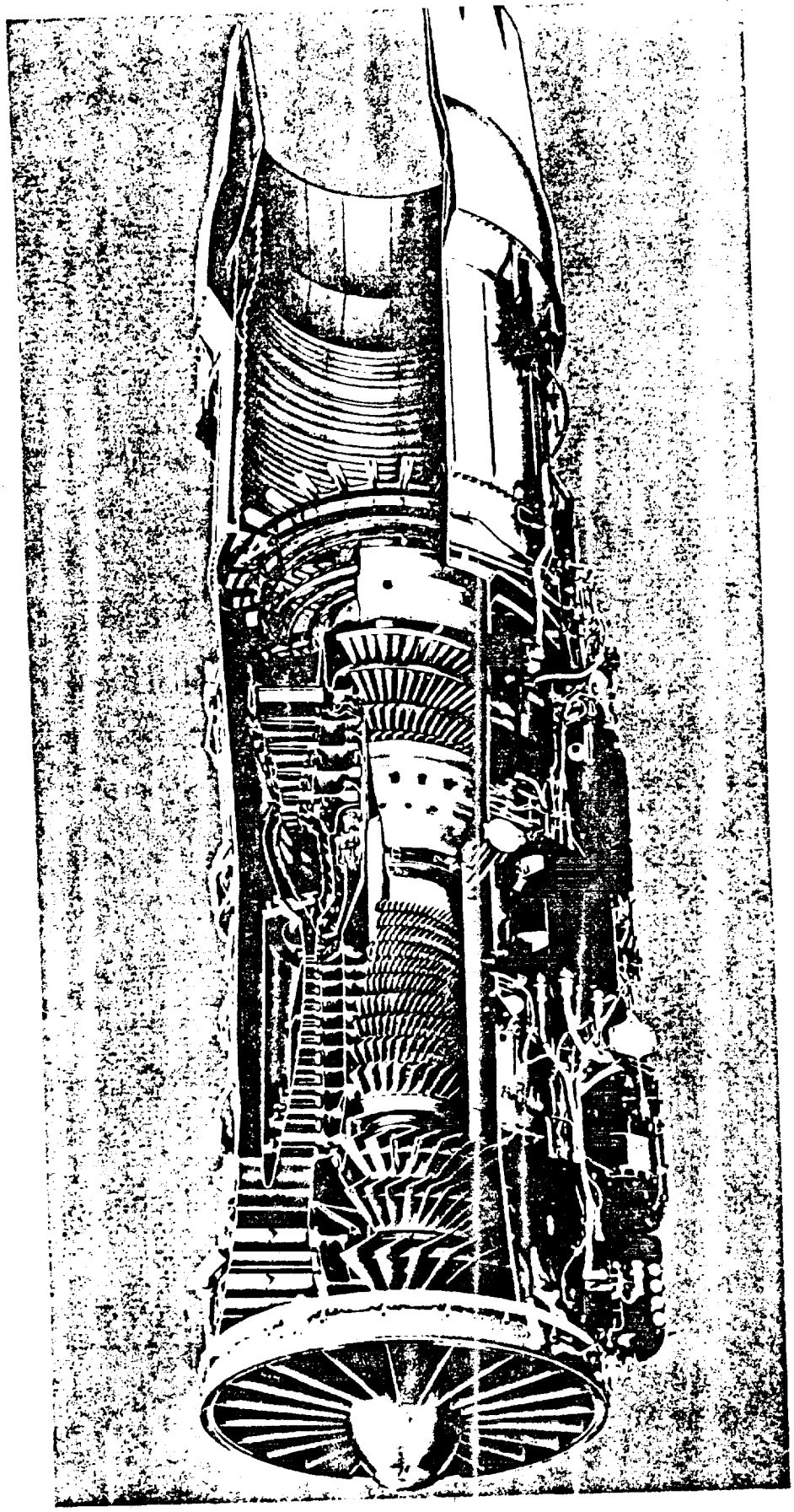

Fig2.1: The F100 Engine.

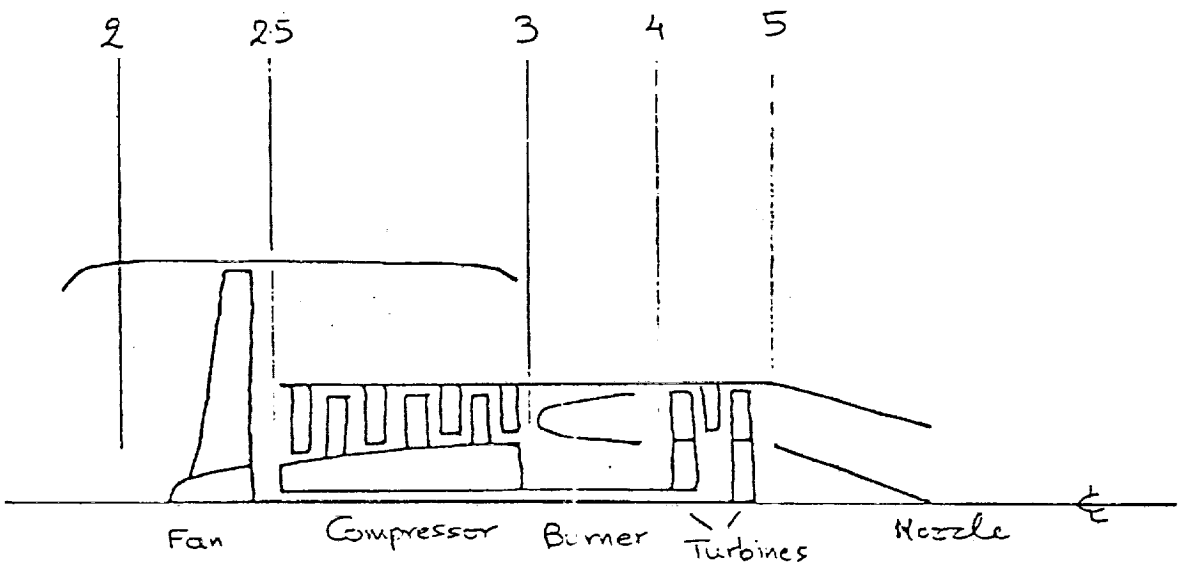

Fig2.2: Schematic Diagram of a Turbofan Engine.

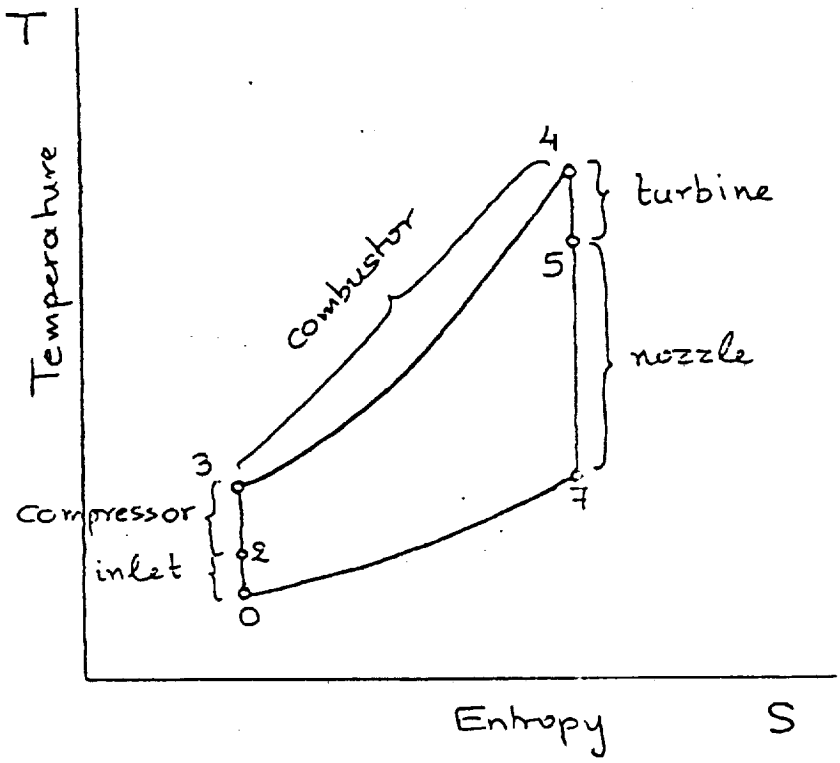

Fig2.3: Temperature-Entropy Diagram:
The Brayton Cycle.

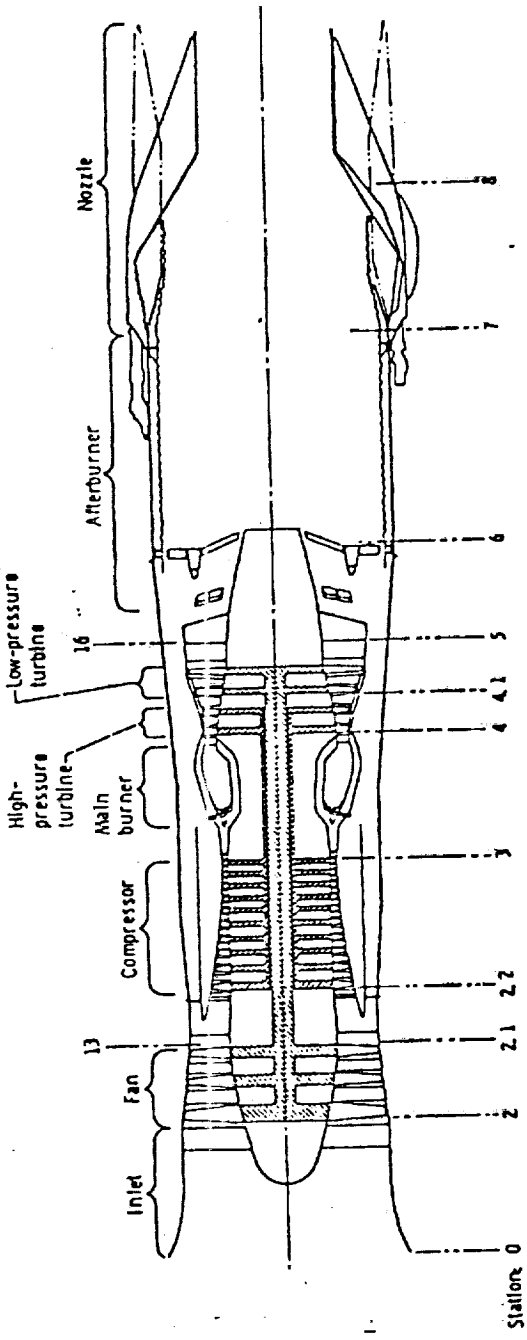

Fig2.4: Schematic of the F100 Engine (from [1]).

To increase the efficiency of the process, the compressor stage further increases the temperature and pressure of the air. At the burner, fuel is mixed with the air and the mixture is burned at approximately constant pressure. This is the stage where thermal energy is added to the gas which will eventually be converted to mechanical work. The motion in the T-S diagram is shown as a motion along a constant pressure line from point 3 to point 4. To complete the cycle, the expanded gas is passed through a turbine, where part of the work is extracted to power the compressor; at the same time the temperature of the gases drops and so does the pressure. Finally, the exit nozzle has a similar effect to the turbine, with the result that, for a well designed engine, the exit pressure corresponds to the ambient conditions, point 7 in (Fig. 2.3.) The thermodynamic cycle we just described is called the Brayton cycle.

Significant improvement to the propulsive efficiency (the ratio of the thrust delivered to the airplane frame to the net mechanical power in the exhaust) can be accomplished with a turbofan engine. A second turbine is added downstream of the first one. It powers a fan (see Fig. 2.2) that pumps air, which is bypassed from the main airflow. This secondary flow either appears directly as a second thrust component or is mixed with the main flow downstream of the turbines and before the exit nozzle (as is the case for the F100 engine, Fig. 2.4).* The ratio of the bypassed flow to the main flow through the gas generator is denoted by α, the bypass ratio. Large commercial turbofan engines have a big α, while engines like the F100 have a smaller bypass ratio, in our case near 1.

---

*Since two turbines and compressors are present, we use the notation: at entry of high compressor, station number 2.5, and at exit of high turbine, station number 4.5.

The afterburner, present in the F100 engine (Fig. 2.4) but not in use at our operating point, provides additional thrust, but only for short intervals of time; this is because the fuel which is burned there is mixed with air at a higher temperature but also higher mach number and thus the process is considerably less economical.

2.2.2 Engine Performance and Limitations

In the previous section we described the general principles of operation of the F100 engine. The description applied mainly to the steady-state running of the engine; for the purposes of control, however, we are interested in the transient behavior of the engine, as it moves from one operating point to another. In any engine simulation, this behavior is captured by component diagrams and dynamics that are used to integrate them.

A component diagram (see for example Fig. 2.5 and 2.6) relates the important nondimensional groups of variables that describe an engine component. In the compressor diagram (Fig. 2.5) the variables are the corrected airflow at the inlet and the pressure ratio (the ratio of output to input pressure). Also sketched are the lines of constant (rotational) speed. We see that higher speeds are associated, in general, with high pressure ratios and bigger airflows. A significant feature of the compressor as well as the fan diagram, is the limit line at the top of the diagram, the surge line.

Surge phenomena in turbomachinery are very undesirable. They lead to significant deterioration of the component performance, for example loss of pumping ability of the compressor (in other words of the ability of the stator-rotor

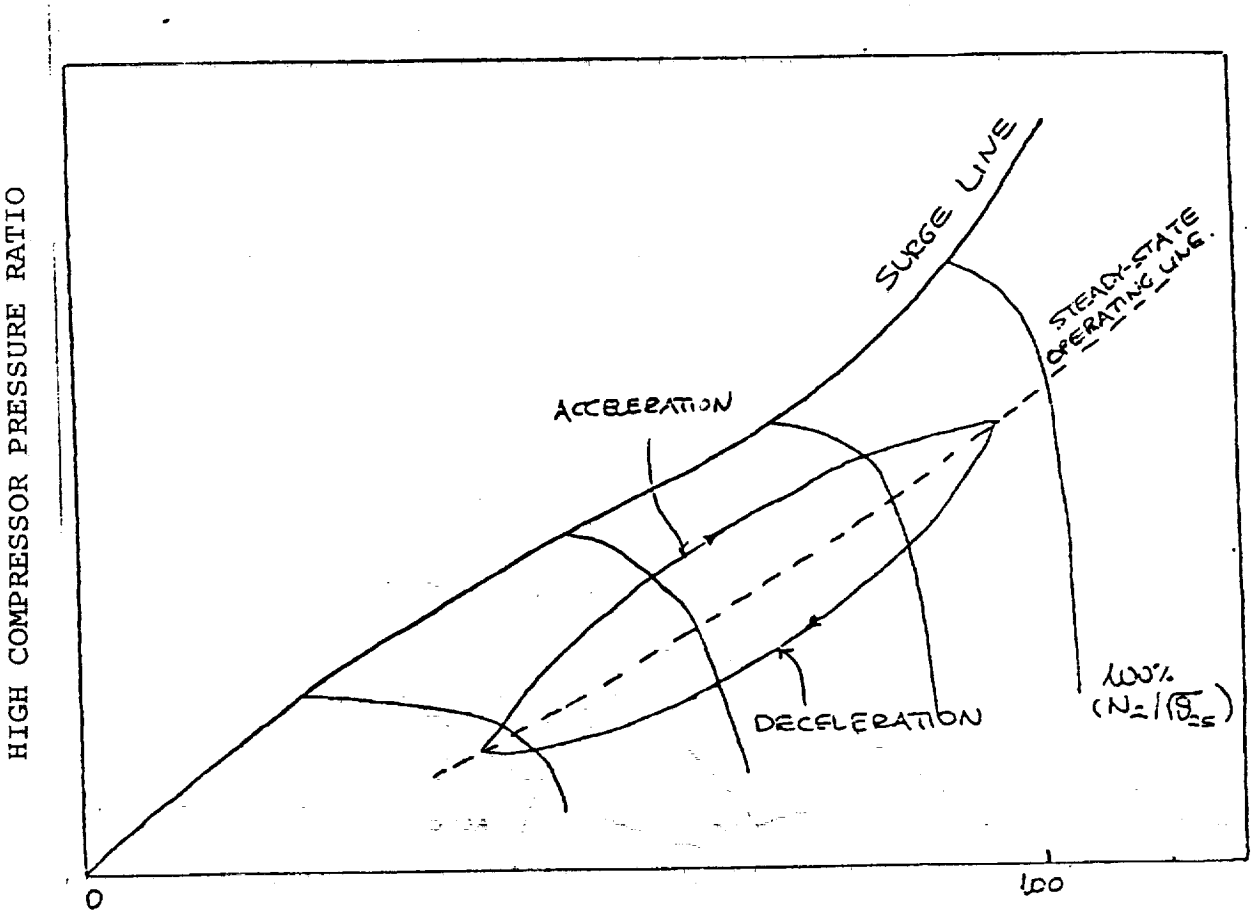

Fig2.5: A Typical Compressor Diagram.

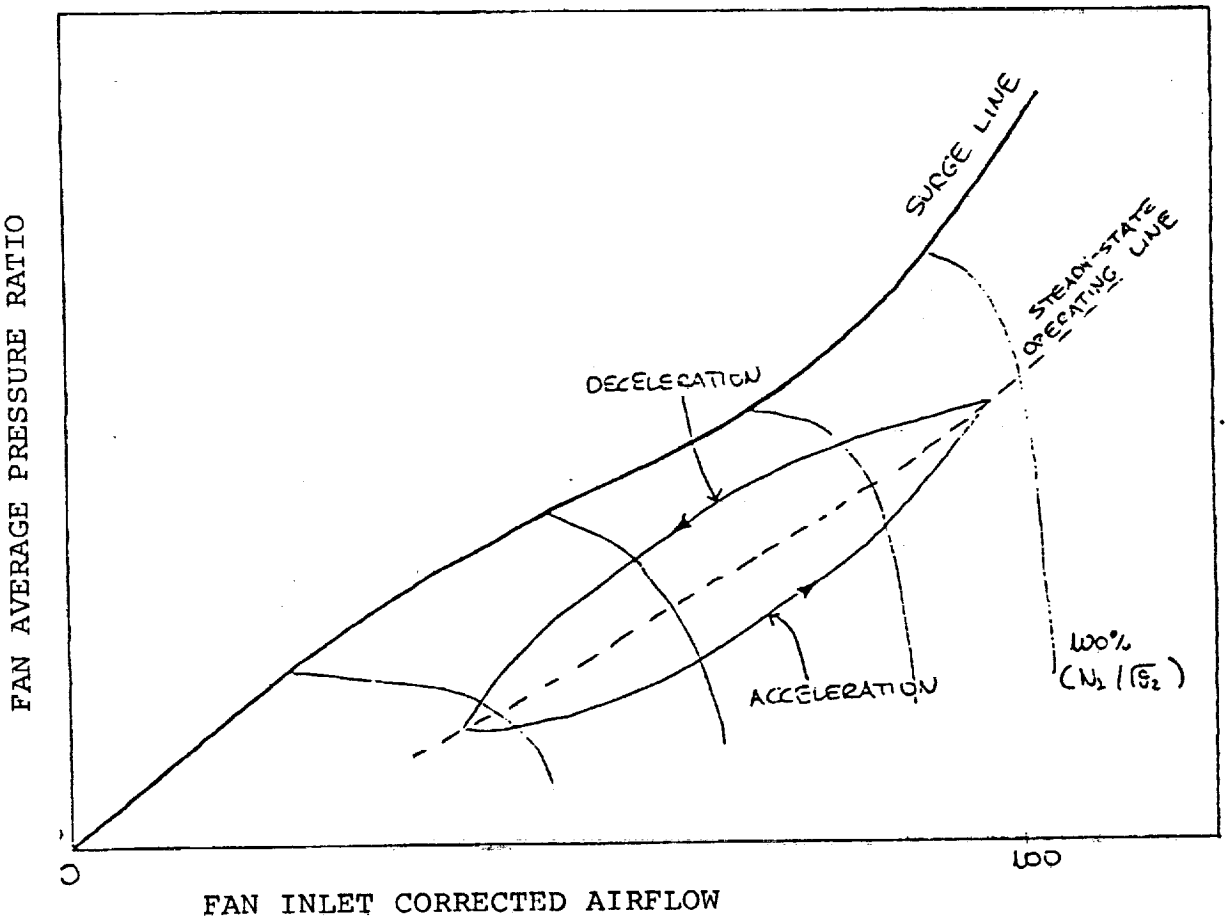

Fig2.6: A Typical Fan Diagram.

sequences to deflect the flow sufficiently). This surging can be accompanied by rotating stall phenomena (see Dixon [4]) which lead to vibration and noise for the engine.* For our purposes, therefore, surge should be avoided and the trajectories of control should stay clear of the surge line.

A good engine design will make the component (compressor, fan or turbines) operate along a steady-state operating line (dashed line in Fig. 2.5 and 6) which stays sufficiently far from the surge line. During transients, however, stall margins can deteriorate. In Fig. 2.5 possible approximate paths are indicated away from the steady-state line, while accelerating or decelerating the engine. Note that stall margin during deceleration increases for the compressor but decreases for the fan.

The operating point for which the linear model used is valid is at almost full power while at rest at sea level. This mode of operation is characterized by the fact that the engine components are choked or, in rough terms, that no further increase in through-flow is possible. Choking is also characterized by the fact that disturbances (e.g. pressure changes) cannot travel upstream, since the sonic velocity has been reached by the flow. Choking, contrary to surge, is not an undesirable state and it leads to some simplification in describing the operation of the engine.

In an engine simulation like the one for the F100 engine from which the linear model was obtained by linearization, the component diagrams are put together to form a complete description of the engine dynamics (Fig. 2.7). Nonlinear

---

*The way surge can be achieved is for example, through reduction of the airflow at constant speed. Surge phenomena are only incompletely explained to date, since they are associated with unstable and turbulent flow.

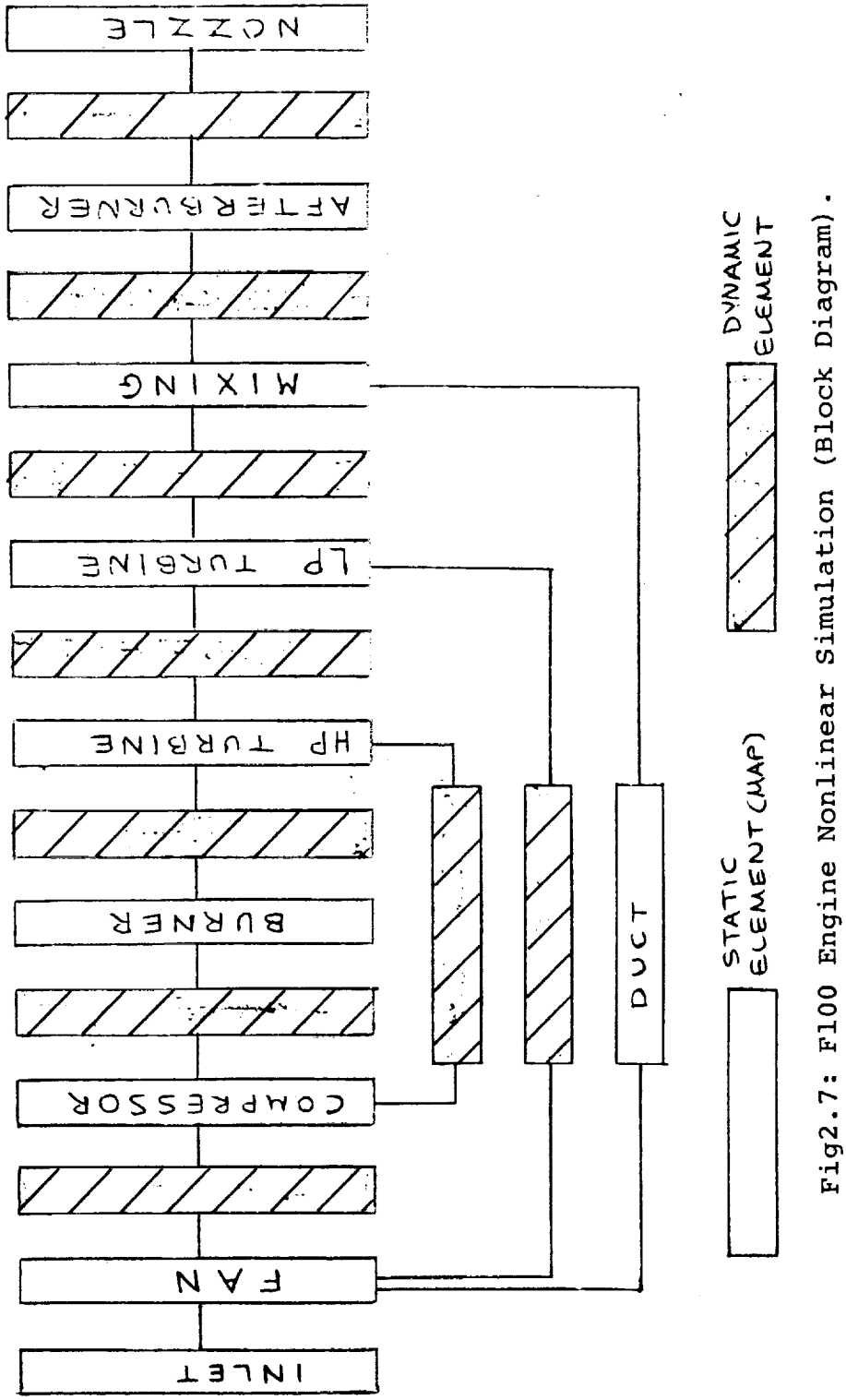

Fig2.7: F100 Engine Nonlinear Simulation (Block Diagram).

differential equations are used to simulate the behavior of the engine off equilibrium.

A modern turbofan engine operates, because of its high-performance requirements, very near its structural and materials limits. Care should be taken in the design stage to avoid excessive vibrations or noise. Lighter and stronger materials are used to stretch the efficiency of the thermodynamic cycle to the limit. At the entry point of the high-temperature turbine, the gases may have temperatures very near the limit of the turbine blades; cooling is often necessary and excursions to higher temperatures can only last a few seconds.

For the design problem of the ALMC conference, the above limitations were never explicit. This will by necessity be true for our design as well. Meaningful data were not available to the author and one must be content with keeping track of the departures of our variables from their reference positions.

Engine Operation

Let us briefly describe how the control task is accomplished. The Power Lever Angle (PLA), ranging from 0 to 100 percent (full setting) is a general thrust command given by the pilot. The on-board computer then translates this power setting into values of an appropriate set of reference variables (for example shaft speeds, etc.). The control system them tries to achieve this change in reference settings. Since in steady-state we want no error between reference and real outputs the requirement is that integrator action is included in the controller design. This is accomplished in the proposed design.

Choice of Outputs

The set of measured variables does not coincide with the set of desirable controlled variables. Thrust cannot be directly measured and neither can the two stall margins of the engine (see Table 2.1).

Thus, one has to make a choice, to some extent arbitrary, as to what to include in the set of outputs. Provided there is strong correlation between the values of the selected variables and the set of variables that one aims to control, the control action will be effective. In our case, the selection will be from among the set of directly measurable states.

The complete set of engine states of the linear model is given in Table 2.2. Most of them can be directly measured. The choice of outputs will be from among these state variables.

The two shaft speeds are two of the four outputs selected. As will be seen in section 2.3, they include the dominant dynamics, at least in the range of control selected.

The fast turbine engine temperature, $T_{4.5}$ is also selected as the third output variable. It gives an indication of whether the engine limitations are exceeded.

The fourth output variable choice is one of the pressures. We select P_3, the compressor discharge pressure. The state P_3 is fairly dominant as the eigenvector analysis reveals, although it is associated with a faster pole (at -175).

Control Inputs: The F100 turbofan jet engine is a true multivariable control example because of the existence of more than one control variable. The main one

TABLE 2.1

Engine Outputs : Original Set *

Y1= Engine Net Thrust Level (lb)

Y2= Total Engine Airflow (lb/sec)

Y3= Turbine Inlet Temperature (°R)

Y4= Fan Stall Margin

Y5= Compressor Stall Margin

TABLE 2.2

List of Engine States and New Outputs with units

X1= Fan Speed (N1) - RPM

X2= Compressor Speed (N2) - RPM

X3= Compressor Discharge Pressure (P_{t3}) - PSIA

X4= Interturbine Volume Pressure ($P_{t4.5}$) - PSIA

X5= Augmentor Pressure (P_{t7}) - PSIA

X6= Fan Discharge Temperature ($T_{t2.5}$) - °R

X7= Duct Temperature ($T_{t2.5c}$) - °R

X8= Compressor Discharge Temperature (T_{t3}) - °R

X9= Burner Exit Fast Response Temperature (T_{t4hi}) - °R

X10= Burner Exit Slow Response Temperature (T_{t4lo}) - °R

X11= Burner Exit Total Temperature (T_{t4}) - °R

X12= Fan Turbine Inlet Fast Temperature ($T_{t4.5hi}$) - °R

X13= Fan Turbine Inlet Slow Temperature ($T_{t4.5lo}$) - °R

X14= Fan Turbine Exit Temperature (T_{t5}) - °R

X15= Duct Exit Temperature (T_{t6}) - °R

X16= Duct Exit Temperature (T_{t7}) - °R

* Taken from [1]

New Set of Outputs: Y1=X1

Y2=X2

Y3=X3

Y4=X12+X13

is (the traditional and only control variable of the past) fuel flow. Returning to the componentwise description of the engine for a moment, the observation is that for fixed geometry of the compressors, fan and turbines we get efficient operation over a limited range of speeds. This can be easily accounted for if we consider the elementary stage of any turbomachinery, a blade row (stationary or nonstationary). We can then see that the angle geometry of the row (the angle at which the blades are positioned relative to the flow) critically determines the ability of the machine to exchange kinetic energy from the flow with rotational energy of the blade row. If, as is the case in modern jet engine designs, we allow for a variable geometry (for practical purposes in the stator rows) then we streamline the efficiency of the component. The F100 engine provides two variable geometry control inputs, one at the fan stage (at the inlet stationary guide vane) and the other at a stator stage of the compressor. The fourth control input considered in our design will be the exit nozzle area. Varying the nozzle area affects the thrust delivered to the aircraft. Also exit nozzle area is used to control the internal pressure.

A list of the inputs with units can be found in Table 2.3.

2.2.3 Sensors and Actuators

To make the linear model as accurate as possible, it is required to include dynamics for the output sensors and the input actuators (Fig. 2.8). A description of the approximate linear dynamics used to represent them follows ([1]).

TABLE 2.3

Engine Control Inputs with Units

U1= Main Burner Fuel Flow (WFMB) -lb/hr

U2= Exit Nozzle Area (A_j) - ft^2

U3= Inlet Guide Vane Position (VG_1) - deg

U4= High Variable Stator Position (VG_2) - deg

Sensors

With the exception of the fan turbine inlet temperature sensor, all the sensors can be represented by first-order lags with transfer functions $\frac{1}{s\tau_i+1}$. The time constants τ_i are in general very small. The tachometers measuring the two shaft speeds have time constants of 0.03-0.05 sec. The pressure sensors are also fast with time constants of about 0.05 sec. All these are fast and will therefore be omitted.

The transfer function of the fan turbine inlet temperature sensor is shown in Fig. 2.9a and a Bode plot of it is given in Fig. 2.9b. The sensor is of this form because it has to be protected from its high-temperature environment. One of the time constants (5.49 sec.) is slower than all the time constants of the engine. It is therefore a main control consideration to achieve fast responses in the presence of this slow sensor. It should be noted that the zero associated with the sensor is at -0.47 rad/sec, between the two poles. This keeps the bandwidth of the sensor wide.

Actuators

The actuator dynamics are more complicated than the sensor dynamics. This is so because they must provide work and are as a result physically larger. A major source of error will lie in the approximations that will be made for these dynamics.

Fuel Flow Actuator

The fuel flow actuator is a hydromechanical system composed of a fuel pump and a metering valve.

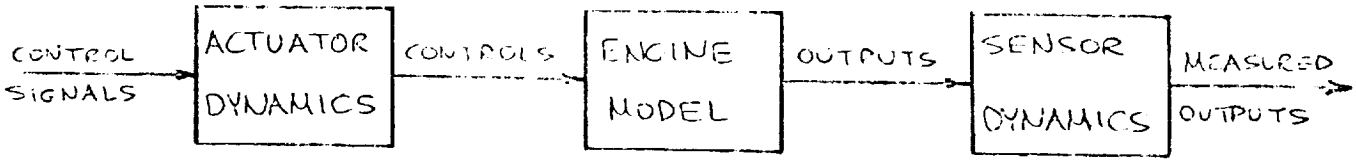

Fig2.8: The overall Plant with Sensors and Actuators.

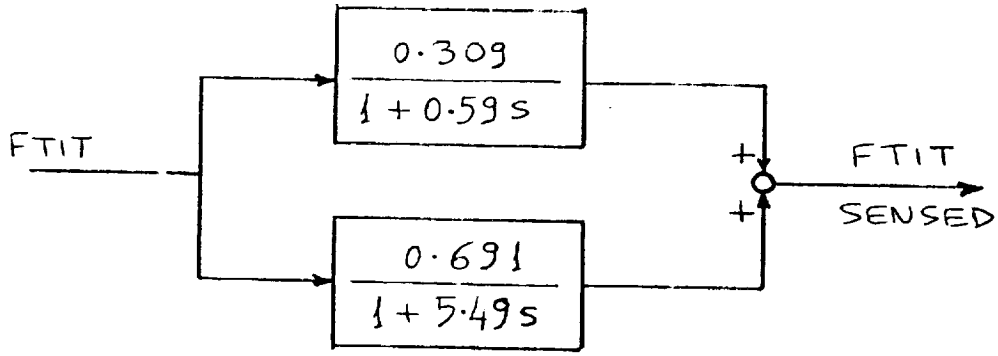

Fig2.9a: The Fan Turbine Inlet Temperature(FTIT) Sensor Dynamics.

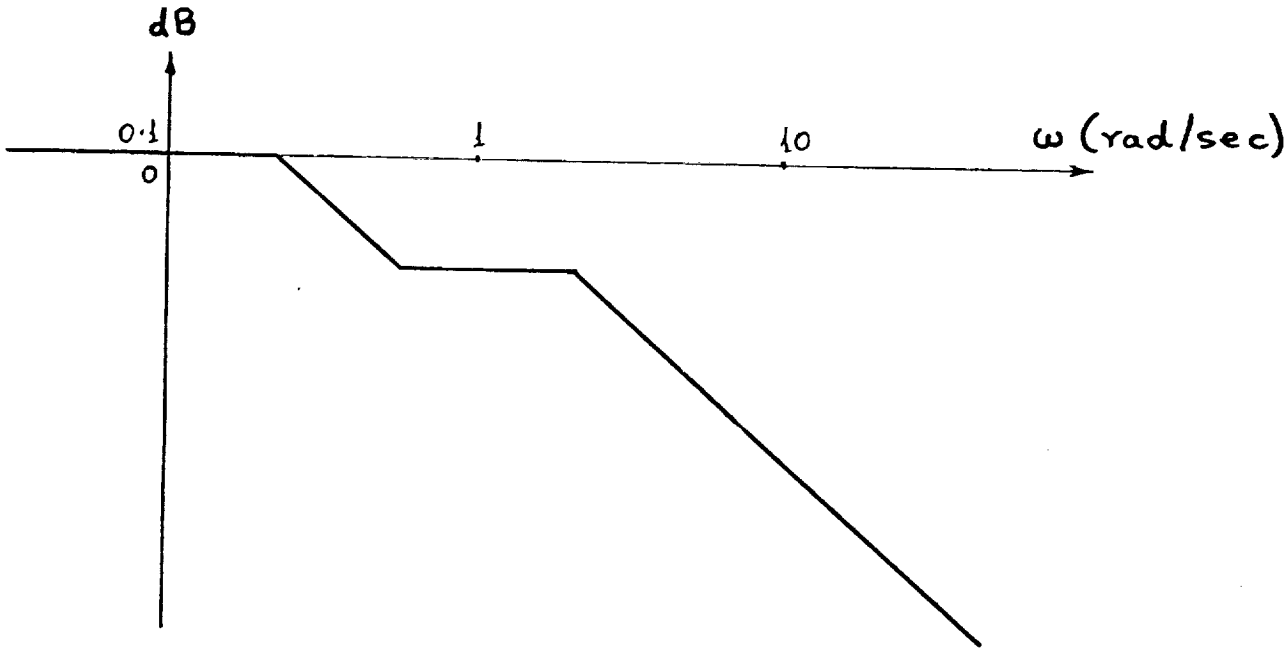

Fig2.9b: Bode plot of the FTIT Sensor Transfer Function.

The metering valve is positioned by a fuel-actuated piston which in turn is driven by an electrically controlled servovalve. Feedback about the position of the metering valve shaft is provided by a position sensor which is a source of backlash. Both the metering valve and the fuel pump servo regulator are represented by first-order systems (Fig. 2.10). Only the dynamics of the fuel pump are kept, however, since the time constant of the valve is 0.02 sec.

Exit Nozzle Actuator

The nozzle area actuator has two parts (Fig. 2.11) The first part, the servo dynamics, is fast and will be omitted. The second part, an air-driven motor controller has second-order dynamics. The characteristics of this motor vary with flying conditions. At our operating point it has a bandwidth of about 38 rad/sec and a damping ratio ζ=0.56. Because it is highly undamped, these dynamics are included.

Fan and Compressor geometry actuators

The linearized models for the two variable geometry actuators are shown in Fig. 2.12 and 2.13. These models are further simplified to yield the approximate models shown. The fast time-constants are omitted and the resulting feedback transfer functions yield the first-order systems with bandwidths of 12 and 40 rad/sec.

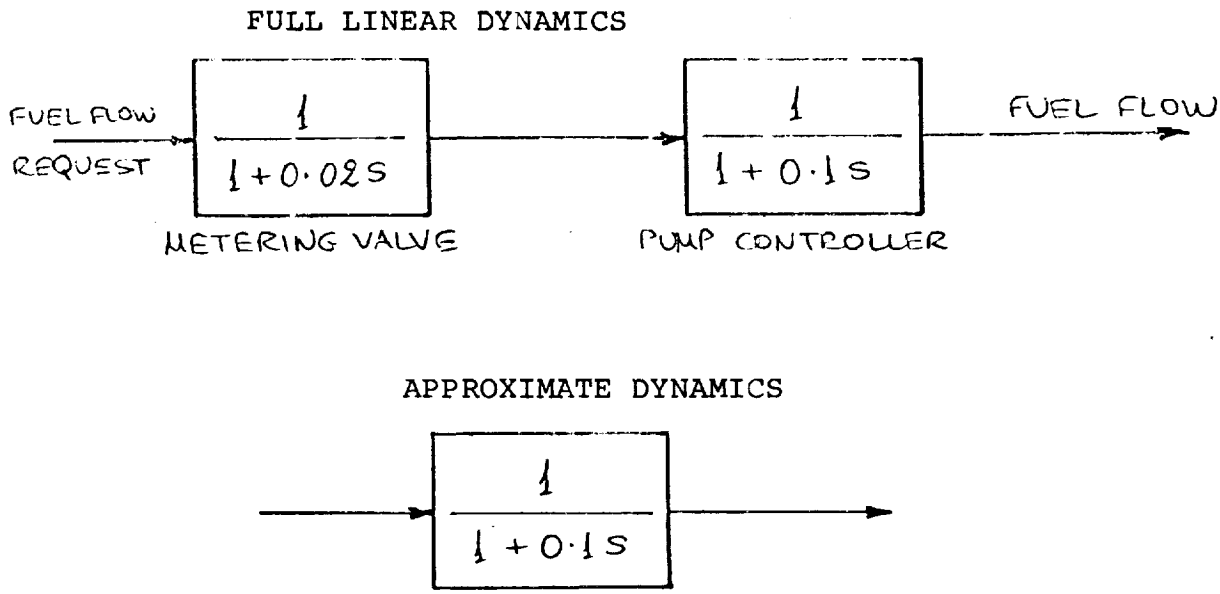

Fig2.10: Fuel Flow Actuator Dynamics.

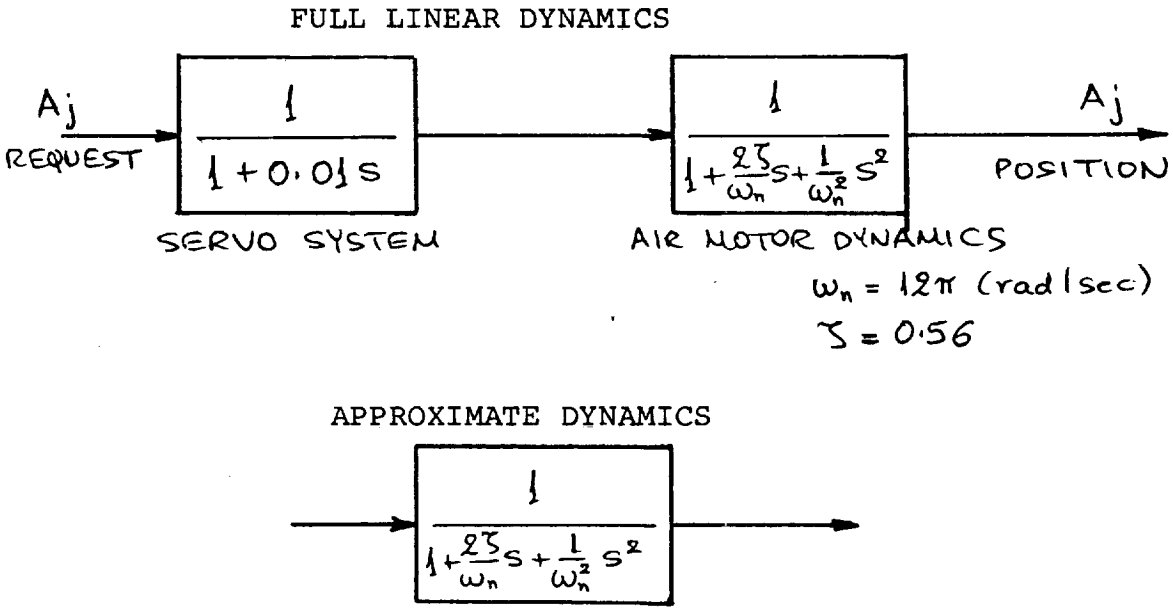

Fig2.11: Exit Nozzle Area (A_j) Dynamics.

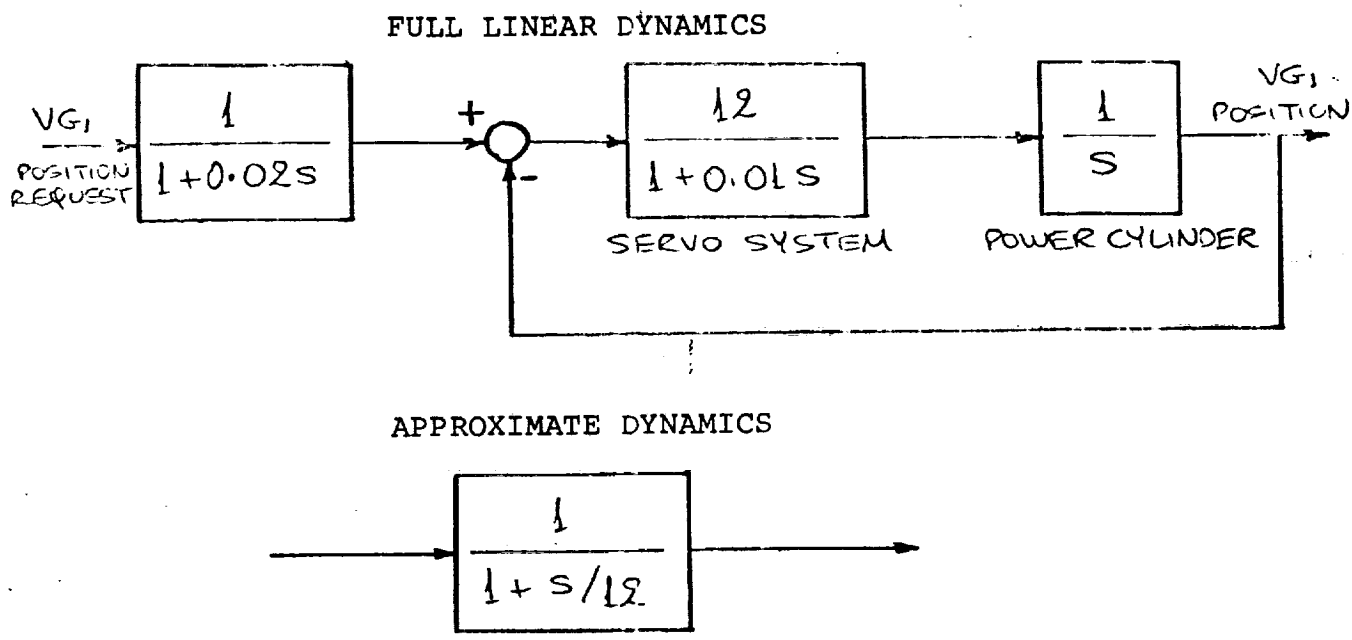

Fig2.12: Fan Variable Geometry (VG_1) Dynamics.

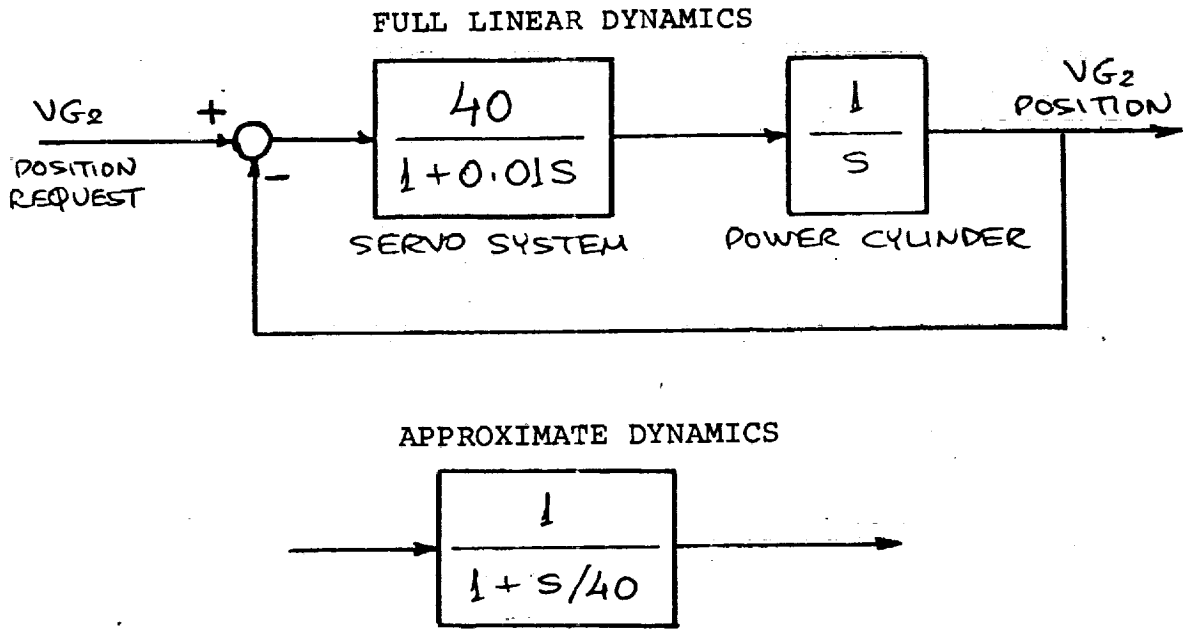

Fig2.13: Compressor Variable Geometry (VG_2) Dynamics.

2.3 Engine Dynamic Characteristics

2.3.1 Introduction

The previous section described the operation of the engine in qualitative terms. Next we discuss the engine dynamics quantitatively, based on the linear model at the operating point of 83° power level angle (see Appendix A).

For this, we need a detailed description of the dynamics that make up the engine response, their frequency characteristics and their relative importance.

This will help in the selection of those parts of the engine dynamics which it is important to affect directly for the purposes of control.

2.3.2 The Pole-Zero Structure

The F100 jet engine is a complex physical system that can at best be only approximately modelled by a mathematical system. Events in the engine can be broadly classified according to the time scales characterizing them as follows. Air flows are the fastest category, having time scales of the order of 10^{-2} sec. Then come fuel flows, at about 10^{-1}sec and also guide vane (variable geometry) and nozzle area response times. Finally, the dominant dynamics of angular rotor acceleration, of the order of 1-10 sec.

Table 2.4 list the poles of the linear system augmented by the significant sensor and actuator dynamics. We see that the spread of the poles corresponds to the spread described above. It is desirable to associate poles with engine states so that the classification of the dynamics given is verified.

To accomplish this, we give an eigenvector analysis of the linear system. Fig. 2.4 plots, for each eigenvalue, the dominant components of its normalized

TABLE 2.4

Augmented System Poles

1) -0.18204
2) -0.64773
3) -1.6810
4) -1.9057
5) -2.6184
6) -6.7148+j1.312
7) -6.7148-j1.312
8) -10.
9) -12.
10) -17.805+j4.7811
11) -17.805-j4.7811
12) -18.592
13) -21.056+j31.259
14) -21.056-j31.259
15) -21.327+j0.8208
16) -21.327-j0.8208
17) -38.678
18) -40.
19) -47.126
20) -50.661
21) -59.161
22) -175.67
23) -577.04

Fig2.14: Eigenvector Analysis : Main Components of Normalized Eigenvectors (see Table2.2 for names of states).

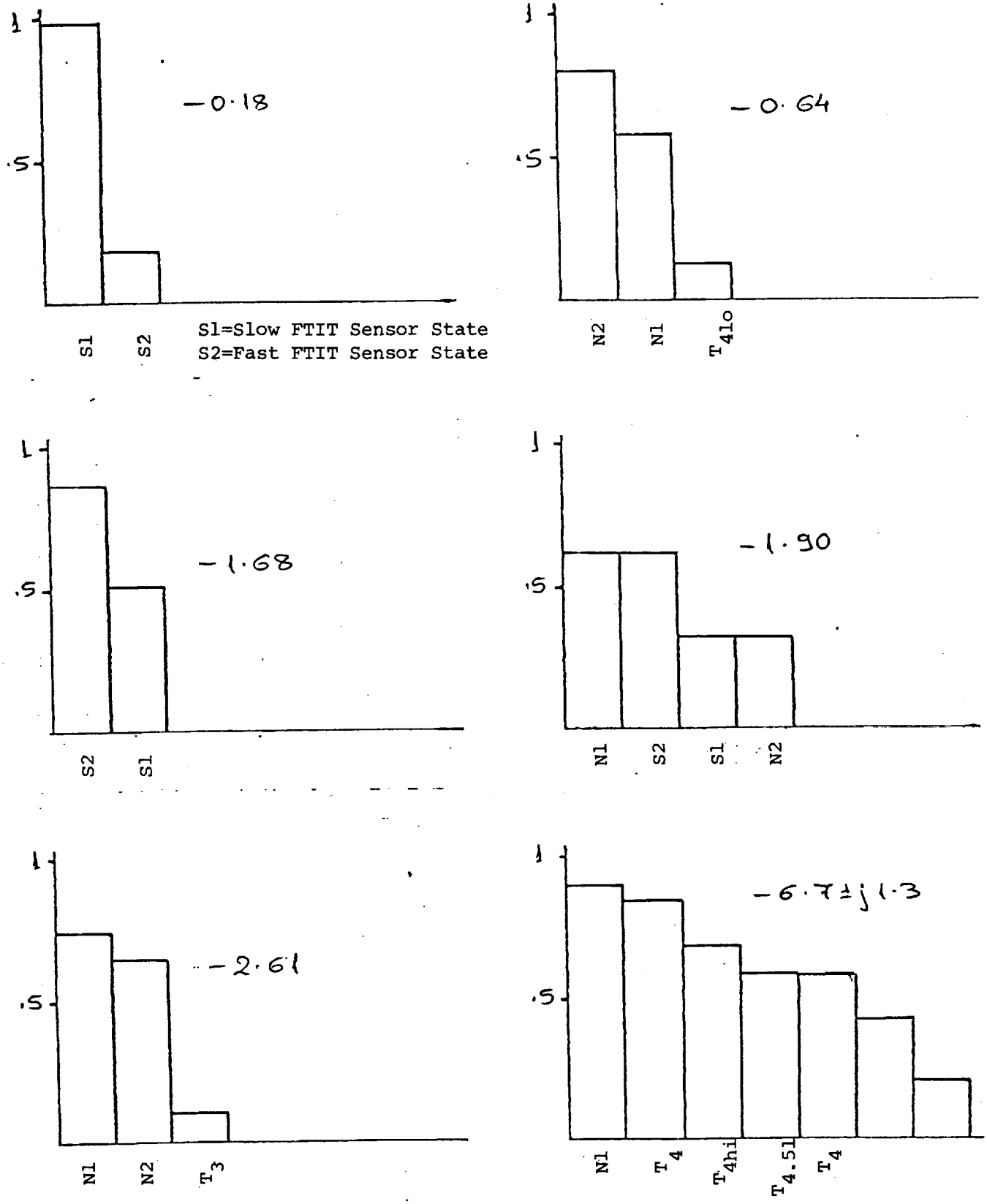

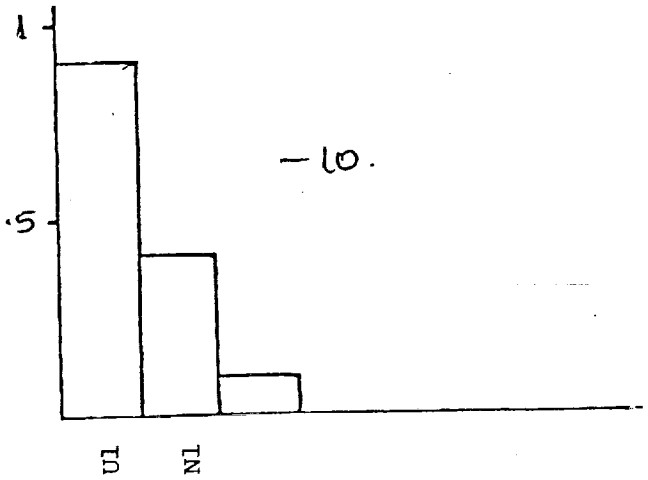

U1=Fuel Flow Actuator State

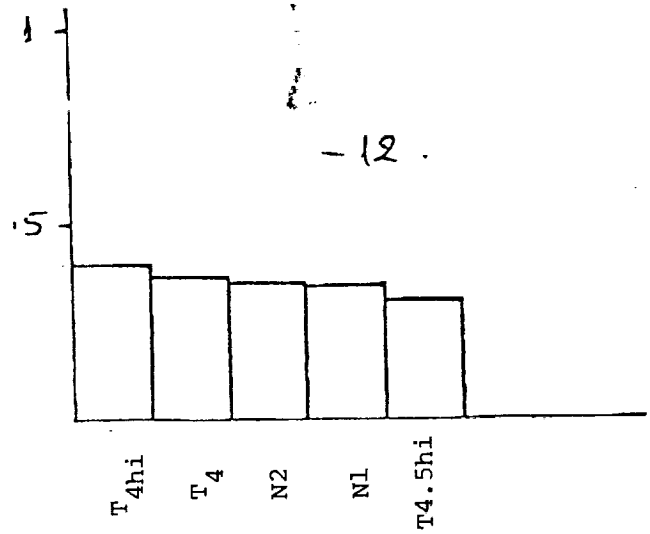

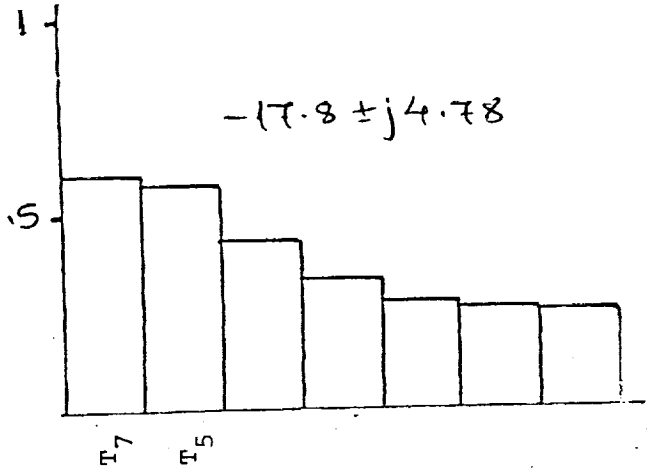

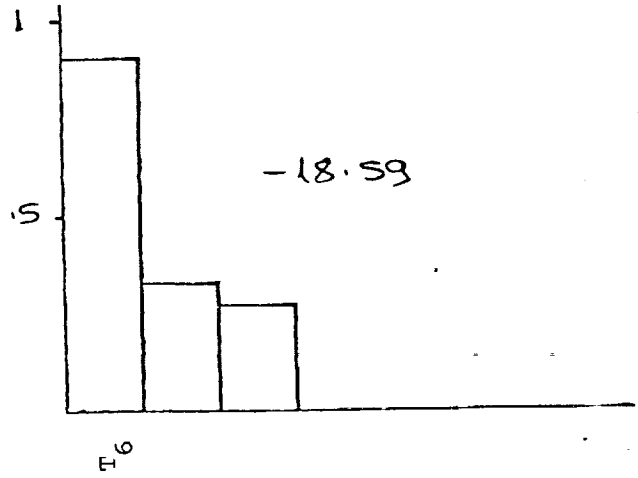

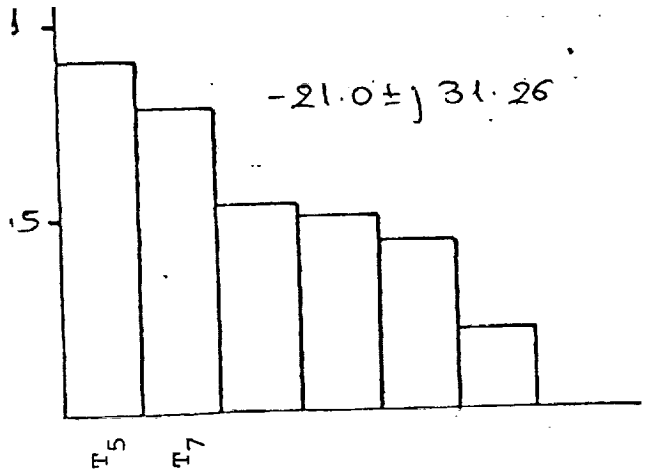

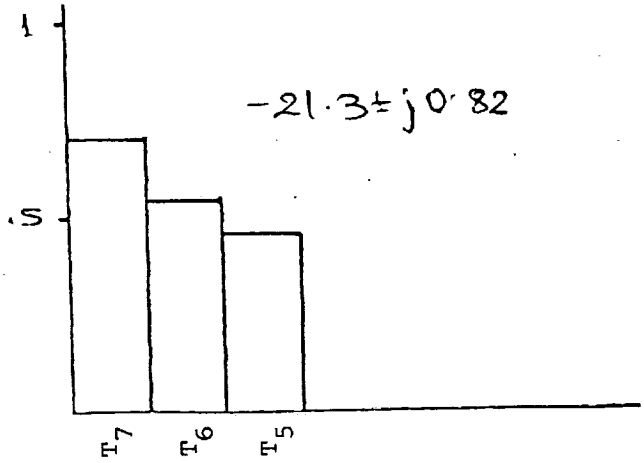

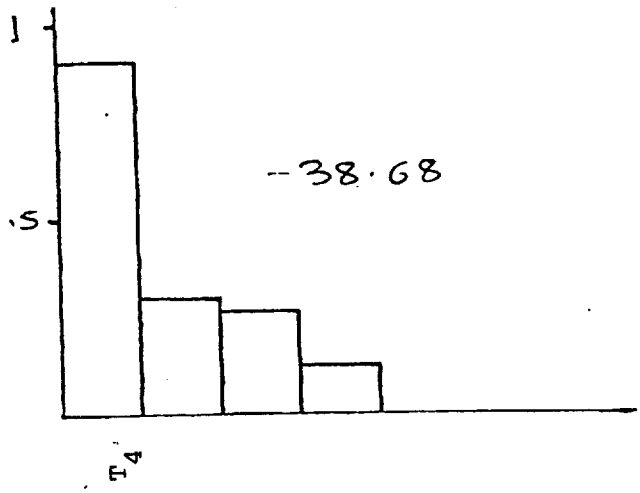
1
.5
-38.68
T_4

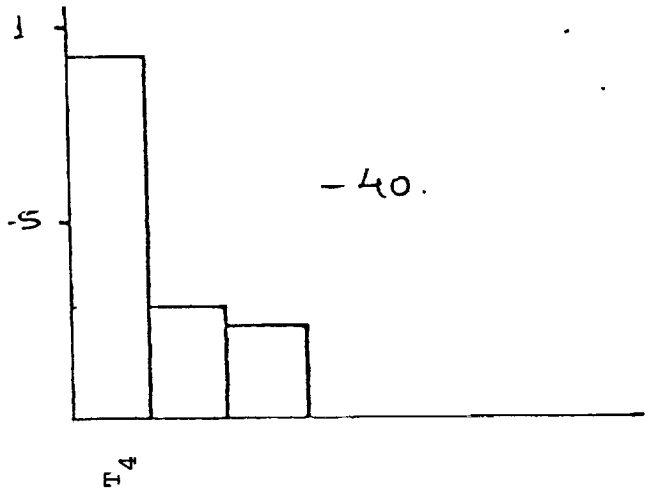
1
.5
-40.
T_4

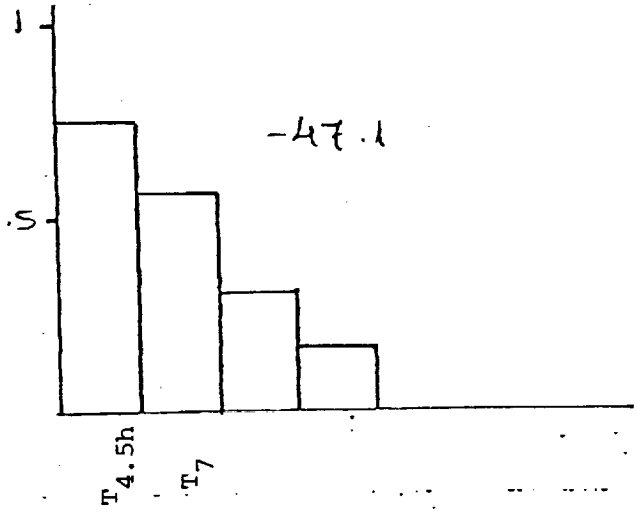
1
.5
-47.1
$T_{4.5h}$
T_7

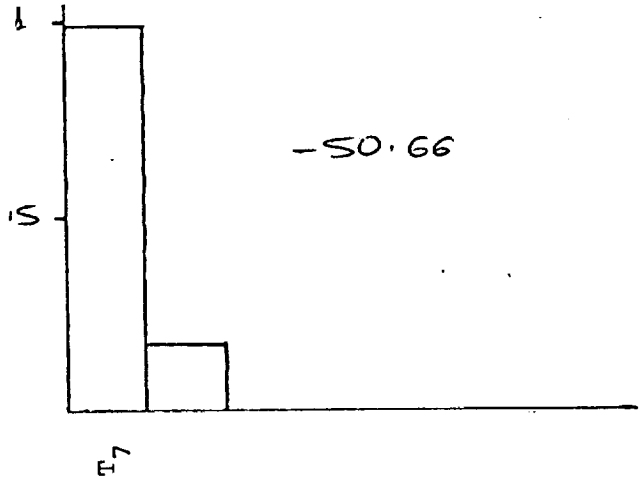
1
.5
-50.66
T_7

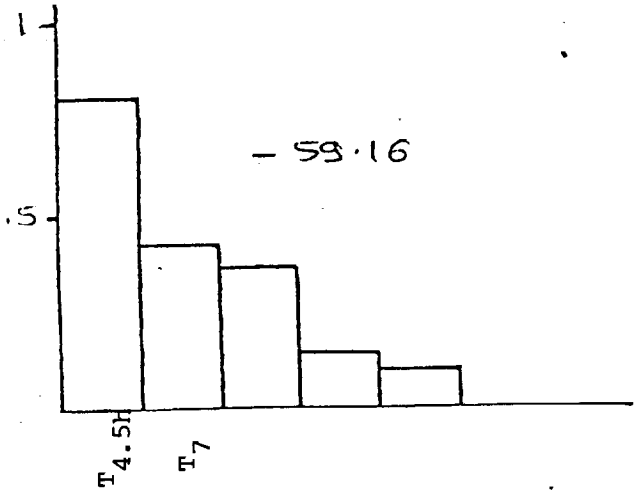
1
.5
-59.16
$T_{4.5h}$
T_7

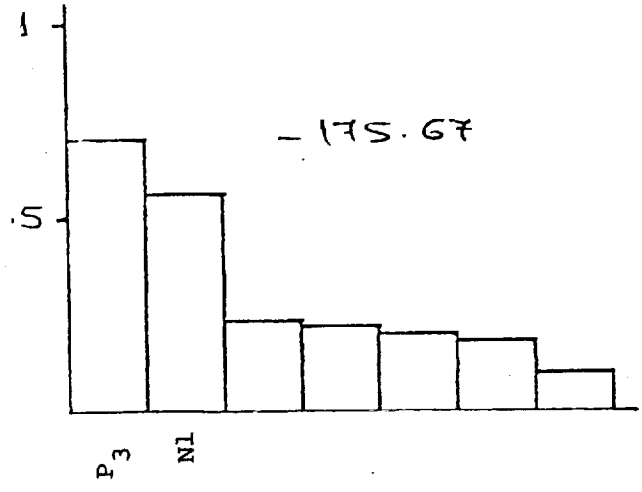
1
.5
-175.67
P_3
N1

eigenvector. This gives an indication of the directions (in this case states) in which each eigenvalue is most important. A fairly strong association of states with poles emerges from Fig. 2.14. In general, pressures and temperatures are associated with fast poles, while the shaft speeds with the relatively slower ones.

Modal analysis

To decide which dynamics are dominant, we use the modal decomposition of the system ([2],[13]).

Given a system in state-space form:

$$\dot{\underline{x}}(t) = \underline{A}\,\underline{x}(t) + \underline{B}\,\underline{u}(t)$$

$$\underline{y}(t) = \underline{C}\,\underline{x}(t)$$

with distinct eigenvalues, one can write an additive decomposition of its transfer function $\underline{G}(s)$:

$$\underline{G}(s) = \underline{C}(s\underline{I}-\underline{A})^{-1}\underline{B} = \sum_{i=1}^{n} \frac{\underline{R}_i}{s+\lambda_i} = \sum_{i=1}^{n} \frac{\underline{R}_i/\lambda_i}{1+s/\lambda_i}$$

where $\underline{R}_i = \underline{C}\,\underline{u}_i\underline{v}_i^T\underline{B}$ are the residue matrices. The vectors $\underline{u}_i$ are the right eigenvectors and $\underline{v}_i^T$ are the row elements of the inverse eigenvector matrix. Note that the last expression has the advantage that the frequency-dependent terms $\frac{1}{1+s/\lambda_i}$ are normalized (i.e. they all go to 1 as $\omega \to 0$).

Now it is easily proved that for an unobservable or uncontrollable pole, the residue matrix is zero. By extension, for any pole, the magnitude of the residue matrix (in the normalized form of the last expression) correlates with how strongly observable and controllable the mode is. It certainly is true that the larger the residue term $\frac{R_i}{\lambda_i}$ the larger the contribution of the corresponding pole to the response of the system (at least for sufficiently low frequencies).

For the above reasons, it is useful to calculate the norm of these residue matrices. The choice of a norm is not critical. We have used the following three norms: $\left(\text{where } \frac{R_i}{\lambda_i} = \underline{A} = (a_{ij})\right)$

1) The singular value norm: $\sigma_{max}(\underline{A})$.

2) The row norm: $\max_i \left(\sum_j |a_{ij}| \right)$

3) The column norm: $\max_j \sum_i |a_{ij}|$

Linearization

The residue matrix norms are dependent on the scaling of the system. It is therefore useful at this point to consider the nature of the linear model.

It is derived from the nonlinear description of the engine which can be written as follows:

$$\dot{\underline{x}}(t) = \underline{f}(\underline{x}(t),\underline{u}(t)) \qquad (2.2)$$

$$\underline{y}(t) = \underline{g}(\underline{x}(t),\underline{u}(t)) \qquad (2.3)$$

where $\underline{x}(t)$ is the state vector, $\underline{y}(t)$ the output and $\underline{u}(t)$ the input vectors. The function $\underline{f}$ is such that at a steady-state point $\underline{x}_o(t)$, $\underline{y}_o(t)$, $\underline{u}_o(t)$

$$\underline{f}(\underline{x}_o(t),\underline{u}_o(t))=0 \qquad (2.4)$$

We can then write, using a first-order Taylor expansion:

$$\dot{\underline{x}}(t) = \underline{f}(\underline{x}_o(t),\underline{u}_o(t)) + \nabla_{\underline{x}}\,\underline{f}(\underline{x}_o(t),\underline{u}_o(t))(\underline{x}(t)-\underline{x}_o(t)) + \\ + \nabla_{\underline{u}}\underline{f}(\underline{x}_o(t),\underline{u}_o(t))(\underline{u}(t)-\underline{u}_o(t)) \qquad (2.5)$$

and

$$\underline{y}(t) = \underline{g}(\underline{x}_o(t),\underline{u}_o(t)) + \nabla_{\underline{x}}\underline{g}(\underline{x}_o(t),\underline{u}_o(t))(\underline{x}(t)-\underline{x}_o(t)) + \\ + \nabla_{\underline{u}}\underline{g}(\underline{x}_o(t),\underline{u}_o(t))(\underline{u}(t)-\underline{u}_o(t)) \qquad (2.6)$$

From these and using (2.4) we obtain a linearized model, with:

$$\underline{A} = \nabla_{\underline{x}}\underline{f}(\underline{x}_o(t),\underline{u}_o(t))$$

$$\underline{B} = \nabla_{\underline{u}}f(\underline{x}_o(t),\underline{u}_o(t))$$

$$\underline{C} = \nabla_{\underline{x}}g(\underline{x}_o(t),\underline{u}_o(t))$$

$$\underline{D} = \nabla_{\underline{u}}g(\underline{x}_o(t),\underline{u}_o(t))$$

It is important to realize that all quantities are now incremental (departures from steady-state). In block diagram form, the control will act on the system shown in Fig. 2.15.

Thus the input/output and state vectors of the linear system are not the real physical variables but their increments from equilibrium. Thus a rescaling of the linear model cannot be based on the nominal values. The conclusion is that it is valid to examine the residue matrices of the original system. Later on in chapter 3 we shall discuss the scaling issue in more detail.

Table 2.5 lists the norms of the residue matrices. In agreement with previous authors we find that there are dominant dynamics. They are those associated with

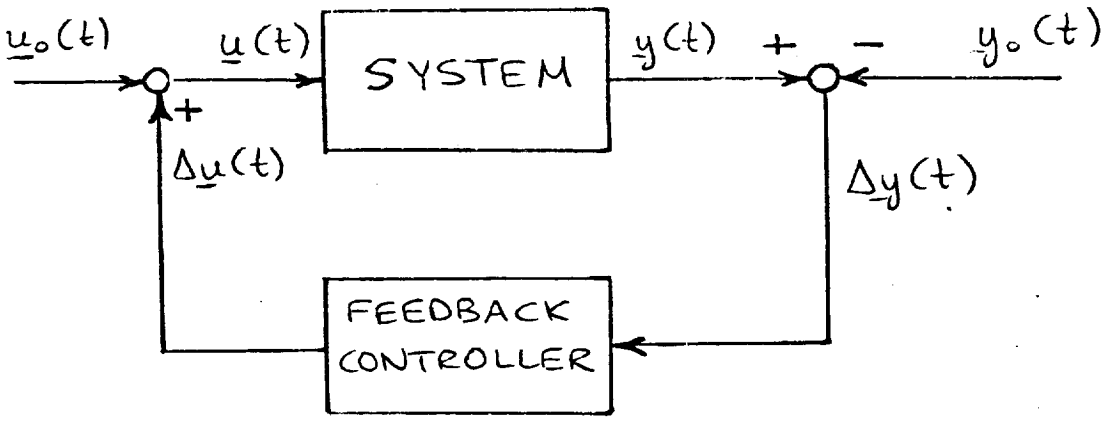

Fig2.15: Control Action on the Incremental Linear System.

TABLE 2.5

Residue Matrix Norms

	EIGENVALUE	Singular Value Norm	Row Norm	Column Norm
1	-0.18204	154.3	157.1	154.3
2	-0.64773	226.9	187.1	321.7
3	-1.6810	227.76	230.4	227.76
4	-1.9057	306.3	253.1	501.6
5	-2.6184	1267.6	983.4	1839.2
6	-6.7+j1.3	1488.45	1487.6	1869.7
7	-6.7-j1.3			
8	-10.	0.47	0.47	0.51
9	-12.	22.1	15.77	33.8
10	-17.8+j4.8	166.2	153.8	237.6
11	-17.8-j4.8			
12	-18.592	1.13	1.04	1.8
13	-21.+j31.3	20.07	13.8	33.34
14	-21.-j31.3			
15	-21.3+j0.8	15.9	13.35	24.2
16	-21.3-j0.8			
17	-38.678	137.75	191.8	119.4
18	-40.	76.6	75.7	88.2
19	-47.126	47.3	48.17	65.5
20	-50.661	8.9	9.6	10.9
21	-59.161	19.45	16.2	29.95
22	-175.67	0.9	0.72	1.45
23	-577.04	1.87E-3	2.3E-3	2.3E-3

the poles at -2.6 and -6.7±j1•3 (rad/sec). From the eigenvector analysis we know that the principal state components for these poles are the two shaft speeds. The complex pair of poles has, however, other states that are quite dominant.

Zeros

Table 2.6 lists the multivariable zeros for the augmented 4 input-4 output linear system. There are no right-half plane (or non-minimum phase) zeros.

Some non-minimum phase zeros can appear when we reduce the system in chapter 3. Thus the zeros of the original system are not directly relevant in the control design.

Open-Loop transfer function

For a multivariable system, the best extension of a Bode plot is a plot of the (frequency-dependent) singular values of the transfer function.

The singular values of the open-loop transfer function of the linear model are plotted in Fig. 2.16.

The d.c. levels of the loops are not important since they are a function of scaling. In an open-loop setting, a loop is fast if it remains flat over a comparatively wide range of frequencies. If it rolls-off fairly soon it is slower.

Based on this we note that the upper loop in Fig. 2.16 is the slowest. It starts rolling off at about 2×10^{-1}. Since the slowest pole is at -0.18 rad/sec. it is this pole that causes the early roll-off.

TABLE 2.6

Multivariable Zeros (Finite)

1) -0.47288
2) -0.64905
3) -2.1283
4) -19.412
5) -20.018
6) -20.873

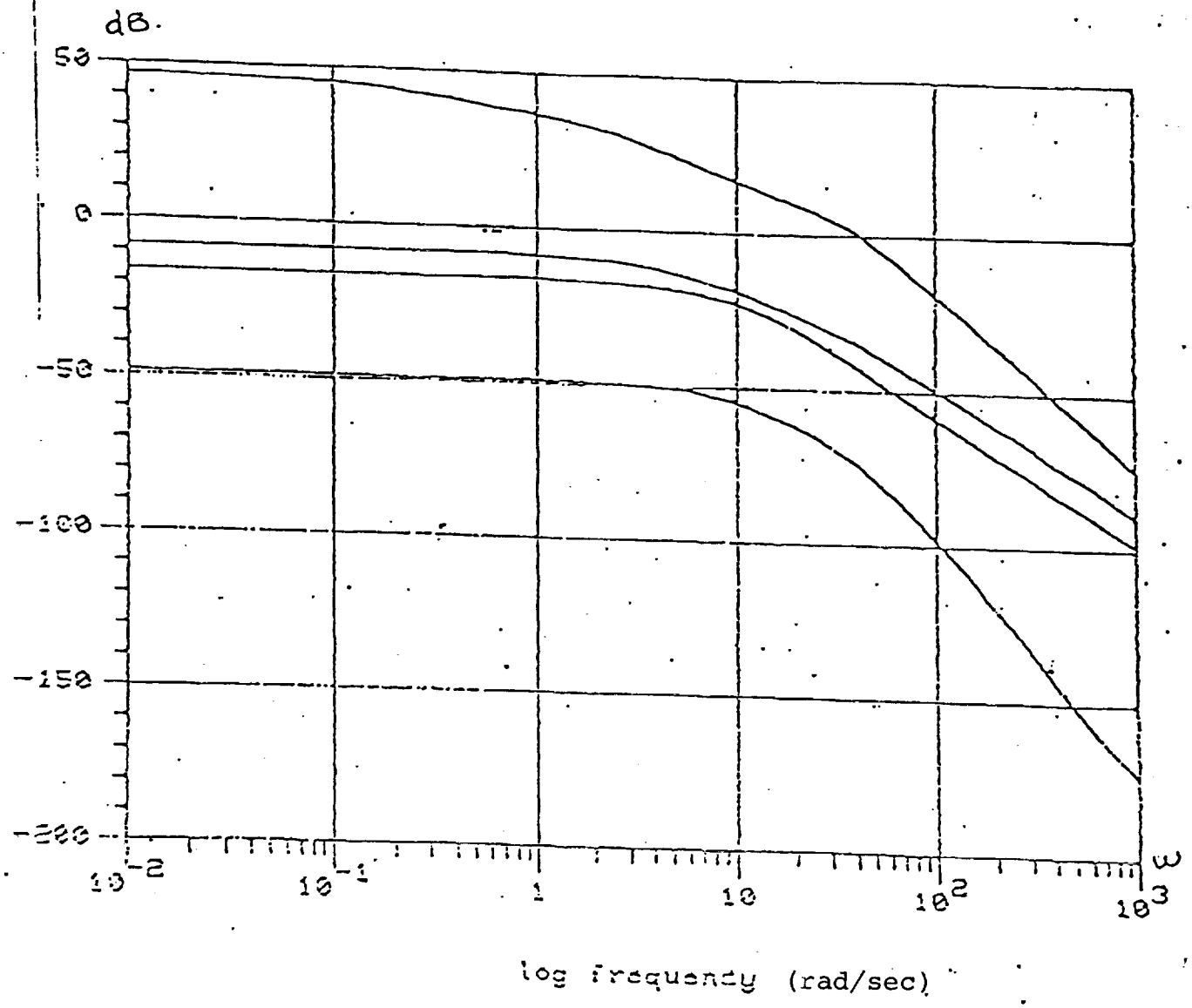

Fig2.16: Open-Loop Tranfer Function: Plot of its Four Singular Values versus Frequency.

2.4 Performance Specifications

We now summarize the specifications that we require of the control design.

First, we need a bandwidth requirement. This will apply to the designed loop transfer function that includes the controller and the plant. A fast loop in a feedback setting means a high crossover frequency.

In accordance with the control specifications given in [22], we require all settling times to be around 2-3 sec. This means that we require the engine to reach about 90% of the change in the set of reference input values in that time. In terms of bandwidth, we require a minimum crossover at around 2-3 rad/sec.

A tight crossover pattern is desirable (i.e. a small spread of the singular values near crossover). Taking into account also the robustness requirement, we arrive at a desirable maximum crossover frequency of around 15 rad/sec. As we shall see in Chapter 3 the simpler the reduced model the more the omitted dynamics and hence the lower the allowable maximum crossover. Thus the figure above is a compromise between fast control and simplicity of design.

The second main control specification is that integral control action is required. This is because (see [1]) it is required to have zero steady-state error to step inputs.

This specification will be met by placing integrators in the four input channels. The integrators come before the plant because the physical point at which the references are injected and where we require the zero steady-state error is at plant output. The integrators are then part of the controller which comes before the plant in the feedback loop.

2.5 Summary

In the present chapter we have set the problem in the form in which we plan to address it. Our goal is to build a compensator which will control efficiently the engine around this operating point.

The description of the engine characteristics gives the required background for doing 'sensible' things with control. The limits of our 'thruth' model are revealed through the examination of the sensor and actuator dynamics.

The basic data on the dynamic behavior of the engine are given and analyzed. The residue matrix analysis sets the stage for model reduction.

The chapter ends by summarizing the set of specifications for control and by outlining the proposed line of attack. It is shown that it is reasonable and that it will accomplish the desired goal. We are now ready to start our control design. The next chapter will deal with model reduction and chapter 4 with the details of control.

3. MODEL REDUCTION

3.1 Introduction

Model reduction means the approximation of a linear state-space system by another of a lower state dimension.

In a control design setting, model reduction is an approximation stage and thus can be approached by a variety of techniques. The engineering practice of neglecting the faster dynamics of a system is a form of model reduction. Singular perturbation methods therefore provide one way of doing model reduction (see, e.g. [18]).

In this chapter, a model reduction technique is presented that has the following features: it is a pole-preservation, state aggregation technique which yields a reduced model that is robust for use in a feedback control system design. The proposed methodology includes a stage of modal analysis (to guide in the selection of poles to be included in the reduced model) and a singular value characterization of modeling error which facilitates control of the robustness properties. A significant feature of our procedure is that it employs such a decomposition of the original system that the single-input single-output analogy is strongest; the way the approximation works is very transparent when viewed in the frequency domain for a scalar system.

In section 3.2 we present our model reduction scheme; we show how it is derived from the residue matrix (or modal) decomposition of the system and we relate it to previous reduction methodologies in order to demonstrate the completeness of our method as against the existing ones. The reduced model is analyzed in a feedback loop configuration in section 3.3 where the norm characterization

of error is found adequate. This leads to a discussion of robustness as it relates to model reduction, in section 3.4. Finally the F100 example is given in section 3.5, where a 13th-order reduced model is derived from the original 23rd order for carrying out the multivariable control designs of chapter 4.

3.2 The Residue Method for Model Reduction

3.2.1 Preliminary Considerations

The purpose of any approximation method which also aims to reduce the order of a linear system is to find another state-space system (of the desired lower order) which 'comes close' to the original system in some sense while preserving the physical control and output variables. A useful interpretation of this closeness is an input-output one: the output associated with the lower-order system is required to be close to the output of the original, for a sufficiently wide class of input signals. And yet this is not enough: one must remember that the reduced model will be used to design a controller. There is no guarantee that a feedback system will be even stable when the same controller is used in a control loop with the original system. Proximity in the input-output sense is not enough to ensure proximity in the feedback sense.

The above is a shortcoming of most previous aggregation methods. Only recently has one been able to address it satisfactorily (see the work of M. Vidyassagar [23]). In this thesis, the issue of model reduction for feedback control is addressed directly, but without having recourse to the algebraic machinery of [23]. Instead,

we shall use an old concept in control: the bandwidth, in this case its multivariable extensions. By making explicit a bandwidth over which our model is accurate, we can go ahead and design a controller, which is only limited by the bandwidth requirement.

Note that the proposed method will not be reducible to a form of singular perturbation: a clear separation in frequency between slow and fast dynamics is not needed and it is possible that a very slow pole is ignored.

3.2.2. The Procedure

Let us start with the original system in state space form:

$$\dot{\underline{x}}(t) = \underline{A}\,\underline{x}(t) + \underline{B}\,\underline{u}(t) \tag{3.1}$$

$$\underline{y}(t) = \underline{C}\,\underline{x}(t) \tag{3.2}$$

where the dimension of the state is n and the dimension of the input and output are the same: $\underline{u},\underline{y} \in R^p$.

The associated transfer function matrix is:

$$\tilde{\underline{G}}(j\ ) = \underline{C}(j\omega\underline{I}-\underline{A})^{-1}\underline{B} \tag{3.3}$$

We shall introduce a model reduction procedure in a number of steps. It will be seen that the method combines elements of previous reduction techniques, with important modifications and from the viewpoint of residue analysis.

1) State aggregation: Assume a linear relationship between the original state $\underline{x}(t)$ and an aggregate state $\underline{z}(t)$:

$$\underline{z}(t) = \underline{K}\,\underline{x}(t) \tag{3.4}$$

the dimension of $\underline{z}$ is r, with $r<n$.

Furthermore, assume that the state $\underline{z}(t)$ has its own dynamic equation:

$$\dot{\underline{z}}(t) = \underline{F}\,\underline{z}(t) + \underline{G}\,\underline{u}(t) \tag{3.5}$$

Substitution of the state aggregation equation (3.4) yields the following relations:

$$\underline{F}\,\underline{K} = \underline{K}\,\underline{A} \tag{3.6a}$$

$$\underline{G} = \underline{K}\,\underline{B} \tag{3.6b}$$

Thus, given a matrix $\underline{K}$, the matrices $\underline{F}$ and $\underline{G}$ can be calculated from the above. This is the state aggregation stage. Appropriate choices of the $\underline{K}$ matrix can accomplish quite general model approximations. The most common method is to choose $\underline{K}$ so as to preserve in the reduced model some selected poles of the original system.

2) Pole Preservation: Let the eigenvalue-eigenvector decomposition of the system $\underline{A}$ matrix be:

$$\underline{A} = \underline{U}\,\underline{\Lambda}\,\underline{U}^{-1} \quad \text{or} \tag{3.7a}$$

$$\underline{\Lambda} = \underline{U}^{-1}\underline{A}\,\underline{U} \tag{3.7b}$$

Consider the case where the eigenvalues of $\underline{A}$, $\lambda_i(\underline{A})$, $(i=1,2,\ldots,n)$ are distinct. Then:

$$\underline{\Lambda} = \text{diag}\{\lambda_i(\underline{A})\} \tag{3.8}$$

and the eigenvector set can be normalized to form a basis for R^n. Write:

$$\underline{U} = [\underline{u}_1, \underline{u}_2, \ldots, \underline{u}_n] \tag{3.9}$$

and

$$\underline{U}^{-1} = \begin{bmatrix} \underline{v}_1^T \\ \underline{v}_2^T \\ \vdots \\ \underline{v}_n^T \end{bmatrix} \tag{3.10}$$

Suppose, it is desired to have the eigenvalues of the reduced model be:

$\{\lambda_{i_1}(\underline{A}),\ldots,\lambda_{i_r}(\underline{A})\}$, a particular subset of the eigenvalue set of $\underline{A}$.

Now define the state aggregation matrix:

$$\underline{K} = (\underline{T})^{-1} \begin{bmatrix} \underline{v}_{ij}^T \\ \vdots \\ \underline{v}_{ir}^T \end{bmatrix} \tag{3.11}$$

where the matrix $\underline{T}$ is block diagonal:

$$\underline{T} = \begin{bmatrix} \underline{T}_1 & & 0 \\ & \underline{T}_2 & \\ & & \ddots \\ 0 & & \underline{T}_j \end{bmatrix} \tag{3.12}$$

(where $\sum^{j} \dim(T_k)=r$).

A block corresponding to a real eigenvalue is just one: $\underline{T}_k=j$. For a pair of complex eigenvalues.

$$\underline{T}_k = \begin{bmatrix} 1/2 & -j/2 \\ 1/2 & j/2 \end{bmatrix} \tag{3.13a}$$

and hence:

$$(\underline{T}^{-1})_k = \begin{bmatrix} 1 & 1 \\ j & -j \end{bmatrix} \tag{3.13b}$$

Fact 3.1: The eigenvalues of $\underline{F}$ are exactly the $\{\lambda_{ij},\ldots,\lambda_{ir}\}$. The matrix $\underline{F}$ is block diagonal:

$$\underline{F} = \begin{bmatrix} \underline{F}_1 & & 0 \\ & \ddots & \\ 0 & & \underline{F}_j \end{bmatrix}$$

where $\underline{F}_k = \lambda_\ell(\underline{A})$ for some λ_ℓ real and $\underline{F}_k = \begin{bmatrix} \mathrm{Re}(\lambda_m) & \mathrm{I}_m(\lambda_m) \\ -\mathrm{Im}(\lambda_m) & \mathrm{Re}(\lambda_m) \end{bmatrix}$ for a complex pair of eigenvalues $\mathrm{Re}(\lambda_m) \pm j\ \mathrm{Im}(\lambda_m)$. Finally, the matrices $\underline{F}$ and $\underline{G}$ are real.

Proof: All parts can be checked easily. Use:

$$\underline{K}^{-1} = [\underline{u}_{ij} \ldots . \underline{u}_{ir}]\ \underline{T} \tag{3.14}$$

the right inverse of $\underline{K}$, to check that:

$\underline{F} = \underline{K}\ \underline{A}\ \underline{K}^{-1}$ is indeed block diagonal and real. Since $\underline{K}$ is real, $\underline{G}$ also is.

Remarks:

1) The case of eigenvalues of higher multiplicity can also be treated by this method (see [5]).

2) So far we have only obtained a state equation. The method has not given us a way of choosing an output equation. This will be done presently, using the point of view of residue analysis.

3) Residue Analysis: For the case of distinct eigenvalues, it is known that the transfer matrix of the system has an additive decomposition given by:

$$\underline{\tilde{G}}(j\omega) = \sum_{i=1}^{n} \frac{\underline{R}_i}{j\omega+\lambda_i} = \sum_{i=1}^{n} \frac{\underline{R}_i/\lambda_i}{1+j\omega/\lambda_i} \qquad (3.15)$$

where $\underline{R}_i = \underline{C}\,\underline{u}_i\,\underline{v}_i^T\,\underline{B}$ are the residue matrices. This form is the equivalent of the partial fraction expansion in scalar systems. Its advantage is that it isolates the frequency-dependent part of the transfer function matrix in the scalar terms $\frac{1}{j\omega+\lambda_i}$. We saw in section 2.3 that the magnitude of a residue matrix provides a measure of how important the contribution of the corresponding pole is in forming the system output vector. Let us examine the terms of the expansion (3.15) from the point of view of approximation.

Isolating the normalized terms $r_1(j\omega) = \frac{1}{1+j\omega/\lambda_i}$ (which all go to one as $\omega \to 0$), let us suppose we have fixed a bandwidth ω_o, over which we want our model to be valid. Figure 3.1 shows three different cases: (i) $|\lambda_i| > \omega_o$; (ii) $|\lambda_i| < \omega_o$, (iii) $|\lambda_i| << \omega_o$.

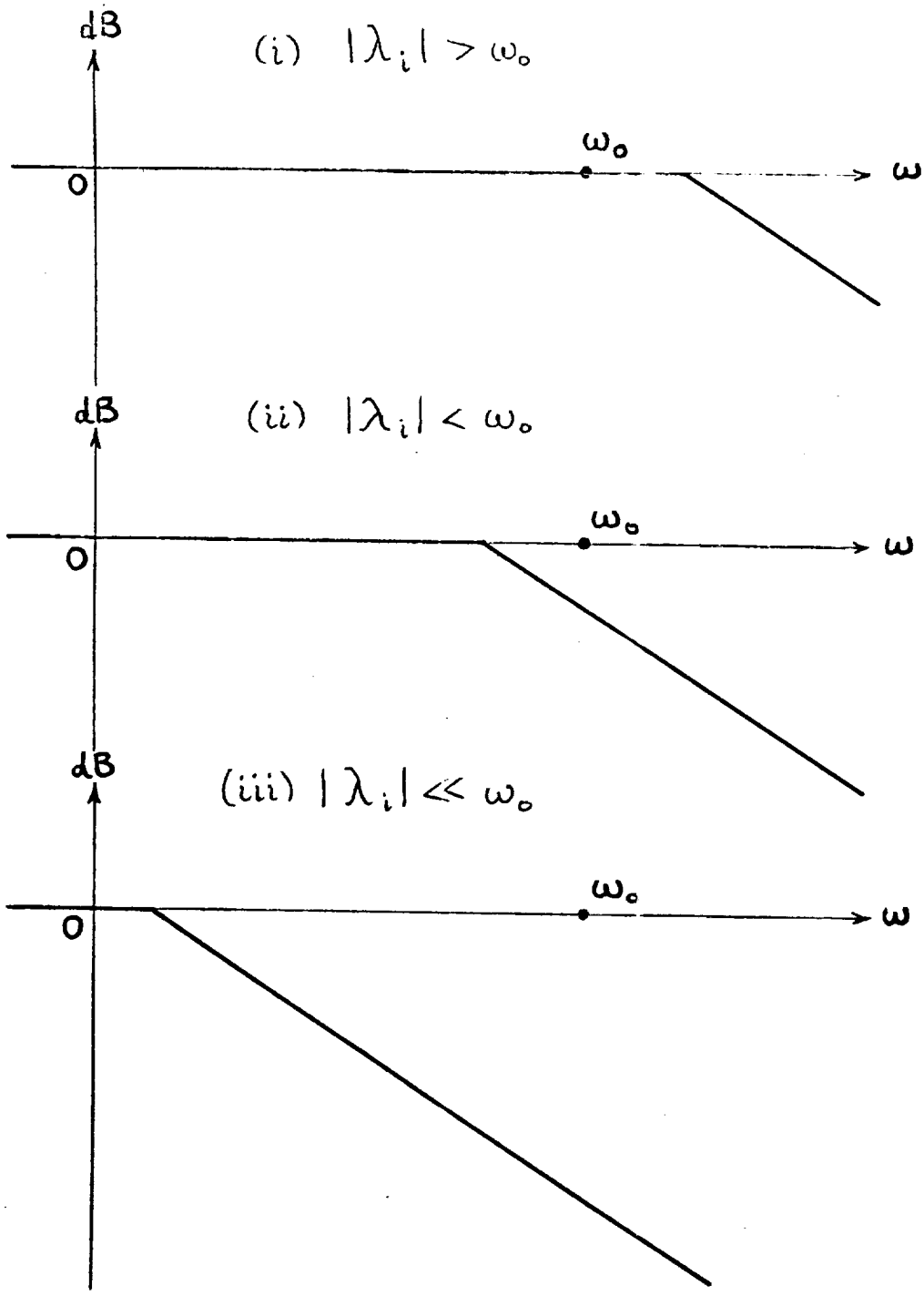

Fig3.1: Bode Plots of $\dfrac{1}{1+jw/\lambda_i} = r_i(jw)$

It is easily seen that in case (i), the residue term will be approximately constant over the bandwidth of interest. This is not the case in Fig. 3.1 (ii), while in Fig. 3.1 (iii) the magnitude has dropped off considerably by the time ω_o is reached.

The above suggest a way of approximating the various terms in (3.15). Terms related to poles which are faster than ω_o can be taken to be constant:

$$\text{(i)} \qquad \frac{\underline{R}_i/\lambda_i}{1+j\omega/\lambda_i} \approx \frac{\underline{R}_i}{\lambda_i}, \quad |\lambda_i| > \omega_o \tag{3.16}$$

Terms on the low side of ω_o should be kept as they are. If, however, a pole is too slow, we may choose to either omit it altogether, or approximate it by an intermediate value

$$\text{(iii)} \qquad \frac{\underline{R}_i/\lambda_i}{1+j\omega/\lambda_i} \approx 0 \quad \text{or} \quad \frac{\underline{R}_i/\lambda_i}{1+j\bar{\omega}/\lambda_i} \tag{3.17}$$

$$\text{where } |\lambda_i| < \bar{\omega} < \omega_o$$

If we keep all terms either as they are or as constant (according to (3.16)) then the advantage is that we preserve the d.c. gain, since

$$\underline{\tilde{G}}(0) = \sum_{i=1}^{n} \frac{\underline{R}_i}{\lambda_i}$$

Otherwise, we are introducing a low-frequency error, which will be small if the residue term is small. Table 3.1 summarizes the options for approximation of the various terms.

TABLE 3.1: Term Approximations

$\lvert\lambda_i\rvert$	$\lVert R_i \rVert / \lvert\lambda_i\rvert$	TERM APPROXIMATION
$\ll \omega_o$	SMALL	0
	LARGE	$r_i(j\omega) R_i / \lambda_i$
NEAR ω_o	SMALL	R_i / λ_i
	LARGE	$r_i(j\omega) R_i / \lambda_i$
$> \omega_o$	ALL VALUES	R_i / λ_i

Let us now pick the option of preserving the d.c. gain. The approximation of the system transfer function is:

$$\underline{G}(j\omega) = \sum_{i=1}^{r} \frac{\underline{R}_i/\lambda_i}{1+j\omega/\lambda_i} + \sum_{i=r+1}^{n} \frac{\underline{R}_i}{\lambda_i} \tag{3.18}$$

Remarks:

1) The problem of choosing the eigenvalues to be present in the reduced model is solved using the residue matrix method.

2) The residue method suggests a convenient way of obtaining an output equation for the approximate model. The way this is done is given in the following fact:

Fact 3.1: The approximate transfer function

$$\underline{G}(j\omega) = \sum_{i=1}^{r} \frac{\underline{R}_i/\lambda_i}{1+j\omega/\lambda_i} + \sum_{i=r+1}^{n} \frac{\underline{R}_i}{\lambda_i}$$

can be realized by the following state-space system of order r:

$$\dot{\underline{z}}(t) = \underline{F}\,\underline{z}(t) + \underline{G}\,\underline{u}(t)$$

$$\underline{y}(t) = \underline{H}\,\underline{z}(t) + \underline{D}\,\underline{u}(t)$$

where the state z(t) is related to the original state by a constant state aggregation matrix:

$$\underline{z}(t) = \underline{K}\,\underline{x}(t)$$

Remarks:

1) This realization procedure is known as the Gilbert diagonal realization procedure [7].

2) There exist reduction methods where the output equation is chosen so as to match a number of moments of the original and the approximate transfer functions (see, for example, the partial realization technique [5]). The difference is that these methods do not include a $\underline{D}$ matrix in the output equation while we do.

Proof: The proof will be constructive. For i=1,...,r, arrange the residue terms in $\tilde{\underline{G}}$ as:

$$\underline{R}_i = \underline{C}\,\underline{u}_i\,\underline{v}_i^T\underline{B} = (\underline{C}\,\underline{u}_i)(\underline{v}_i^T\underline{B})$$

Form: $\underline{H}' = \underline{C}[\underline{u}_1 \ldots \underline{u}_r]$, $\underline{G}' = [\underline{v}_1 \ldots \underline{v}_r]^T\underline{B}$

and $\underline{D} = \sum_{i=r+1}^{n} \frac{\underline{R}_i}{\lambda_i}$.

with $\underline{F}' = \mathrm{diag}\{\lambda_i\}$ we see that $(\underline{F}',\underline{G}',\underline{H}',\underline{D})$ is a (complex) realization i=1,...,r of G. This is because, since $\underline{F}'$ is diagonal, its eigenvectors are just the basis vectors $\underline{e}_i$, i=1,...,r and, therefore, the residue terms of the reduced system are:

$$\underline{H}'\,\underline{e}_i\underline{e}_i^T\underline{G}' = \underline{C}[\underline{u}_1,\ldots,\underline{u}_r]\underline{e}_i\,\underline{e}_i^T[\underline{v}_1 \ldots \underline{v}_r]^T\underline{B} = \underline{C}\,\underline{u}_i\underline{v}_i^T\underline{B} .$$

To finish the proof we need to show that we can get a real realization $(\underline{F},\underline{G},\underline{H},\underline{D})$ for the same $\underline{G}$. This is because the transformation T acts on the state space matrices as:

$$\underline{F} = \underline{T}^{-1}\underline{F}'\underline{T}, \quad \underline{G} = \underline{T}^{-1}\underline{G}, \quad \underline{H} = \underline{H}'\underline{T}$$

so that $\underline{T}$ is a similarity transform and hence the transfer function associated with $(\underline{F}',\underline{G}',\underline{H}'\underline{D})$ is the same as $\underline{G}$. □

3.3 Model Errors

We have posed the model reduction problem as a transfer function approximation problem. One can apply the framework of robustness theory in considering the errors resulting from the approximation stage.

The characterization of error in the robustness framework is the maximum singular value, as a function of frequency, of the error transfer function. It is known (see e.g. [13]) that we can define an additive error, a multiplicative, a subtraction and a division error. Of these, we choose the multiplicative error. The reason is that the multiplicative error is a relative error: it makes sense to talk about a 10% error, for example, while an absolute error is dependent on the units used.

Let $\tilde{\underline{G}}$ and $\underline{G}$ be the true and approximate loop transfer functions. The multiplicative error, $\Delta\underline{G}_{\mu}$ can be defined in one of two ways:

$$\Delta\underline{G}_{\mu 1} = (\tilde{\underline{G}}-\underline{G})\underline{G}^{-1} \tag{3.19}$$

or

$$\Delta\underline{G}_{\mu 2} = \underline{G}^{-1}(\tilde{\underline{G}}-\underline{G}) \tag{3.20}$$

For $\tilde{\underline{G}}$ and $\underline{G}$ as in section 3.2; we have:

$$\Delta\underline{G}_{\mu 1}(j\omega) = \left[\sum_{i=r+1}^{n} \frac{-j\omega}{j\omega+\lambda_i}\underline{R}_i\right]\left[\sum_{i=1}^{r}\frac{\underline{R}_i}{j\omega+\lambda_i} + \sum_{i=r+1}^{n}\frac{\underline{R}_i}{\lambda_i}\right]^{-1}$$

$$= \sum_{i=r+1}^{n} \frac{-j\omega}{j\omega+\lambda_i}\underline{R}_i\underline{G}^{-1}(j\omega) \tag{3.21}$$

$\Delta\underline{G}_{\mu 2}(j\omega)$ is defined similarly.

Now consider Fig. 3.2. It shows a feedback loop where part of the loop transfer function $\tilde{\underline{G}} = \tilde{\underline{G}}_3\tilde{\underline{G}}_2\tilde{\underline{G}}_1$ is approximated, so that $\underline{G} = \tilde{\underline{G}}_3\underline{G}_2\tilde{\underline{G}}_1$.

It is obvious that $\underline{G}_2$ is the general point at which an approximation can be made. Let $\tilde{\underline{G}}_2$ represent the plant and $\tilde{\underline{G}}_1$ and $\tilde{\underline{G}}_3$ the pre- and post-compensators. We are interested in the propagation of the multiplicative error in $\tilde{\underline{G}}_2$ as we add $\tilde{\underline{G}}_1$ and $\tilde{\underline{G}}_3$ to the loop.

Let $c_1(j\omega)$ and $c_3(j\omega)$ be the frequency-dependent condition numbers of $\tilde{\underline{G}}_1(j\omega)$ and $\tilde{\underline{G}}_3(j\omega)$, i.e:

$$c_1(j\omega) = \frac{\sigma_{max}(\tilde{\underline{G}}_1(j\omega))}{\sigma_{min}(\tilde{\underline{G}}_1(j\omega))} \quad \text{and} \quad c_3(j\omega) = \frac{\sigma_{max}(\tilde{\underline{G}}_3(j\omega))}{\sigma_{min}(\tilde{\underline{G}}_3(j\omega))}$$

We then have:

Fact 3.2: For the configuration in Fig. 3.2, let $c_1(j\omega)$ and $c_3(j\omega)$ be the frequency-dependent condition numbers of $\tilde{\underline{G}}_1(j\omega)$ and $\tilde{\underline{G}}_3(j\omega)$. Then, assuming the inverses $\tilde{\underline{G}}_1^{-1}$, $\tilde{\underline{G}}_2^{-1}$, $\underline{G}_2^{-1}$, $\tilde{\underline{G}}_3^{-1}$ exist:

1) $$||\Delta\underline{G}_{\mu 1}(j\omega)||_2 \leq c_3(j\omega)||(\tilde{\underline{G}}_2-\underline{G}_2)\underline{G}_2^{-1}||_2$$

2) $$||\Delta\underline{G}_{\mu 2}(j\omega)||_2 \leq c_1(j\omega)||\underline{G}_2^{-1}(\tilde{\underline{G}}_2-\underline{G}_2)||_2$$

Proof: Easily computed.

$$\Delta\underline{G}_{\mu 1} = (\tilde{\underline{G}}-\underline{G})\underline{G}^{-1} = (\tilde{\underline{G}}_3\tilde{\underline{G}}_2\tilde{\underline{G}}_1-\tilde{\underline{G}}_3\underline{G}_2\tilde{\underline{G}}_1)(\tilde{\underline{G}}_3\underline{G}_2\tilde{\underline{G}}_1)^{-1} =$$

$$= \tilde{\underline{G}}_3(\tilde{\underline{G}}_2-\underline{G}_2)\tilde{\underline{G}}_1\tilde{\underline{G}}_1^{-1}\underline{G}_2^{-1}\tilde{\underline{G}}_3^{-1} = \tilde{\underline{G}}_3(\tilde{\underline{G}}_2-\underline{G}_2)\underline{G}_2^{-1}\tilde{\underline{G}}_3^{-1}$$

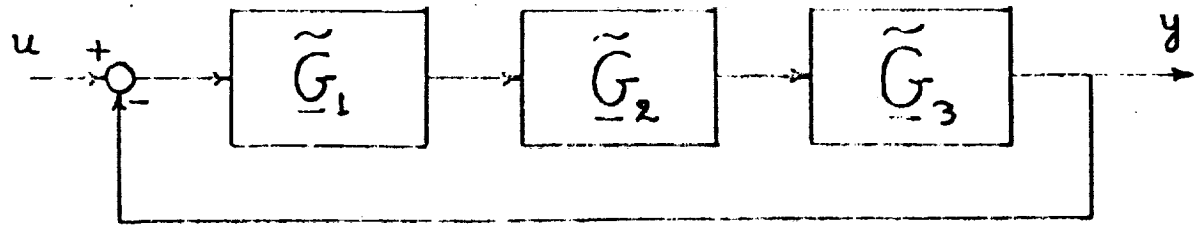

True $\tilde{\underline{G}}$

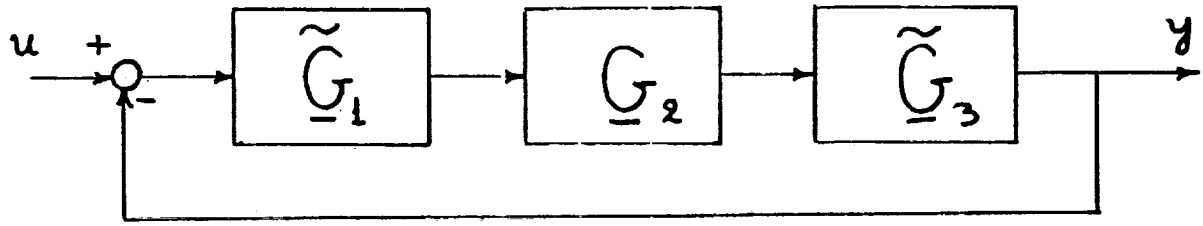

Approximate $\underline{G}$

Fig3.2: General Configuration of Transfer Function Approximation in a Feedback Loop.

Hence: $$||\Delta G_{\mu 1}||_2 = ||\tilde{G}_3(\tilde{G}_2 - G_2)G_2^{-1}\tilde{G}_3^{-1}||_2$$

$$\leq ||\tilde{G}_3||_2 ||(\tilde{G}_2 - G_2)G_2^{-1}||_2 \; ||\tilde{G}_3^{-1}||_2$$

(by sub-multiplicativity of norms)

and since, for the 2-norm:

$$||\tilde{G}_3^{-1}||_2 = \sigma_{max}(\tilde{G}_3^{-1}) = \frac{1}{\sigma_{min}(\tilde{G}_3)}$$

the result i) follows.

2) follows similarly. □

Remarks: 1) As a design guideline, we would like to keep these condition numbers low so as to control the loop error more effectively. 2) If $\tilde{G}_3 = I$ (no post-compensation) then the loop error coincides with the error in G_2. Thus the multiplicative error $\Delta\tilde{G}_{\mu 1}$ is invariant under all pre-compensators. This is the final reason for having chosen this characterization of error.

Some further properties of $\Delta G_{\mu 1}$ are developed in the following two facts. Assume $G^{-1}(j\omega)$ exists, for all ω.

Fact 3.3: The multiplicative error $\Delta G_{\mu 1}$ for the reduced model obtained in section 3.2 goes to zero for $\omega \to 0$ and to $-I$ for $\omega \to \infty$.

(Note that the statement applies to $\Delta G_{\mu 1}$ itself and not to its norm; of course, the singular values will all go to 1 at high frequencies and to 0 for low).

Proof: From (3.21) it is obvious that, as $\omega \to 0$, the elements of $\Delta \underline{G}_{\mu 1}$ will pointwise go to zero, because of the $-j\omega$ factor in the numerator of the scalar multiplying each term.

Thus:

$$\lim_{\omega \to 0} \Delta \underline{G}_{\mu 1}(j\omega) = \lim_{\omega \to 0} \sum_{i=r+1}^{n} \frac{-j\omega}{\lambda_i + j\omega} \underline{R}_i \underline{G}^{-1}(j\omega) = \underline{0}$$

For $\omega \to \infty$, the frequency-dependent terms of $\underline{G}(j\omega)$ will go to zero, leaving:

$$\lim_{\omega \to 0} \Delta \underline{G}_{\mu 1}(j\omega) = \lim_{\omega \to \infty} \left[\sum_{i=r+1}^{n} \frac{-1}{1+\lambda_i/j\omega} \underline{R}_i \right] \left[\sum_{i=r+1}^{n} \frac{\underline{R}_i}{\lambda_i} \right]^{-1} = -I$$

Roughly speaking, because of the presence of the $\underline{D}$ matrix, the multiplicative error at high frequencies is just formed by dividing $\underline{D}$ by itself; also, since we have matched the d.c. gain, the error at low frequency goes to zero.

A handy bound on the error, which is geometric, can be found in the case when:

$$\| \underline{R}_i \underline{G}^{-1}(j\omega') \|_2 \leq 1, \quad \text{for some } \omega'. \quad i=r+1,\ldots,n \tag{3.22}$$

Fact 3.4: Suppose (3.22) is satisfied. Then:

$$\| \Delta \underline{G}_{\mu 1}(j\omega') \|_2 \leq \sum_{i=r+1}^{n} \left| \frac{j\omega'}{j\omega' + \lambda_i} \right| \tag{3.23}$$

Proof: Write:

$$\Delta \underline{G}_{\mu 1}(j\omega) = \sum_{i=r+1}^{n} \frac{-j\omega}{j\omega + \lambda_i} \underline{R}\, \underline{G}^{-1}(j\omega)$$

Then

$$||\Delta G_{\mu 1}(j\omega')||_2 = ||\sum_{i=r+1}^{n} \frac{-j\omega'}{j\omega'+\lambda_i} R_i G^{-1}(j\omega')||_2 \leq$$

$$\leq \sum_{i=r+1}^{n} \left|\frac{j\omega'}{j\omega'+\lambda_i}\right| ||R_i G^{-1}(j\omega')||_2 \leq \sum_{i=r+1}^{n} \left|\frac{j\omega'}{j\omega'+\lambda_i}\right|$$

Remarks: 1) The requirements is roughly that G is bigger at ω' than any of the omitted residue terms. In particular ω' can be the desired bandwidth. In that case Fact 3.4 gives a guide test whether our error is sufficiently small at that bandwidth.

2) Geometrically, the terms $\left|\frac{j\omega'}{j\omega'+\lambda_i}\right|$ measure the ratio of the length of ω' to the vector that $j\omega'$ forms with each omitted pole.

Let us summarize at this point the reduction method proposed. The residue matrix analysis helps in the selection of the dynamics for the approximate model. A state-space system is obtained through state aggregation.

The approximate plant is now considered as a part of a feedback loop. The multiplicative error in the plant approximation is the total error appearing in the loop.

3.4. Model Reduction and Robustness

3.4.1 The Robustness Requirement

In the previous sections, the properties of the multiplicative error coming out of the model reduction method proposed in this chapter were analyzed. This section shows how robust control of such a reduced model is accomplished.

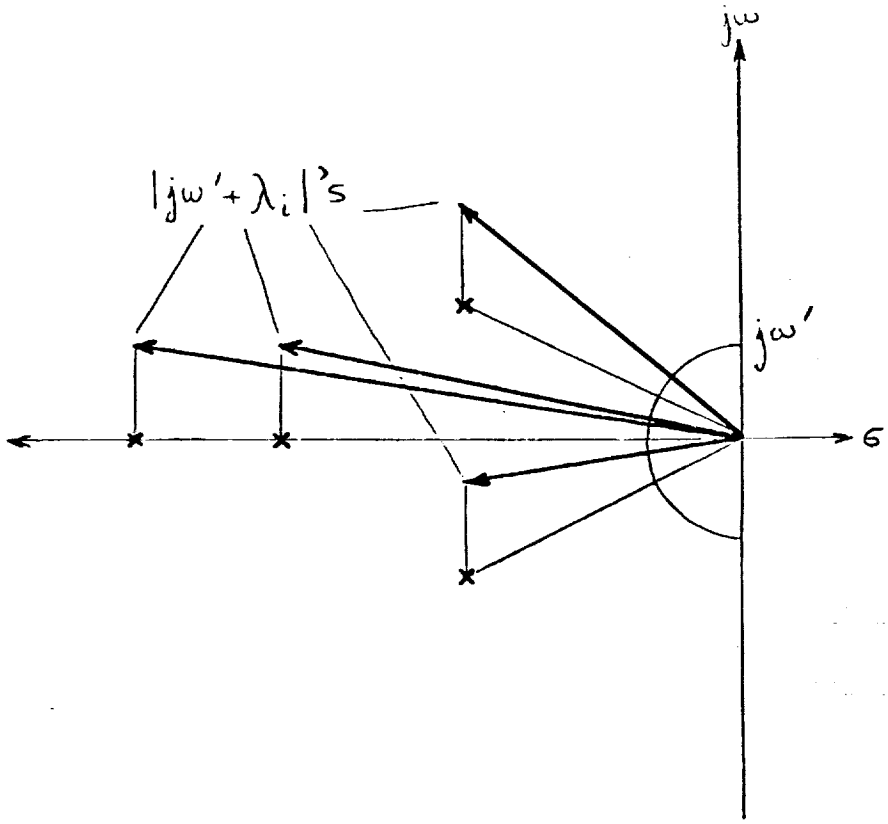

Fig3.3: Geometric Illustration of Fact 3.4:
An Example with 4 omitted poles.

The ideas are not new. They can be found in the recent literature, specifically in Lehtomaki [13] and in [14], [15].

Let $\underline{T}(j\omega)$ be the overall loop transfer function (that includes the reduced model and the designed controller). Let $\Delta\underline{G}_{\mu 1}(j\omega)$ be the multiplicative error as defined in (3.19).

Suppose the system is stable. Then if the reduced model is replaced by the real plant model, the overall system is stable; provided that:

$$\sigma_{min}(\underline{I}+\underline{T}^{-1}(j\omega)) > \sigma_{max}(\Delta\underline{G}_{\mu 1}(j\omega)) \tag{3.24a}$$

for all frequencies ω. The inequality is strict. A stronger inequality (Laub [12]) can be stated:

$$\sigma_{max}[(\underline{I}+\underline{T}^{-1}(j\omega))\Delta\underline{G}_{\mu 1}(j\omega)] < 1 \quad \text{for all } \omega \tag{3.24b}$$

In general, this last inequality is much less conservative than (3.24a). Actually, (3.24a) follows directly from the above, by noting that for any norm the Schwarz inequality is satisfied:

$$||\underline{A}||\,||\underline{B}|| \geq ||\underline{A}\,\underline{B}||$$

and by using the properties of singular values.

What the requirement for robust control is, can now be visualized simply. Fig. 3.4 shows a possible form of the multiplicative error maximum singular value plot. The error maximum singular value goes to zero at low frequencies and to one at high.

The design inverse return transfer function minimum singular value should stay above the error plot, as shown. This is enough to guarantee stability.

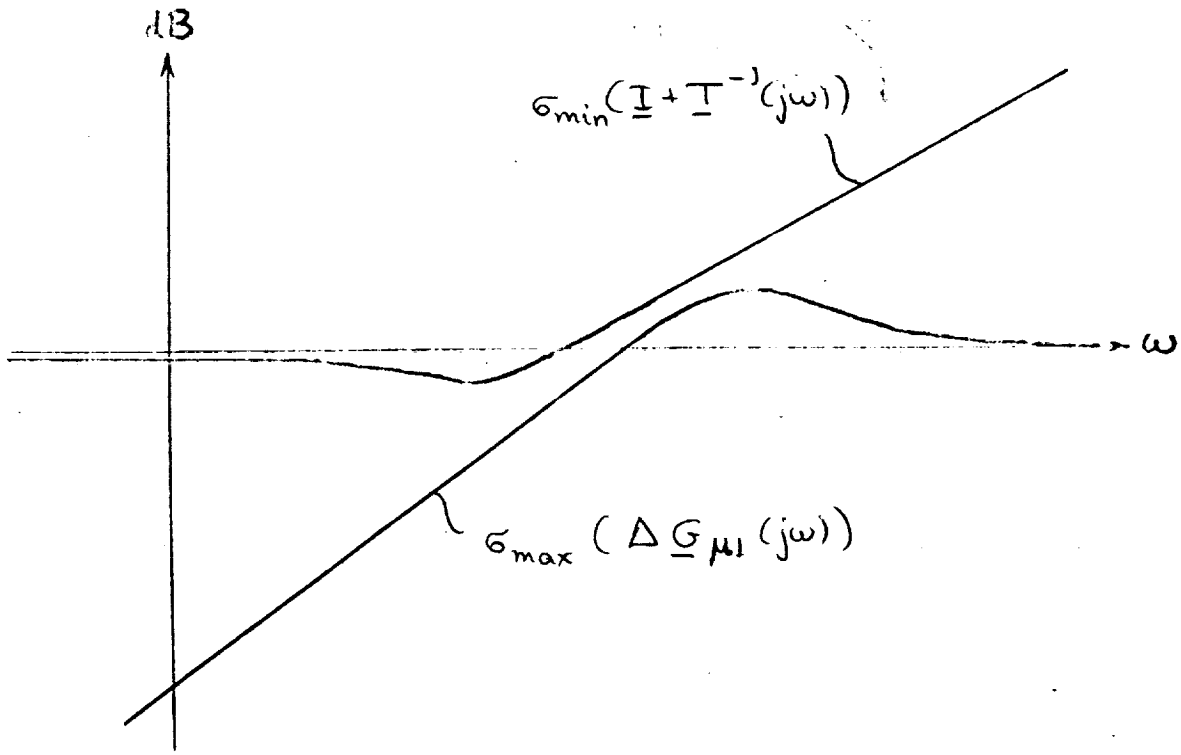

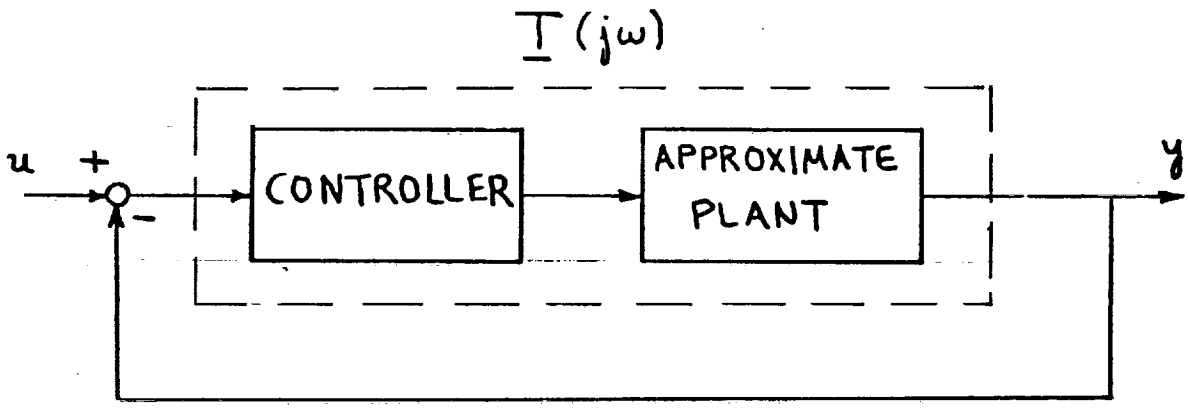

Fig3.4: A Possible Robustness Requirement Plot.

Note that eq. (3.24b) leads to a similar plot, where the requirement is that we stay below the 0dB line. However the error is not shown explicitly and so (3.24a) is preferred.

3.4.2. Scaling and Robustness

A few issues related to scaling will be discussed. Current literature has not treated scaling systematically with the result that the issue is often confused. It will be found that the discussion is also useful with regard to the conservative nature of robustness estimates.

The general framework is given first.

Definition: A scaling transformation of a given linear system is one where the input, output and state vectors are transformed by diagonal matrices with (strictly) positive elements.

If $\underline{u}$, $\underline{y}$, $\underline{x}$ are the original and $\underline{u}_n$, $\underline{y}_n$, $\underline{x}_n$ the transformed vectors, then:

$$\underline{u} = \underline{N}_u \underline{u}_n, \quad \underline{y} = \underline{N}_y \underline{y}_n, \quad \underline{x} = \underline{N}_x \underline{x}_n \tag{3.25}$$

This leads to the following transformations of the system matrices:

$$\begin{aligned} \underline{A}_n &= \underline{N}_x^{-1} \underline{A} \underline{N}_x \\ \underline{B}_n &= \underline{N}_x^{-1} \underline{B} \underline{N}_u \\ \underline{C}_n &= \underline{N}_y^{-1} \underline{C} \underline{N}_x \\ \underline{D}_n &= \underline{N}_y^{-1} \underline{D} \underline{N}_u \end{aligned} \tag{3.26}$$

The state transformation is a special case of a similarity transformation (since $\underline{N}_x$ is non-singular). The others are not. If one considers the transfer function of the system, its transformed form is:

$$\underline{G}_n(s) = \underline{N}_y^{-1}\underline{G}(s)\underline{N}_u \tag{3.27}$$

So that, while $\underline{N}_x$ has cancelled out, $\underline{N}_y$ and $\underline{N}_u$ still appear.

Furthermore, considers the error in going from a true to an approximate model. Then the multiplicative error $\Delta\underline{G}_{\mu 1}$ (as in (3.19)) becomes:

$$(\Delta\underline{G}_{\mu 1})_n = \underline{N}_y^{-1}\ \Delta\underline{G}_{\mu 1}\ \underline{N}_y \tag{3.28a}$$

while $\Delta\underline{G}_{\mu 2}$ (3.20) becomes:

$$(\Delta\underline{G}_{\mu 2})_n = \underline{N}_u^{-1}\ \Delta\underline{G}_{\mu 2}\ \underline{N}_u \quad . \tag{3.28b}$$

Thus $\Delta\underline{G}_{\mu 1}$ is affected by the output scaling and $\Delta\underline{G}_{\mu 2}$ by that of the input.

So far, the discussion was general. The concrete situations in which we face scaling are:

1) Choice of units. Any model of a real system is built according to some set of units for its variables. This choice of units is obviously arbitrary. To express the same model in a different set of units, a rescaling is necessary. The scaling matrices then account for the conversions from one set of units to another.

2) Non-dimensionalizing (or Normalizing) A step further is to make the system equations independent of units. This is accomplished by picking a set of

'nominal' values for the variables of the system and making a scaling transformation using these values in the scaling matrices. The resulting input, output and state variables are then interpreted as fractions of the nominal values. No units appear, so the problem of choosing the units is solved.

One wonders why then all the linear models in the literature are not normalized in this way. The reason is that there is still considerable arbitrariness in the process. To normalize, one needs a set of 'nominal' values. And there is no unique way of picking these values.

An obvious rule is to take these values to be the steady-state values at the operating point at which the linear model has been constructed (Skira and DeHoff in [1]). But this may not be desirable, since the variables of the linear model are incremental (i.e. departures from the steady state). There need be no relation between the steady-state values and the levels at which the variables are used during control.

The overriding question in considering scaling is how arbitrary it is and to what extent scaling changes a model.

Let us take the single-input, single-output case first. There are two remarks to be made:

1) A scaling transformation indeed scales up or down the system transfer function (see (3.27)).

2) The relative error is completely independent of scaling transformations (see (3.28)).

The transfer function of a scalar system is a gain relation: a certain input producing so much output. It is to be expected that this gain depends on the units used to measure the inputs and outputs.

The relative error, however, is not affected by the units used in the SISO case.

The multivariable case differs from the scalar case in that even the relative error depends on the scaling used. It is easy to see from (3.28) that the diagonal elements are not affected. An appropriate normalization, however, can change the off-diagonal elements in such a way as to make the error norm smaller.

And this bring us to the robustness question. To summarize: the robustness requirement translates into an inequality requirement: The designed inverse return difference staying over the error. But we saw that the error is affected by scaling (and hence normalizing) transformations.

The claim is now that the robustness requirements conservativeness can be removed to an extent through an appropriate scaling transformation.

For this, pick a normalizing matrix for the outputs (if $\Delta\underline{G}_{\mu 1}$ is used) $\underline{N}_y$ such that:

$$\sigma_{max}[\underline{N}_y^{-1}\ \Delta\underline{G}_{\mu 1}(j\omega_o)\underline{N}_y] \tag{3.29}$$

is minimized. The frequency ω_o can be near crossover or at an appropriate point of interest.

The minimization indicated above is not easy. Instead one can derive an <u>empirical</u> N_y, based on the behavior of the error near ω_o. Furthermore, since

the diagonal elements are not affected, there is a limit as to what the choice of $\underline{N}_y$ can accomplish. These points will be demonstrated shortly in the discussion of the F100 engine.

The committment to the elements of $\underline{N}_y$ as nominal departures is not binding. The control design may end up using departures that are substantially different. The point is that the robustness requirement is now less conservative.

To summarize, we used the arbitrariness of scaling transformations to get a transformation of the linear model that leads to a better error norm behavior.

3.5 Aggregated F100 model

In this section a reduced model is derived from the augmented F100 linear dynamics. The goal is to derive a model that will allow the control to have a bandwidth of about 15 rad/sec. At the same time, it is desirable to have a simple model. Thus we require the order of the model to be as low as possible, subject to the control bandwidth requirement.

An examination of Table 2.3 shows that at the region of the desired bandwidth are the following poles: $-17.8\pm j4.78$, -18.59 and $-21.3\pm j0.8$. Turning to Table 2.4, the magnitudes of the residue terms corresponding to these poles can be compared. Since the residue corresponding to the pole at -18.59 is small, we choose to omit this pole.

Including everything else up to the complex pair at $-21.3\pm j0.8$ gives a 13th order system. This is now tentatively the reduced model. Table 3.2 lists the included poles. The reduction procedure creates some multivariable zeros

TABLE 3.2: Poles of the Reduced Model.

1)	-0.18204
2)	-0.64773
3)	-1.6810
4)	-1.9057
5)	-2.6184
6), 7)	-6.7148±j1.312
8)	-10
9)	-12
10), 11)	-17.805±j4.7811
12), 13)	-21.327±j0.82083

TABLE 3.3: Zeros of the Reduced Model.

1)	39.023	Non-minimum phase
2)	24.109	
3), 4)	14.663±j17.671	
5), 6)	4.3179±j88.061	
7)	-0.47322	Minimum phase
8)	-0.64886	
9)	-2.1281	
10)	-19.466	
11), 12)	-20.381±j3.1208	
13)	-21.205	

which are, in general different from those of the original system. These zeros are listed in Table 3.3. It is important to note the presence of non-minimum phase (right-half plane) zeros. They, in general, inhibit the robustness recovery process. In our case, they are all outside the desired bandwidth. The smallest zero is at 24.1 rad/sec. It will be seen in the design chapter that robustness recovery is still possible, despite these non-minimum phase zeros.

Having included all the important poles up to the desirable bandwidth does not imply that the multiplicative error will satisfy the bandwidth requirement, as set out in section 3.4. Fig. 3.5 plots the multiplicative error of the tentative reduced model. We see that the maximum singular value of the error crosses over at between 3 and 4 rad/sec. This is not a bandwidth wide enough to base a design upon (given the bandwidth requirement of about 15 rad/sec).

To remedy the situation, we go back to the discussion of scaling in section 3.4.2. By using appropriate nominal values for the departures of the output variables from steady-state (which is equivalent to choosing an N_y matrix), we hope to get a higher crossover frequency.

The minimization of formula (3.29) is not easily done. Instead, the elements of the residue matrices can be examined. In this way, it is possible to come up with good choices for the $\underline{N}_y$ matrix. It is the case that most of the error at high frequencies occurs at elements different than those where the error is concentrated at low-frequencies. Scaling down these elements was possible by choosing an appropriate $\underline{N}_y$ matrix. This improves the characteristics of the error at crossover by pulling the singular values closer. The choice of $\underline{N}_y$ is:

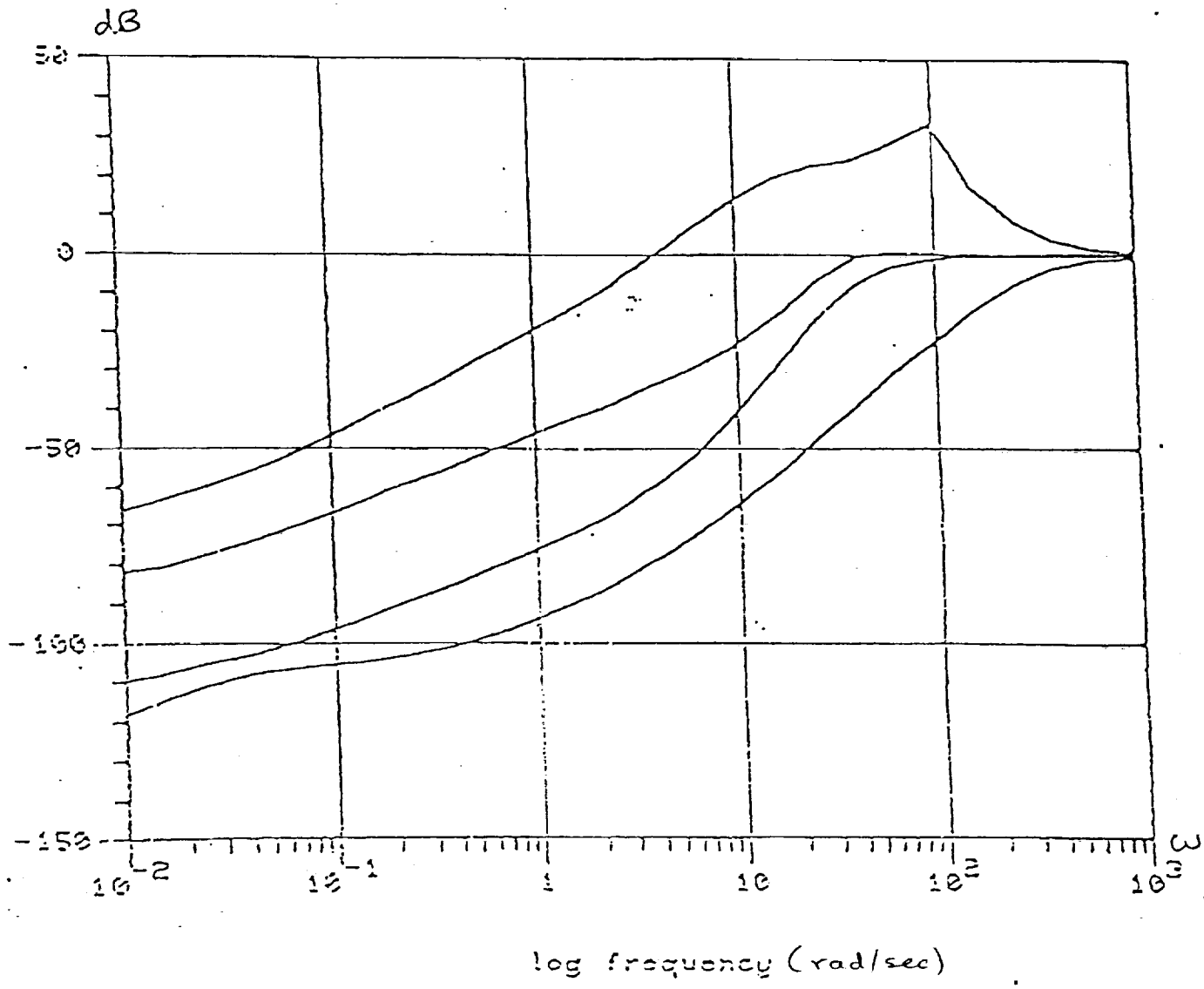

Fig3.5: Unscaled Multiplicative Error; Singular Values vs Frequency.

$$\underline{N}_y = \begin{bmatrix} 10^{-2} & & 0 \\ & 10^{-2} & \\ & & 10^{-1} \\ 0 & & & 1 \end{bmatrix} \tag{3.30}$$

This can be translated into the following nominal departures of the output variables:

$$\begin{aligned} N_1 &= 100 \text{ RPM} \\ N_2 &= 100 \text{ RPM} \\ P_3 &= 10 \text{ PSIA} \\ T_{t4.5} &= 1^\circ \text{ R} \end{aligned} \tag{3.31}$$

Note that only the relative magnitude of these values matters. An overall scaling of $\underline{N}_y$ upwards or downwards as formula (3.28a) indicates, does not affect the multiplicative error.

Figure 3.6 shows that the crossover is now at around 16 rad/sec and is therefore satisfactory.

The reduced model that has been arrive at has these two nice features. First, there is no clear separation of slow (included) and fast (omitted) poles as in the singular perturbation methods [18]. Second, a pole slower than the bandwidth was omitted (since its residue was small), while the reduced model remained satisfactory. The scaled true and approximate transfer functions are plotted in Figs. 3.7 and 3.8.

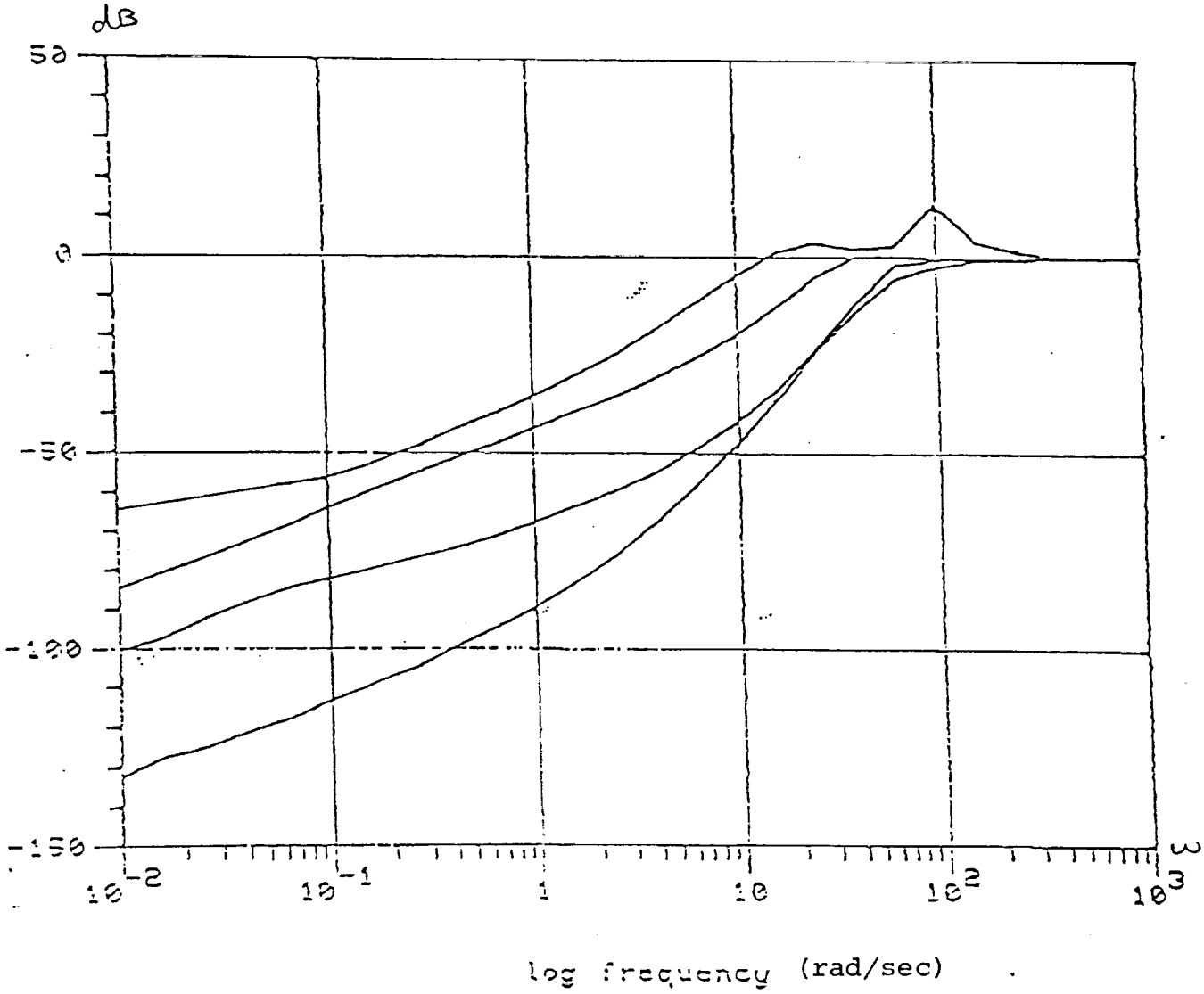

Fig3.6: Scaled Multiplicative Error; Singular Values vs Frequency.

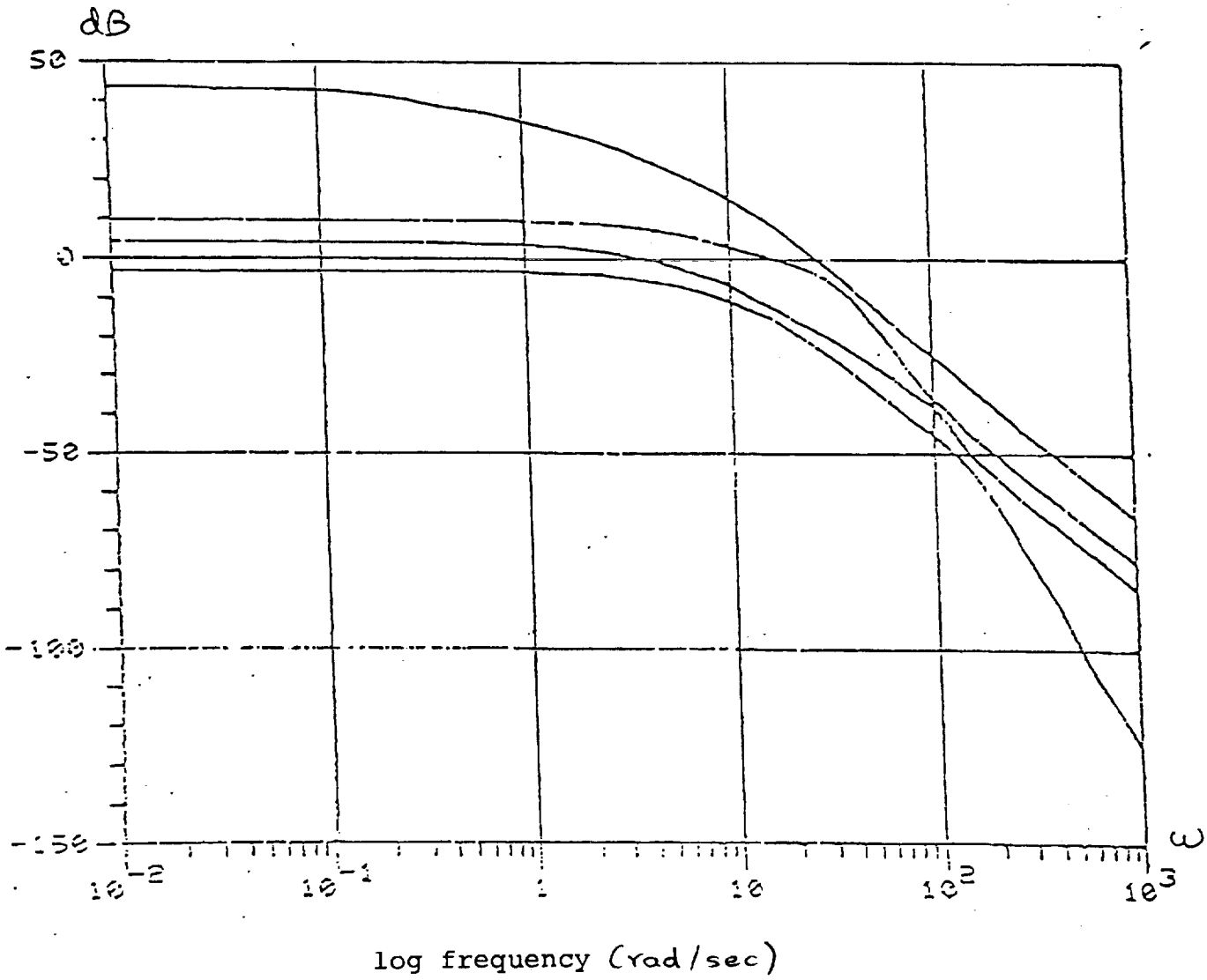

Fig3.7: Full Linear Model Transfer Function (scaled); Singular Values vs Frequency.

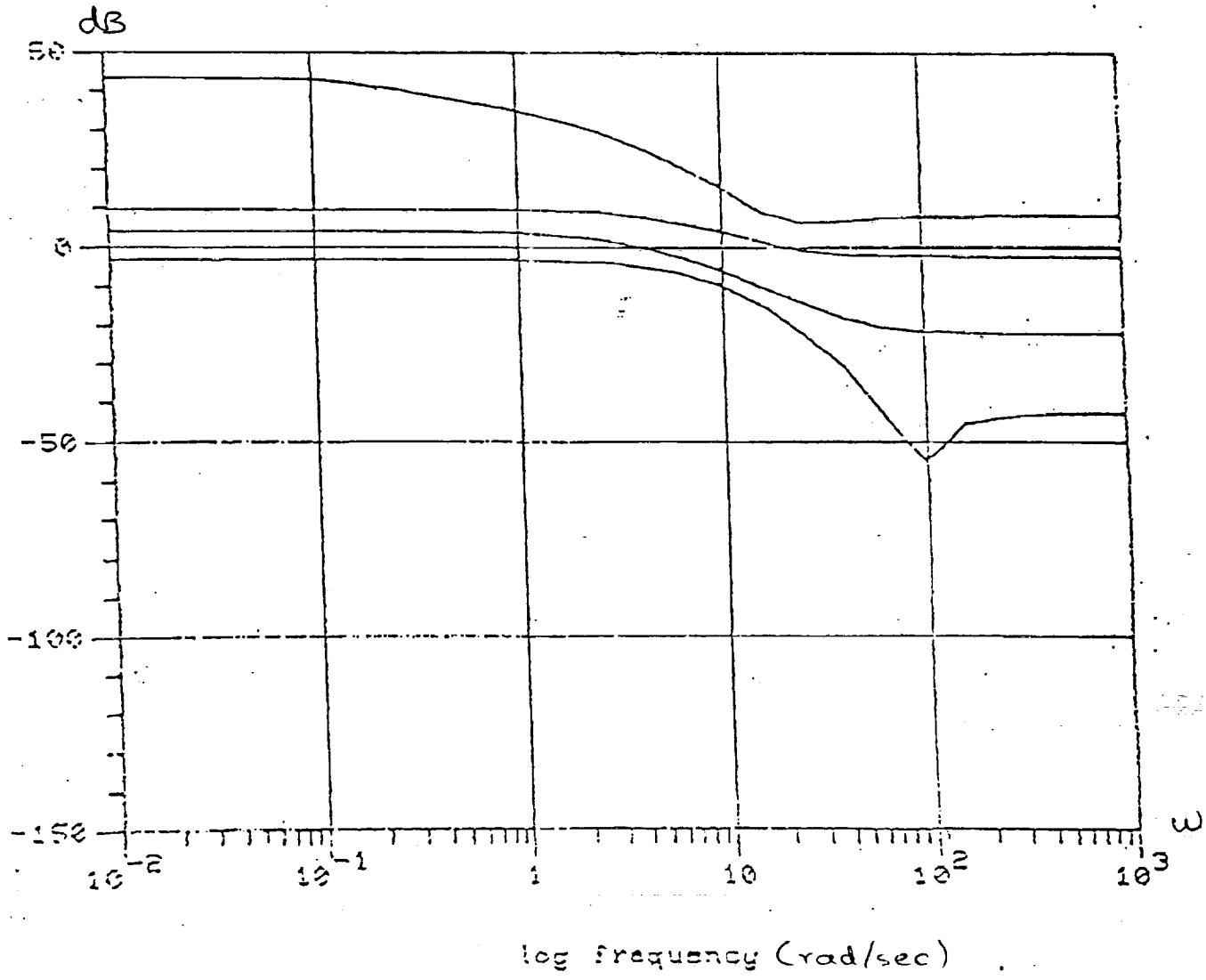

Fig3.8: Reduced Model Transfer Function (scaled); Singular Values vs Frequency.

A further illustration of the second point above is given in Fig. 3.9. The slowest pole (at -0.18) is now left out. It is noticed that, while the high-frequency crossover is not much affected, the error is rather large at low frequencies. Thus, this model could also be used for design, but some design freedom would probably have to be compromised. We do not use this model for design in this work.

3.6 Chapter Summary

The present chapter has introduced ideas that are quite central to the development of the design methodology expounded in this thesis.

Model reduction leads first of all to approximate models whose validity is exactly assessed through the robustness measures. Thus, feedback control can be implemented reliably. The controllers can be made fast, insomuch as the model allows it. Finally, the order of the controller is controlled exactly through the order of the reduced model. This is a particularly attractive feature, as compared to modern algebraic approaches to controller synthesis.

The chapter also included a discussion of another important issue: scaling was examined as a limitation but also as a way of making robustness measures less conservative. The next chapter is the design chapter where the reduced model is used to build a controller.

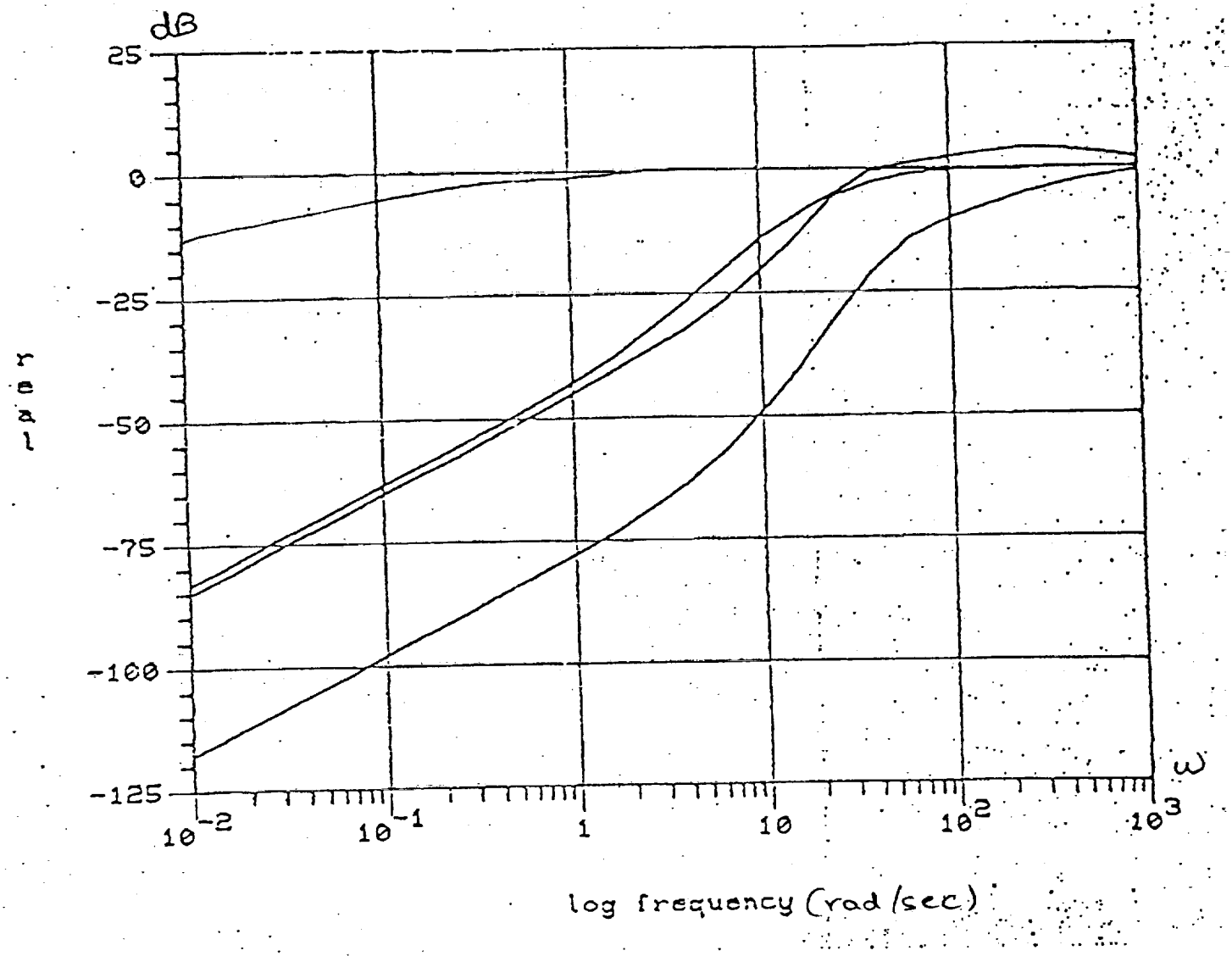

Fig3.9: Multiplicative Error for a 12th-order System (slowest pole at -0.18 omitted); Singular Values vs Frequency.

4. COMPENSATOR DESIGN

4.1 Introduction

We have finally reached the design stage. In this chapter, a compensator will be built that is based on the LQG procedure. The singular-value based loop-shaping approach to LQG will be taken. This means that, having translated the specifications for control into constraints in the frequency-domain it will be attempted to shape the loops of the design (more specifically, the singular values of the overall loop transfer function) so as to meet the specifications. As in traditional control, there are two kinds of specifications: performance requirements and plant uncertainty limitations. In the engine example, for performance we required fast control (all loops crossing over at fast enough frequencies) and zero steady-state error to step changes in the reference signals and output disturbances. The kind of plant uncertainty that will be of concern is that arising from the approximation involved in the model reduction stage.

Section 2 gives an overview of the LQG procedure. Section 3 details the steps of the methodology, which is then applied in Section 4 to the engine example. The robustness recovery stage is described in Section 5. In Section 6 we make sure the specifications have been met.

4.2. A Summary of the LQG Procedure

4.2.1 Preliminary Considerations

In this section a brief summary of the Linear-Quadratic-Gaussian methodology is given. This will, first of all, serve the purpose of fixing the notation.

A more important reason is that we wish to emphasize the modern singular-value loop-shaping perspective of Stein [19],[20]. We thus need a selective exposition geared to that point of view. Finally, we derive some new results which supplement the Stein method. They refer mainly to the connections between the state-space, mathematical structure of the LQG method and the resultant frequency-domain characteristics. This is in keeping with the general philosophy of this thesis which seeks to make maximum use of engineering practice in the frequency domain. Standard references for most of the results in this section are [10], [19].

The LQG procedure is a mathematically elegant method of choosing a stable multivariable controller for a given state-space system. Substantial freedom exists for the designer to pick the parameters of the design. This is more of a disadvantage, since there exist no reliable ways of directly affecting the controller structure through choice of parameters using a purely optimization-based philosophy. One objective of the present work is precisely to expand the possibilities of doing this. In particular, we shall derive ways of controlling both the bandwidth of a controller and its behavior near crossover. More generally we shall get a handle on the spread of the singular values at particular frequency ranges. It is obvious that the above are loop-shaping tools of considerable usefulness.

4.2.2 The LQG Procedure and Loop Transfer Recovery

Start with a state-space description that includes state and observation noises $\underline{\xi}$ and $\underline{\eta}$ that are white.

$$\dot{\underline{x}}(t) = \underline{A}\,\underline{x}(t) + \underline{B}\,\underline{u}(t) + \underline{\Gamma}\,\underline{\xi}(t) \tag{4.1a}$$

$$\underline{y}(t) = \underline{C}\,\underline{x}(t) + \underline{\eta}(t) \tag{4.1b}$$

The intensity matrices of $\underline{\xi}$ and $\underline{\eta}$ are $\underline{I}$ and $\underline{N}$ respectively. Because $\underline{\xi}$ enters the system via $\underline{\Gamma}$, there is no loss in generality in assuming an identity intensity matrix for it.

The LQG compensator for the system (4.1) includes a Kalman filter as a state estimates and the constant LQ gains $\underline{K}_c$. The configuration of the controller is shown in Fig. 4.1. The state estimator dynamics are:

$$\dot{\hat{\underline{x}}}(t) = \underline{A}\,\hat{\underline{x}}(t) + \underline{B}\,\underline{u}(t) + \underline{K}_f(\underline{y}(t)-\underline{C}\,\hat{\underline{x}}(t)) \tag{4.2}$$

and the feedback law is:

$$\underline{u}(t) = -\underline{K}_c\hat{\underline{x}}(t) \tag{4.3}$$

The gain matrices $\underline{K}_c$, $\underline{K}_f$ are given by:

$$\underline{K}_c = \underline{R}^{-1}\underline{B}^T\underline{P} \tag{4.4}$$

$$\underline{K}_f = \underline{\Sigma}\,\underline{C}^T\underline{N}^{-1} \tag{4.5}$$

where $\underline{P}$ and $\underline{\Sigma}$ solve the algebraic Riccati equations:

Controller Algebraic Riccati equation:

$$\text{(CARE):}\quad \underline{A}^T\underline{P} + \underline{P}\,\underline{A} + \underline{Q} - \underline{P}\,\underline{B}\,\underline{R}^{-1}\underline{B}^T\underline{P} = 0 \tag{4.6}$$

Filter Algebraic Riccati equation:

$$\text{(FARE):}\quad \underline{A}\,\underline{\Sigma} + \underline{\Sigma}\,\underline{A}^T + \underline{\Gamma}\,\underline{\Gamma}^T - \underline{\Sigma}\,\underline{C}^T\underline{N}^{-1}\underline{C}\,\underline{\Sigma} = 0 \tag{4.7}$$

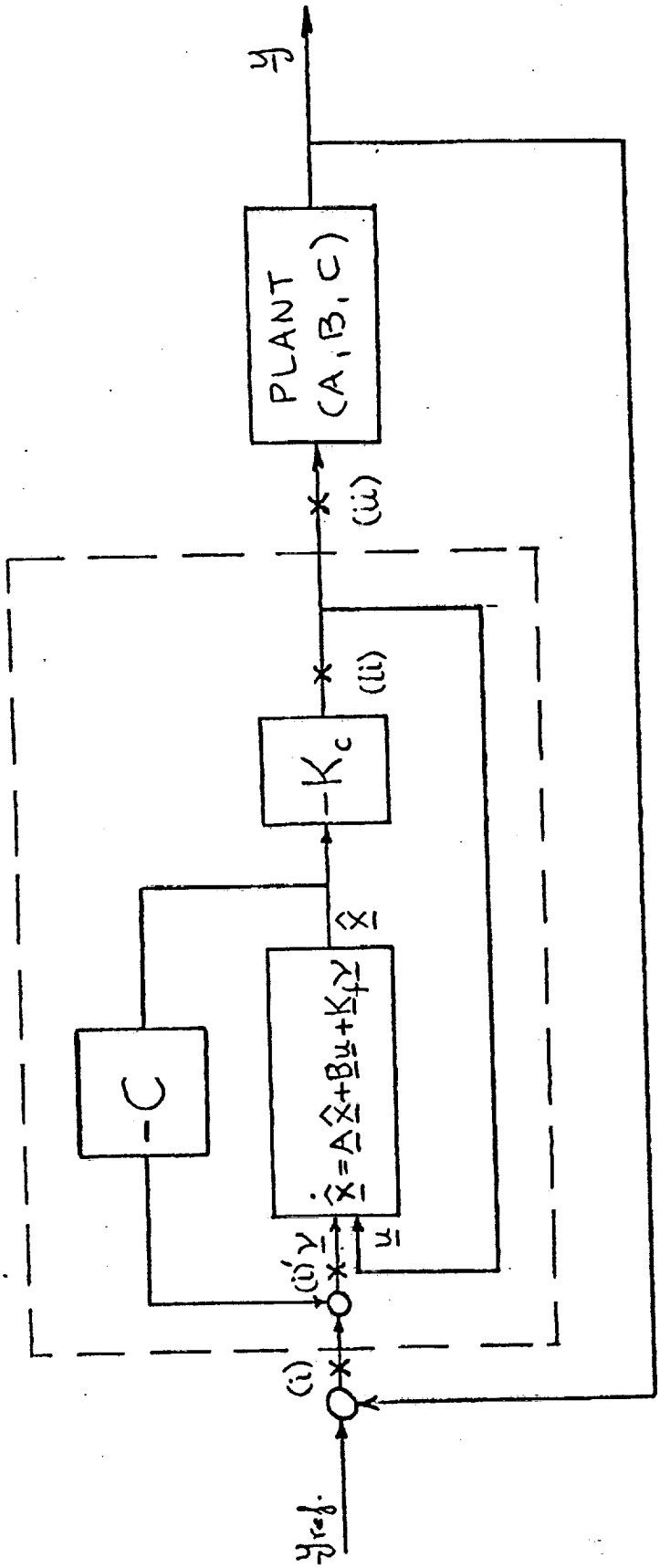

Fig4.1: Structure of the LQG Controller.

The resulting feedback loop (as shown in Fig. 4.1) is stable. Its poles are the eigenvalues of $\underline{A}-\underline{K}_f\underline{C}$ and of $\underline{A}-\underline{B}\ \underline{K}_c$.

In the absence of specific noise data or when the noise sources are not important in the system (as is the case for the engine), there is considerable freedom in selecting the noise statistics. In fact, one can use $\underline{\Gamma}$ and $\underline{N}$ directly as design parameters, together with $\underline{Q}$ and $\underline{R}$.

Robustification:

Now it is shown (see e.g. [21]), that the loop transfer functions (LTF) at points (i)' and (ii)' in the loop (Fig. 4.1) are particularly simple:

$$\text{LTF at (i)':} \qquad \underline{C}\ \underline{\phi}(j\omega)\ \underline{K}_f = \underline{G}_f(j\omega) \tag{4.8a}$$

$$\text{LTF at (ii)':} \qquad \underline{K}_c\ \underline{\phi}(j\omega)\ \underline{B} = \underline{G}_c(j\omega) \tag{4.8b}$$

(where $\underline{\phi}(j\omega) = (j\omega\underline{I}-\underline{A})^{-1}$)

At the physically meaningful points (i) and (ii), however, the loop transfer functions are more complex. The LTF recovery results (due to Kwakemaak [9],[10] and Stein [21]) given a way of recovering the desirable loop transfer functions $\underline{G}_f$ and $\underline{G}_c$ at these real points (i) and (ii).

In the engine example, point (ii) correspond to the entry point to the integrators and not to the input of the plant. Thus, point (ii) is not a meaningful point in our case. We shall limit our considerations to point (i).

The version of the Kwakernaak recovery results that we shall use states that, choosing the LQ parameters as follows:

$$\underline{R} = \underline{I} \tag{4.9a}$$

$$\underline{Q} = \underline{H}^T\underline{H}, \quad \text{where} \quad \underline{H} = q\underline{C} \tag{4.9b}$$

and letting $q \to \infty$, the loop transfer function at point (i) will approach $\underline{G}_f(j\omega)$, pointwise:

$$\underline{C}\,\underline{\phi}(j\omega)\underline{B}\,\underline{K}_c[\underline{\phi}^{-1}(j\omega)+\underline{B}\,\underline{K}_c+\underline{K}_f\underline{C}]^{-1}\underline{K}_f \to \underline{C}\,\underline{\phi}(j\omega)\underline{K}_f \tag{4.10}$$

under the assumption that there are no non-minimum phase zeros of the plant. If there are any, the experience has been that the recovery procedure still works, but the convergence breaks down near the frequencies where the zeros are. No theoretical result that completes the picture exists yet.

Kalman Equalities-Loop Shaping

The reason in doing loop transfer function recovery is that the transfer function $\underline{G}_f$ (or $\underline{G}_c$) is easier to shape. This will be developed in the next section The basic instruments for shaping the loops are the Kalman equalities, derived from the algebraic Riccati equations (4.6) and (4.7).

LQ Kalman Equalities:

Direct: $$[\underline{I}+\underline{G}_c(j\omega)]^*\ \underline{R}[\underline{I}+\underline{G}_c(j\omega)] = \underline{R} + \underline{B}^T\underline{\phi}^*(j\omega)\underline{Q}\,\underline{\phi}(j\omega)\underline{B} \tag{4.11}$$

Inverse: $$[\underline{I}+\underline{G}_c^{-1}(j\omega)]^*\ \underline{R}[\underline{I}+\underline{G}_c^{-1}(j\omega)] = (\underline{G}_c^{-1}(j\omega))^*\underline{R}\,\underline{G}_c^{-1}(j\omega)+((\underline{K}_c)_R^{-1})^T\underline{Q}(\underline{K}_c)_R^{-1} \tag{4.12}$$

KF Kalman Equalities:

$$\text{Direct:} \quad [\underline{I}+\underline{G}_f(j\omega)]\underline{N}[\underline{I}+\underline{G}_f(j\omega)]^* = \underline{N} + (\underline{C}\ \underline{\phi}(j\omega)\underline{\Gamma})(\underline{C}\ \underline{\phi}(j\omega)\underline{\Gamma})^* \tag{4.13}$$

$$\text{Inverse:} \quad [\underline{I}+\underline{G}_f^{-1}(j\omega)]\underline{N}[\underline{I}+\underline{G}_f^{-1}(j\omega)]^* = \underline{G}_f^{-1}(j\omega)\underline{N}(\underline{G}_f^{-1}(j\omega))^* + (\underline{K}_f)_L^{-1}\underline{\Gamma}\ \underline{\Gamma}^T((\underline{K}_f)_L^{-1})^T \tag{4.14}$$

where * denotes the hermitian transpose and $(\underline{K}_c)_R^{-1}$ and $(\underline{K}_f)_L^{-1}$ are the right- and left inverse of $\underline{K}_c$ and $\underline{K}_f$, which exist if and only if $\underline{B}$ and $\underline{C}$ have full rank.

Formulae (4.12) and (4.14) are proved in Appendix B. Some well-known robustness properties follow from these relationships, for the case where $\underline{R} = \rho\underline{I}$ and $\underline{N} = \rho\underline{I}$.

Robustness Properties:

1) $\sigma_{min}[\underline{I}+\underline{G}_c(j\omega)] \geq 1$

2) $\sigma_{min}[\underline{I}+\underline{G}_c^{-1}(j\omega)] \geq 1/2$

3) $\sigma_{min}[\underline{I}+\underline{G}_f(j\omega)] \geq 1$ (4.15)

4) $\sigma_{min}[\underline{I}+\underline{G}_f^{-1}(j\omega)] \geq 1/2$ (4.16)

for all ω.

Properties (2) and (4) are proved in Appendix B. Properties (1) and (3) have been known for a long time.

4.3 Design Methodology

The set-up for control is shown in Fig. 4.2. The feedback loop is composed of the reduced model augmented by the integrators and the LQG controller. The overall compensator $\underline{K}(s)$ thus include the integrators and the LQG controller. For the purposes of robustness it is required that:

$$\text{For all } \omega, \quad \sigma_{max}(\Delta \underline{G}_{\mu l}(j\omega)) < \sigma_{min}[\underline{I}+(\underline{G}(j\omega)\underline{K}(j\omega))^{-1}] \tag{4.17}$$

The steps of the design procedure will be:

1) Design a Kalman filter transfer function, $\underline{G}_f$, that satisfies the robustness requirement and meets the design specifications (good crossover behavior and zero steady-state error on steps).

2) Recover $\underline{G}_f$ approximately by design of the LQ regulator. At this stage, one can only hope that the non-minimum phase zeros will not cause any trouble. Push the recovery sufficiently so that the robustness requirements and design specifications are still met. If not, go back to the first step and modify the Kalman filter appropriately.

Shaping the Kalman filter loop

The design parameters of the Kalman filter are the matrices $\underline{\Gamma}$ and $\underline{N}$. Note that the column dimension of $\underline{\Gamma}$ is arbitrary.

Rewrite the Kalman equality (4.13) for $\underline{N} = \mu \underline{I}$.

$$[\underline{I}+\underline{G}_f(j\omega)][\underline{I}+\underline{G}_f(j\omega)]^* = \underline{I}+\frac{1}{\mu}(\underline{C}\,\underline{\phi}(j\omega)\underline{\Gamma})(\underline{C}\,\underline{\phi}(j\omega)\underline{\Gamma})^*$$

At low frequencies, because of the integrators present in the loop, we can expect $\underline{G}_f(j\omega)$ to be large. In this case it easily follows (Stein [19]) that:

$$\text{For all} \quad \forall i: \sigma_i[\underline{C}\,\underline{\phi}(j\omega)\underline{K}_f] \approx \sigma_i[\underline{C}\,\underline{\phi}(j\omega)\underline{\Gamma}]/\sqrt{\mu} \tag{4.18}$$

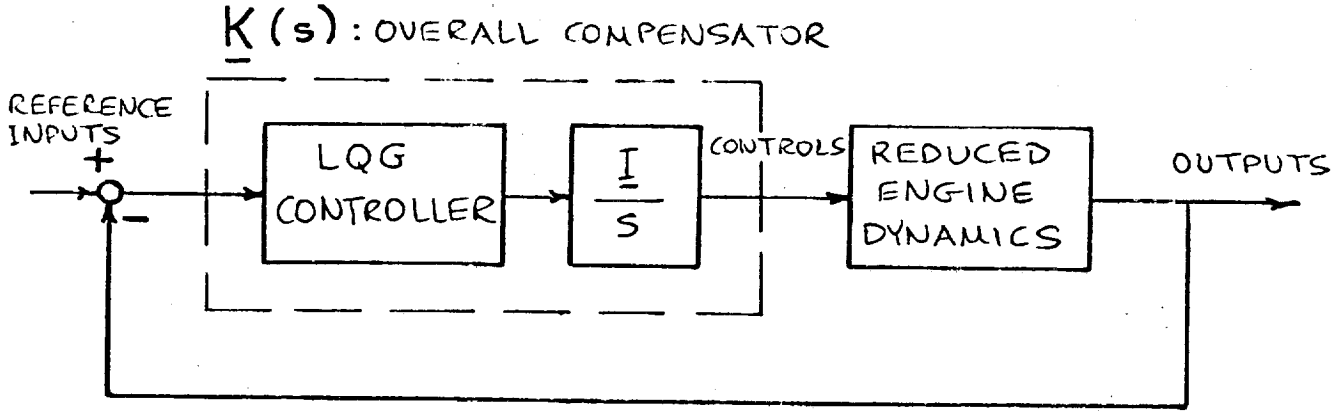

Fig4.2: LQG-based Engine Control Setup.

This is a most useful form. It allows us considerable freedom in shaping the low-frequency end of $\underline{G}_f(j\omega)$. By choosing an appropriate $\underline{\Gamma}$ matrix, we can control the spread of the singular values. Then the choice of μ controls the gain of the loop.

A good choice for $\underline{\Gamma}$ is such as to make $\underline{C}\,\underline{\phi}(j\omega)\underline{\Gamma}\approx\underline{I}$ at low frequencies. For our problem, the integrator-augmented state-space system is:

$$\underline{A} = \begin{bmatrix} \underline{0} & \underline{0} \\ \underline{G} & \underline{F} \end{bmatrix}, \quad \underline{B} = \begin{bmatrix} \underline{I} \\ 0 \end{bmatrix}, \quad \begin{bmatrix} \underline{C} = \underline{D} & \underline{H} \end{bmatrix} \tag{4.19}$$

where $(\underline{F},\underline{G},\underline{H},\underline{D})$ form the reduced model. Choosing

$$\underline{\Gamma} = \begin{bmatrix} \underline{G}(0)^{-1} \\ \underline{0} \end{bmatrix}$$

it is easy to check that:

$$\underline{C}\,\underline{\phi}(j\omega)\underline{\Gamma} = \frac{1}{j\omega}\,\left[\underline{H}(j\omega\underline{I}-\underline{F})^{-1}\underline{G} + \underline{D}\right]\underline{G}(0)^{-1} \tag{4.20}$$

so that, at low frequencies:

$$\underline{C}\,\underline{\phi}(j\omega)\underline{\Gamma} \approx \frac{1}{j\omega}\,\underline{I} \quad . \tag{4.21}$$

Thus $\underline{C}\,\underline{\phi}\,\underline{\Gamma}$ behaves like $\frac{I}{j\omega}$ and we have managed to pull together the singular values of $\underline{G}_f$.

The parameter μ can now be used to control the speed of the loop. A high μ means a slow loop and a small μ gives a faster loop.

If the singular values do not spread out too much as the frequency increases this low-frequency pulling may be enough to give a well-behaved crossover pattern (i.e. all singular values crossing over close to each other). If not, then we may need to sacrifice the low-frequency pulling by using a diagonal $\underline{N}$: $\underline{N}=\text{diag}\{n_i\}$. By adjusting the relative magnitudes of the n_i, one can better control the crossover characteristics of the various singular values.

Note that if instead, we had picked:

$$\underline{\Gamma} = \begin{bmatrix} \underline{D}^{-1} \\ 0 \end{bmatrix}$$

that would have accomplished a pulling of the singular values of $\underline{C}\,\underline{\phi}\,\underline{\Gamma}$ at high-frequencies. However, there is no guarantee that:

$$\sigma_i(\underline{G}_f) \simeq \sigma_i(\underline{C}\,\underline{\phi}\,\underline{\Gamma})$$

since it is not true that $\underline{G}_f$ will be large at high frequencies.

4.4 The Design Sequence

It is time to turn to the F100 engine example and apply the loop-shaping tools discussed so far.

The design model is the 13th-order scaled reduced model derived in chapter 3. To see in what direction the control should be applied, the open loop transfer

function of the scaled reduced model, augmented by the integrators, is plotted in Fig. 4.3. It is noticed that the singular values have a substantial spread (about 30 dB near crossover) and thus the crossover pattern is not satisfactory. At low frequencies, the integrators take over and the singular values all behave like $\frac{1}{s}$. Similarly, at high frequencies, the impract of the $\underline{D}$ matrix of the reduced model is not present; the singular values roll-off at the rate of 20dB decade, due to the effect of the integration. (The reader should compare Fig. 4.3 with Fig. 3.8).

We have two options: try pinching the singular value loops at low or high frequencies. To see how the $\underline{C}\,\underline{\phi}\,\underline{\Gamma}$ loops look like, we plot in Figs. 4.4 and 4.5 the transfer function $\underline{C}\,\underline{\phi}\,\underline{\Gamma}$ for the two choices of $\underline{\Gamma}$:

$$\underline{\Gamma} = \begin{bmatrix} \underline{G}(0)^{-1} \\ \underline{0} \end{bmatrix} \quad \text{and} \quad \underline{\Gamma} = \begin{bmatrix} \underline{D}^{-1} \\ \underline{0} \end{bmatrix}$$

Compared to Fig. 4.3, these transfer functions are essentially rescaled versions of the original transfer function. They differ only in the fact that the $\underline{B}$ matrix, $\begin{bmatrix} \underline{I} \\ 0 \end{bmatrix}$, (see (4.19)) is replaced by a $\underline{\Gamma}$ matrix, given by one of the above two versions.

It is clear that the alignment of the singular values is effective in both cases. However, when the Kalman filter gains $\underline{K}_f$ are designed for these choices of $\underline{\Gamma}$ (with $\underline{N}=\underline{I}$) and $\underline{G}_f(j\omega)$ is plotted (Figs. 4.6,4.7) the difference is apparent.

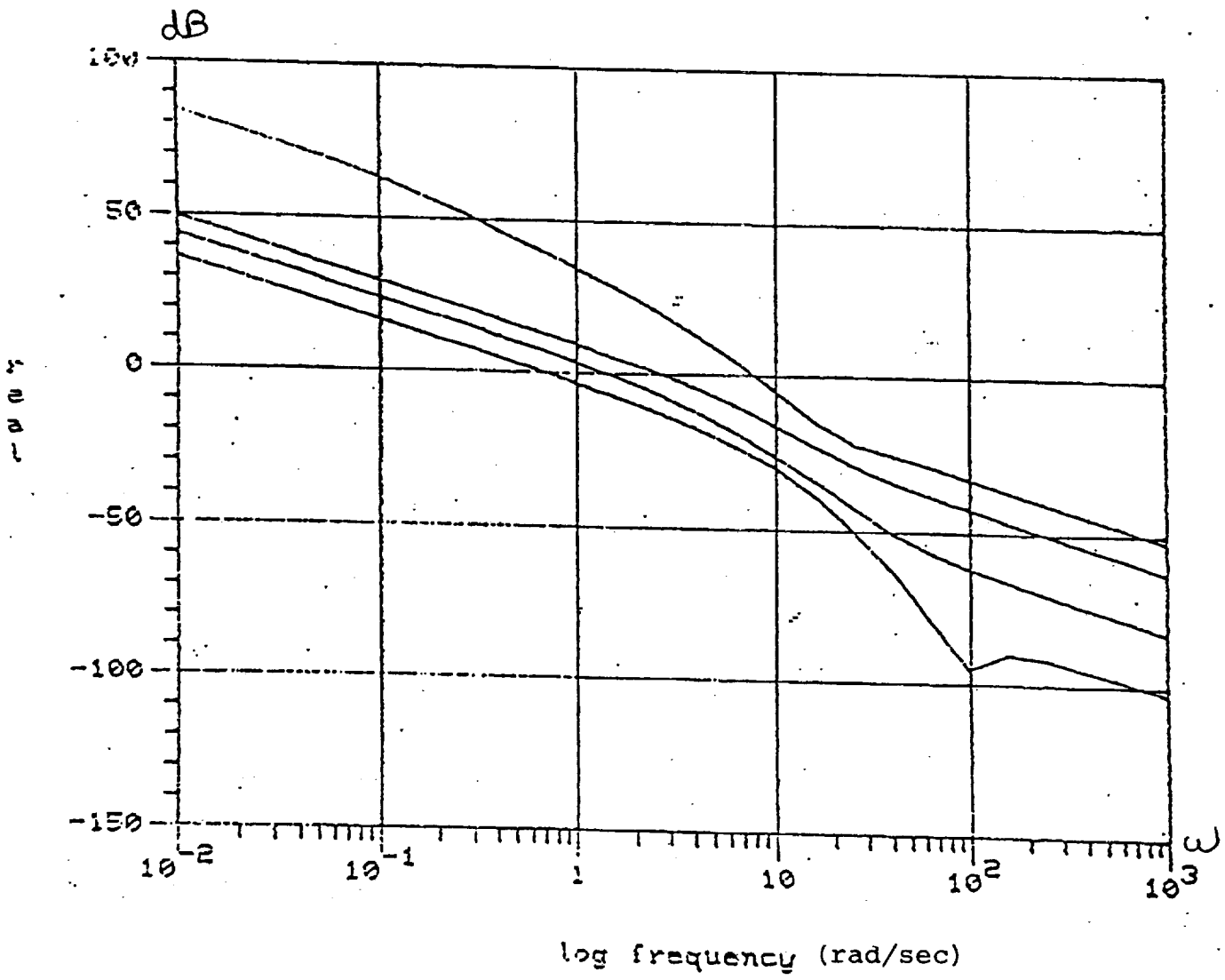

Fig4.3: The Scaled Reduced Model with Integrators; Singular Values vs Frequency.

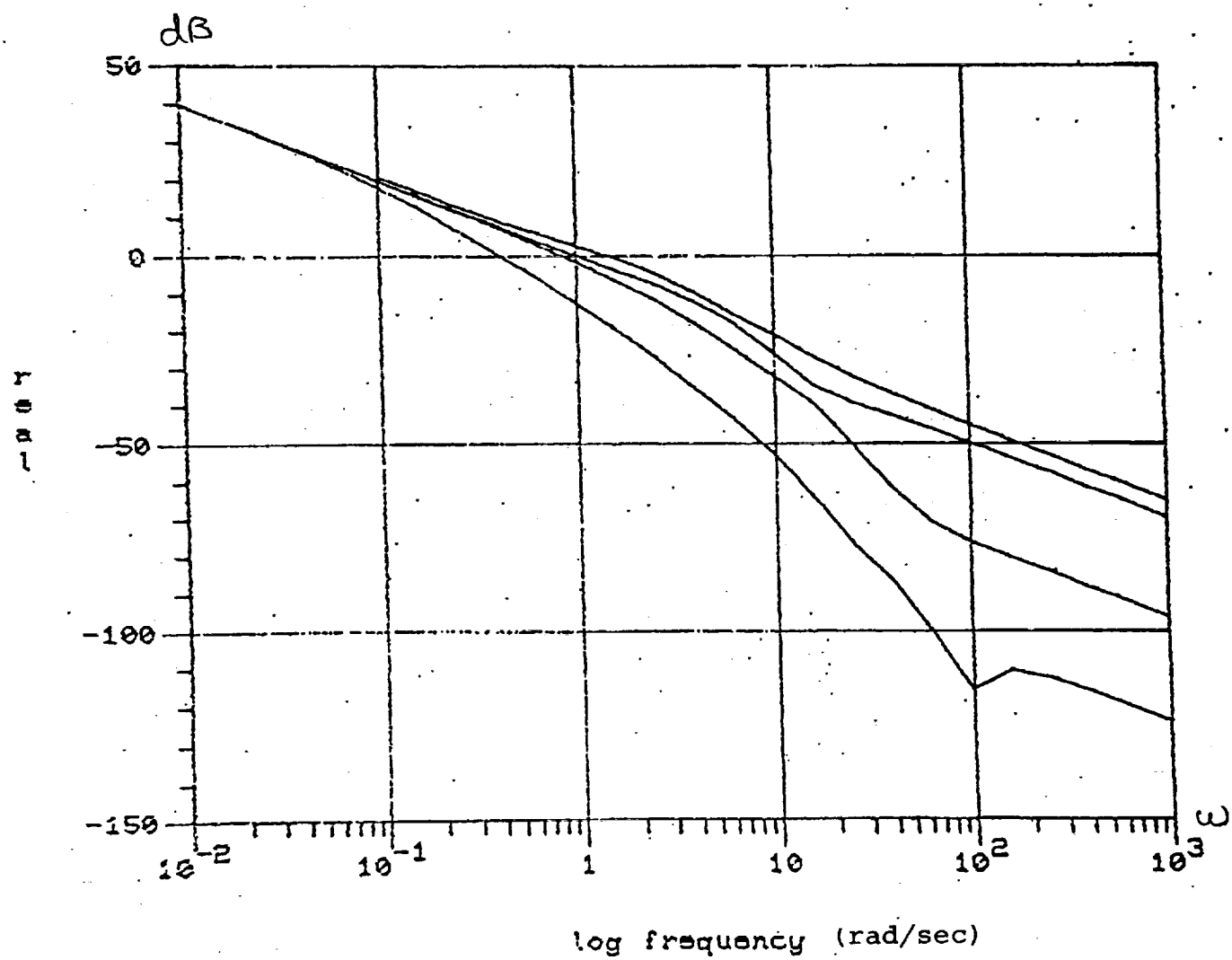

Fig4.4: $\underline{C}\underline{\Phi}(jw)\underline{\Gamma}$ for $\underline{\Gamma} = \begin{bmatrix} \underline{G}(o)^{-1} \\ \underline{O} \end{bmatrix}$;

Singular Values vs Frequency.

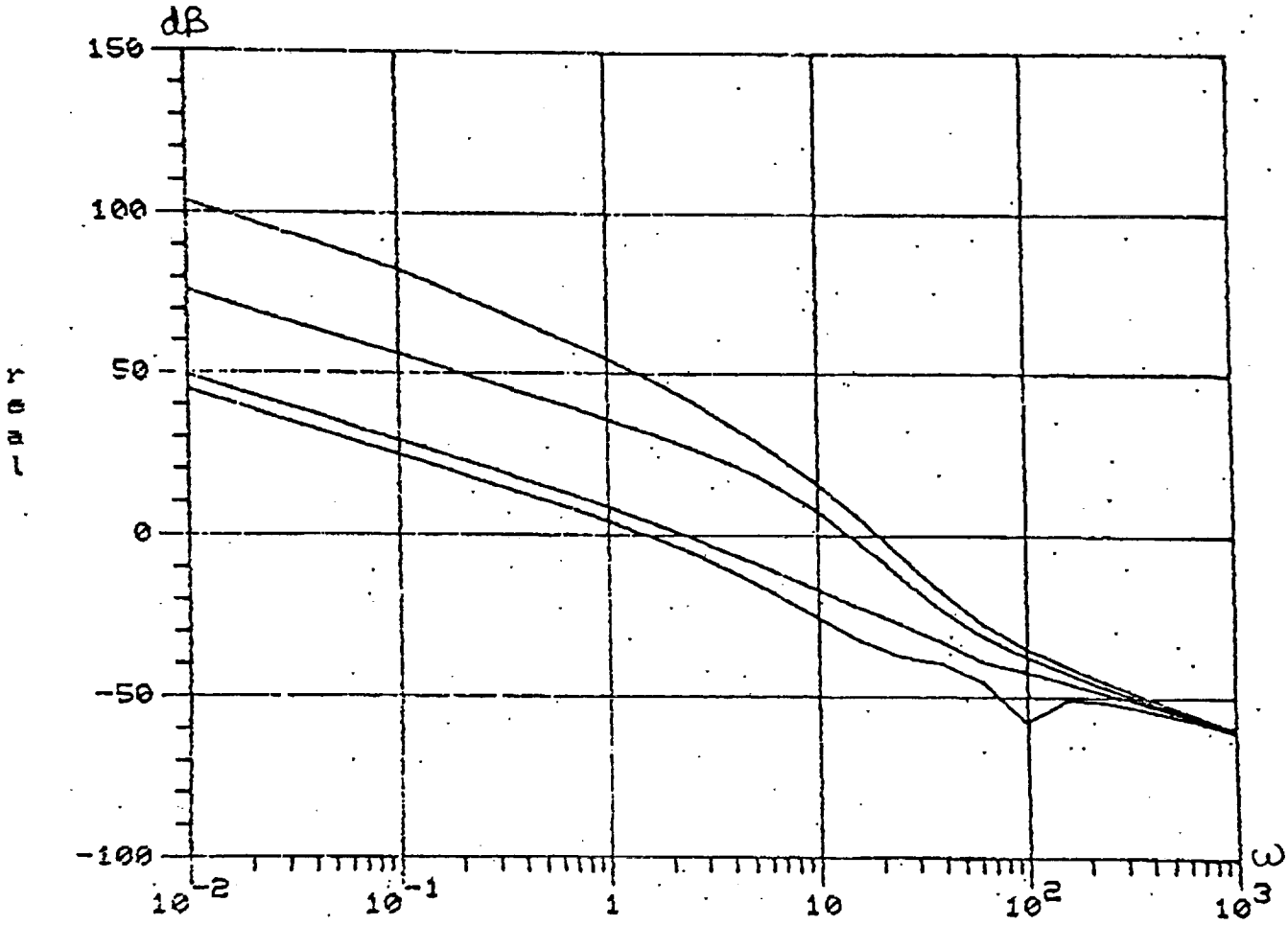

Fig4.5: $\underline{C}\underline{\Phi}(jw)\underline{\Gamma}$ for $\underline{\Gamma} = \begin{bmatrix} \underline{D}^{-1} \\ \underline{0} \end{bmatrix}$;

Singular Values vs Frequency.

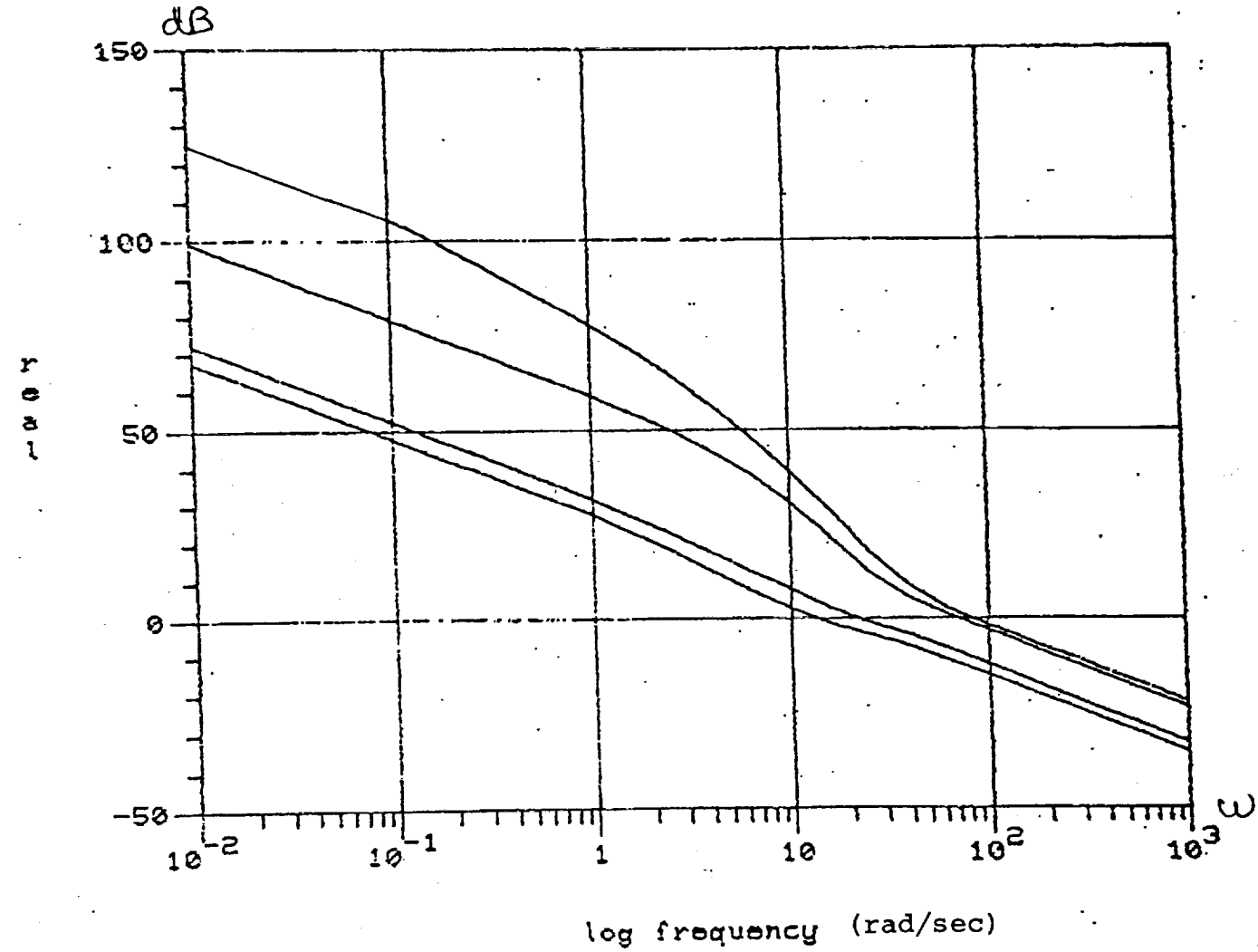

Fig4.6: High-Frequency Alignment Kalman Filter Design $\underline{N}=\underline{I}$, $\underline{\Gamma}=\begin{bmatrix} \underline{D}^{-1} \\ \underline{0} \end{bmatrix}$; Singular Values vs Frequency.

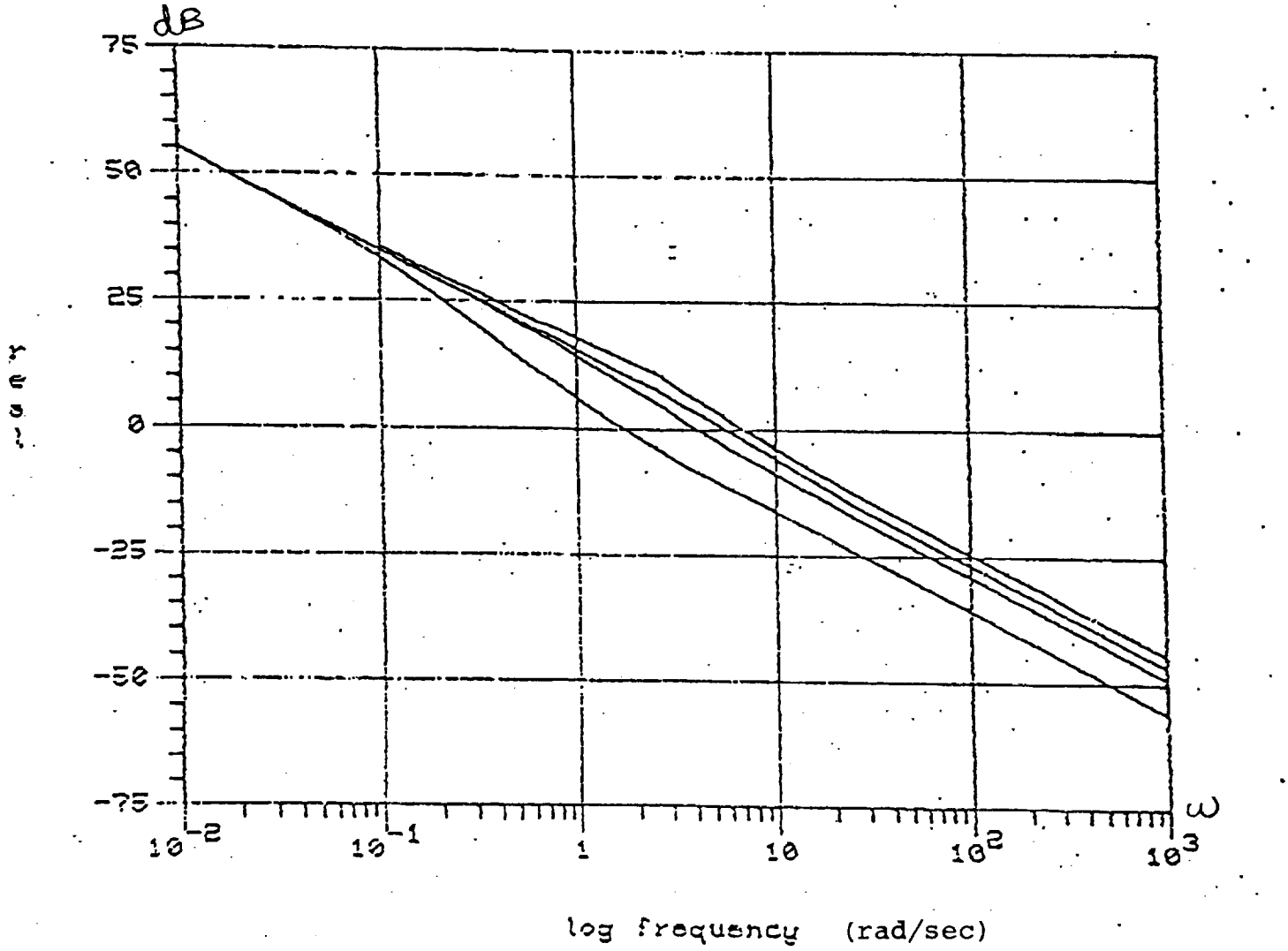

Fig4.7: Low-Frequency Alignment Kalman Filter Design $\underline{N}=\underline{I}$, $\underline{\Gamma}=\begin{bmatrix} \underline{G}(\omega)^{-1} \\ \underline{0} \end{bmatrix}$; Singular Values vs Frequency.

The low-frequency alignment has resulted in a much tighter singular-value spread and, hence, better crossover behavior. Moreover, the high-frequency alignment is not so effective since, as we have noted, the approximation:

$$\sigma_i[\underline{G}_f(j\omega)] \approx \sigma_i[\underline{C}\ \underline{\phi}(j\omega)\underline{\Gamma}]$$

is not valid (Fig. 4.6). Especially because over the desired bandwidth the low-frequency alignment is much more effective, from now on we abandon the high-frequency alignment.

Now the design of Fig. 4.7, for $\underline{N}=\underline{I}$, is still a little slow. In view of the bandwidth requirement (2-3 r/s to 10-15 r/s) we can afford to push the controller a little faster. This is done by scaling $\underline{N}$ down. Fig. 4.8 plots $\underline{G}_f(j\omega)$ for:

$$\underline{\Gamma} = \begin{bmatrix} \underline{G}(0)^{-1} \\ \\ \underline{0} \end{bmatrix} \quad \text{and} \quad \underline{N} = 5\text{x}10^{-3}\underline{I}\ .$$

From Fig. 4.8 we can see that the lowest crossover is now around 3 r/s and the highest at around 12-13 r/s. This is judged as a satisfactory design, from the performance limitations, since it corresponds to settling times of 2-3 secs.

Attempts to pull the singular value loops even closer by a diagonal $\underline{N}$ did not lead to any improvement. Thus Fig. 4.8 is taken to represent the final loop shape that is to be recovered.

Let us note that a diagonal $\underline{N}$ has in a sense already been employed in this design. This is because the reduced model is a rescaled version of the original reduced model, as was explained in section 3.5. And scaling of the $\underline{C}$ matrix of a system corresponds to picking a diagonal $\underline{N}$ matrix in the Kalman filter problem

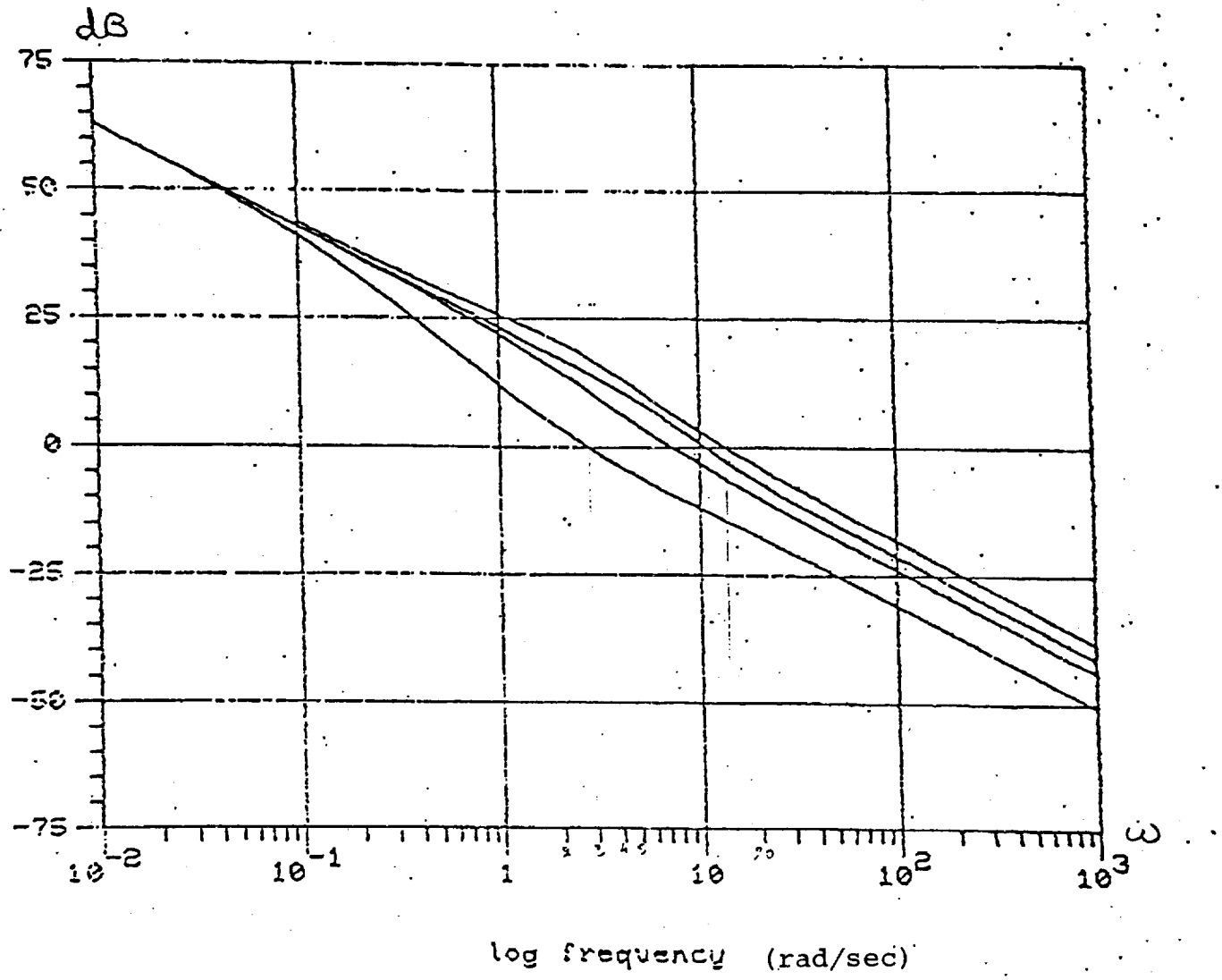

Fig4.8: Low-Frequency Alignment Kalman Filter Design $\underline{N}=5\times10^{-3}\underline{I}$, $\underline{\Gamma}=\begin{bmatrix} \underline{G}(\omega)^{-1} \\ \underline{0} \end{bmatrix}$;

Singular Values vs Frequency.

with elements equal to the inverses square of the nominal values that make up the output scaling matrix. This can be seen from the algebraic Riccati equation of the Kalman filter:

$$\underline{A}\,\underline{\Sigma} + \underline{\Sigma}\,\underline{A}^T + \underline{\Gamma}\,\underline{\Gamma}^T - \underline{\Sigma}\,\underline{C}^T\underline{N}^{-1}\underline{C}\,\underline{\Sigma} = 0$$

Now the robustness requirement (4.17) has to be checked. Fig. 4.9 plots the singular values of $[\underline{I}+\underline{G}_f^{-1}(j\omega)]$. As Fig. 4.10 shows, the designed loop meets the robustness requirement, since $\sigma_{min}[\underline{I}+\underline{G}_f^{-1}(j\omega)]$ is above $\sigma_{max}[\underline{\Delta}\,\underline{G}_{\mu 1}(j\omega)]$ for all frequencies.

This is not, however, the complete design. Step 2 of section 4.3 is still to come. We must recover the designed transfer function $\underline{G}_f(j\omega)$ by designing the LQ compensator.

4.5 Loop Transfer Recovery (LTR)

As we have seen, we need to recover the desirable Kalman transfer function $\underline{G}_f$. For this, we pick the parameters $\underline{R}$ and $\underline{Q}$ of the LQ regulator to be:

$$\underline{R} = \underline{I}, \quad \underline{Q} = \underline{H}^T\underline{H} \quad \text{with} \quad \underline{H} = q\underline{C}$$

where the scalar q is increased until we get a satisfactory recovery of $\underline{G}_f$. The results are illustrated in Figs. 4.11 to 4.14. Fig. 4.11 corresponds to q=100. We see that the recovery is quite good (compare Fig. 4.8 with Fig. 4.11), up to the point where we have the right-half plane zeros (around 20 r/s). Note that an interesting feature of the recovery process is that the Kalman filter transfer

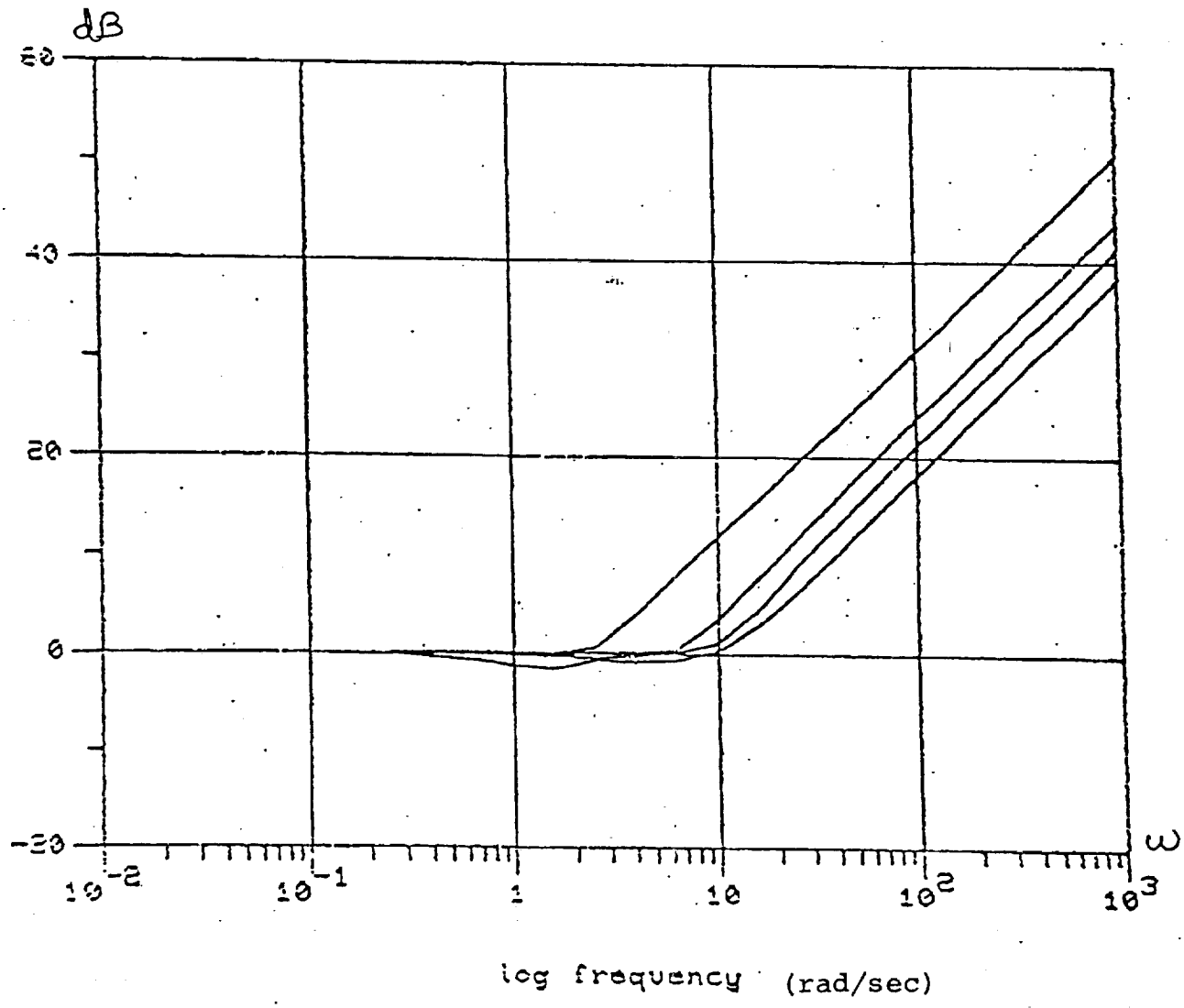

Fig4.9: Plot of Designed Inverse Return Difference Function $(\underline{I}+\underline{G}_f^{-1}(j\omega))$; Singular Values vs Frequency.

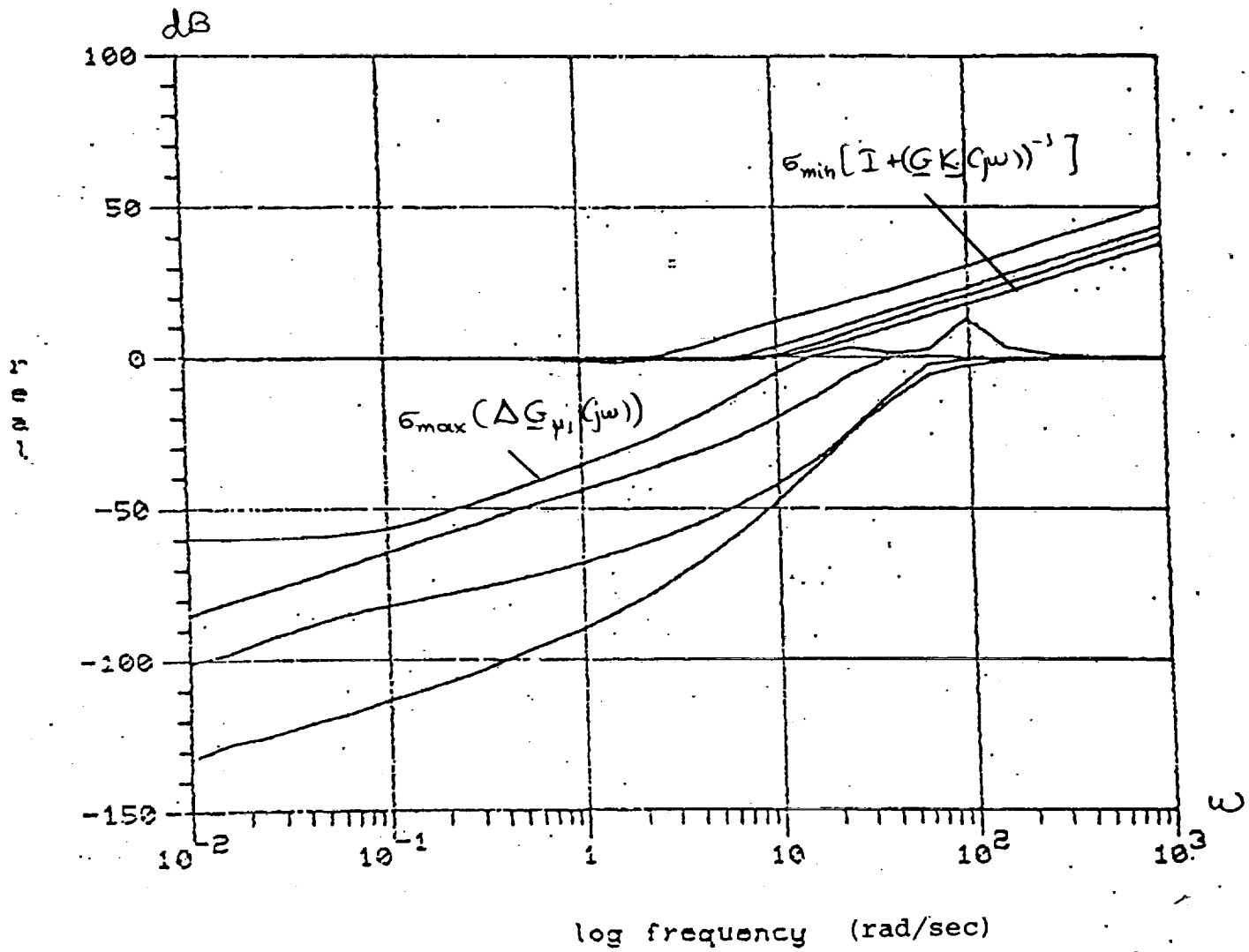

Fig4.10: Robustness Requirement Plot:
Inverse Return Difference Function
staying over the Multiplicative Error.

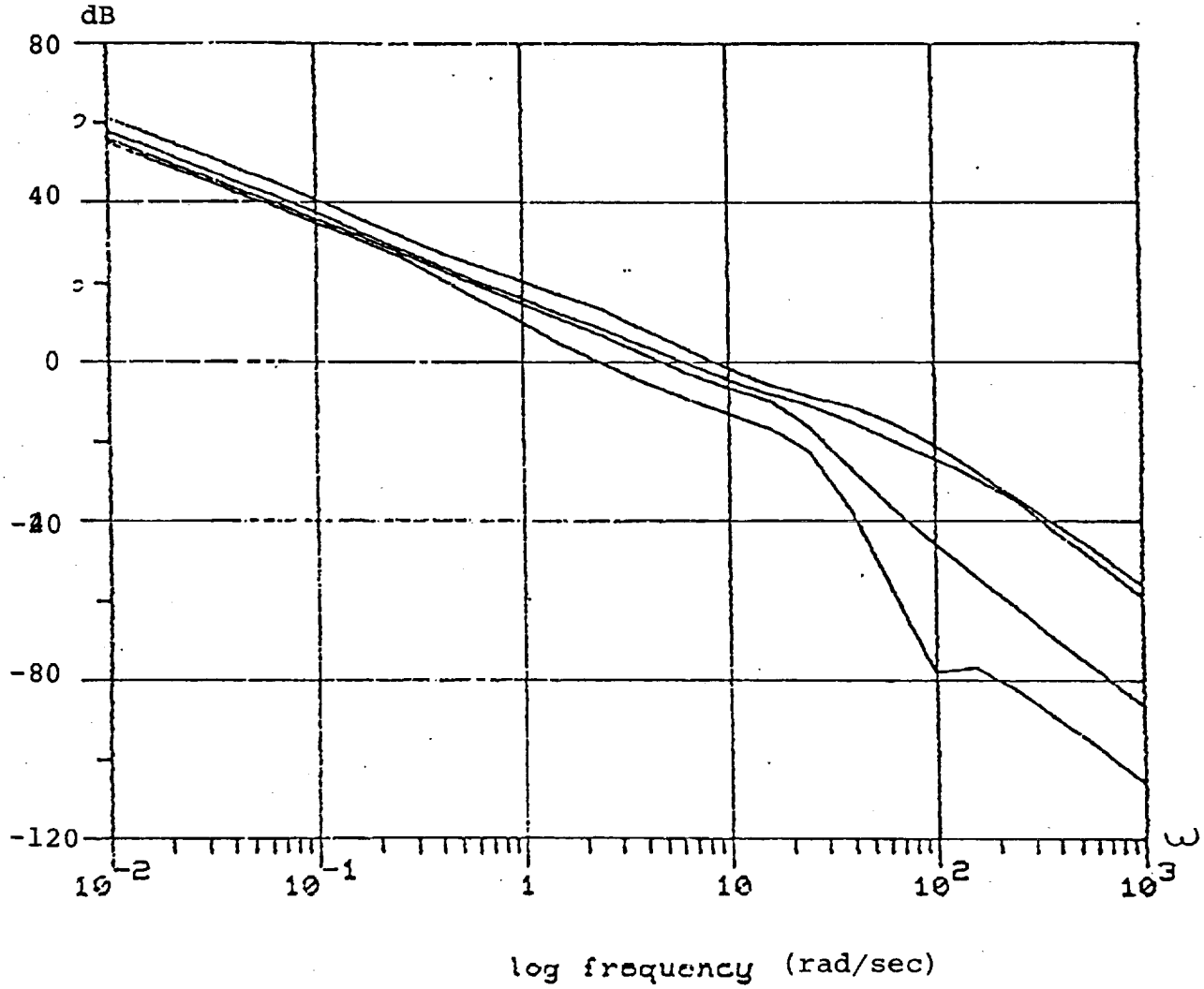

Fig4.11: Loop Transfer Recovery: q=100 ; Singular Values vs Frequency.

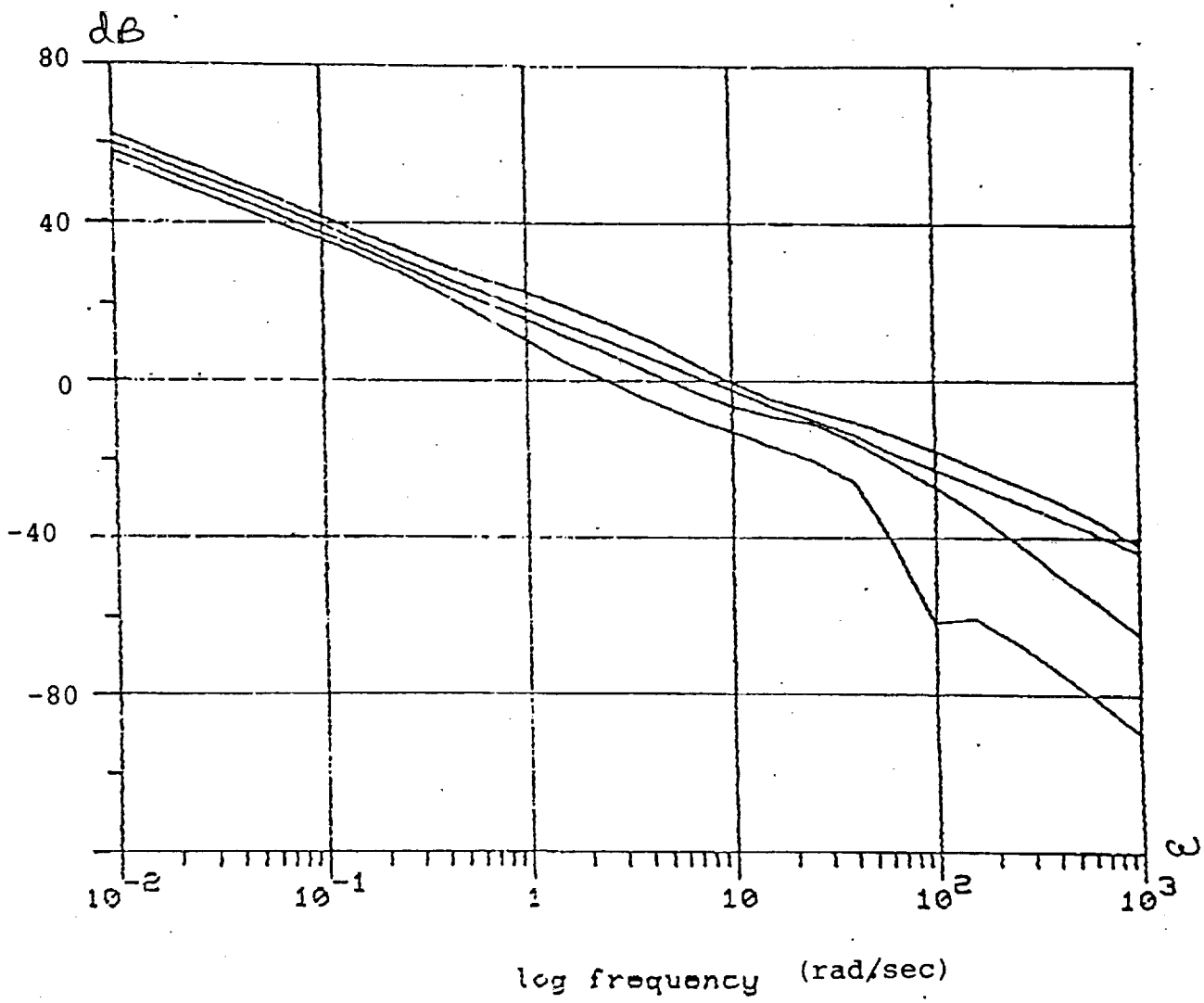

Fig4.12: Loop Transfer Recovery: $q=10^3$; Singular Values vs Frequency.

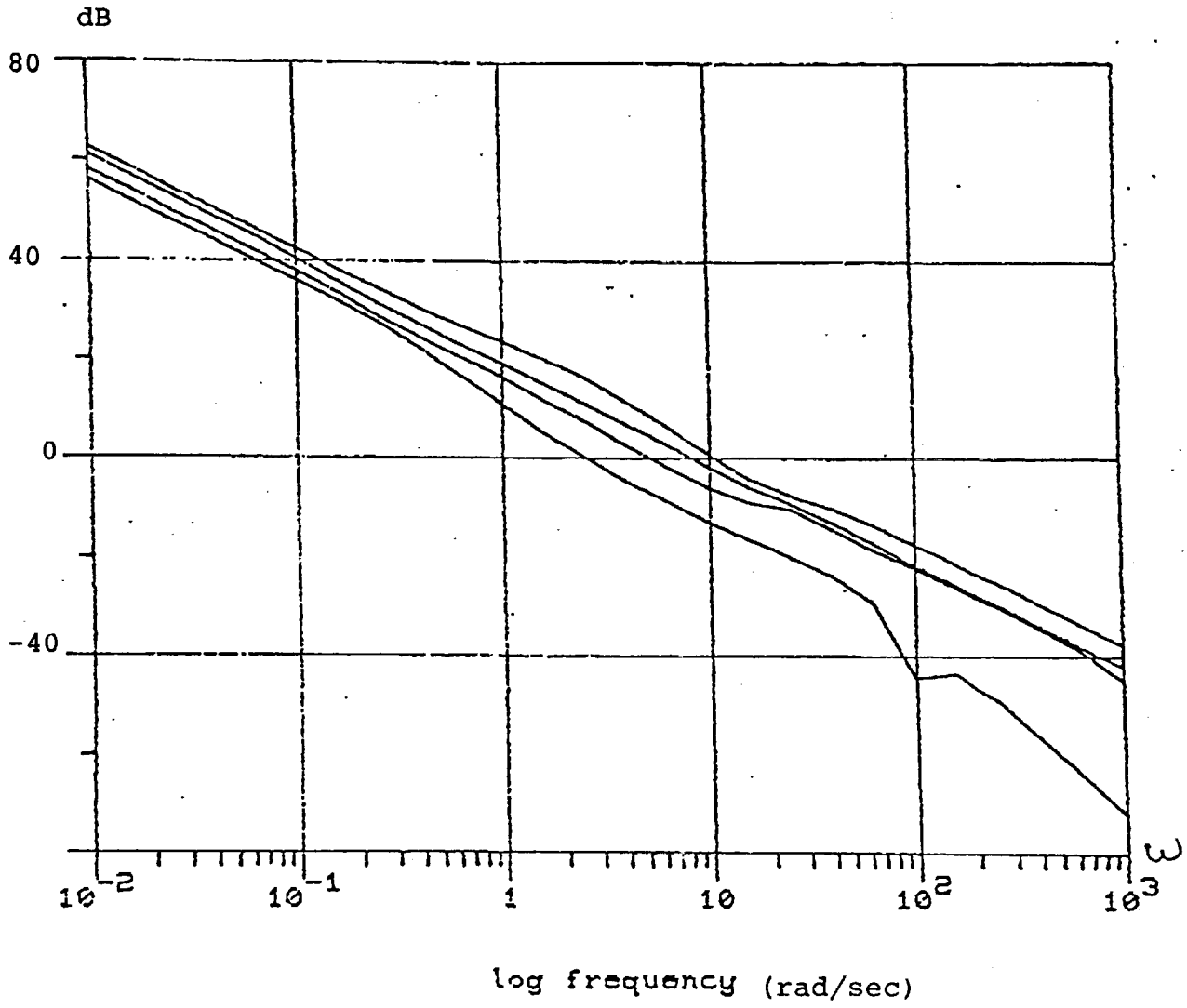

Fig4.13: Loop Transfer Recovery: $q=10^4$; Singular Values vs Frequency.

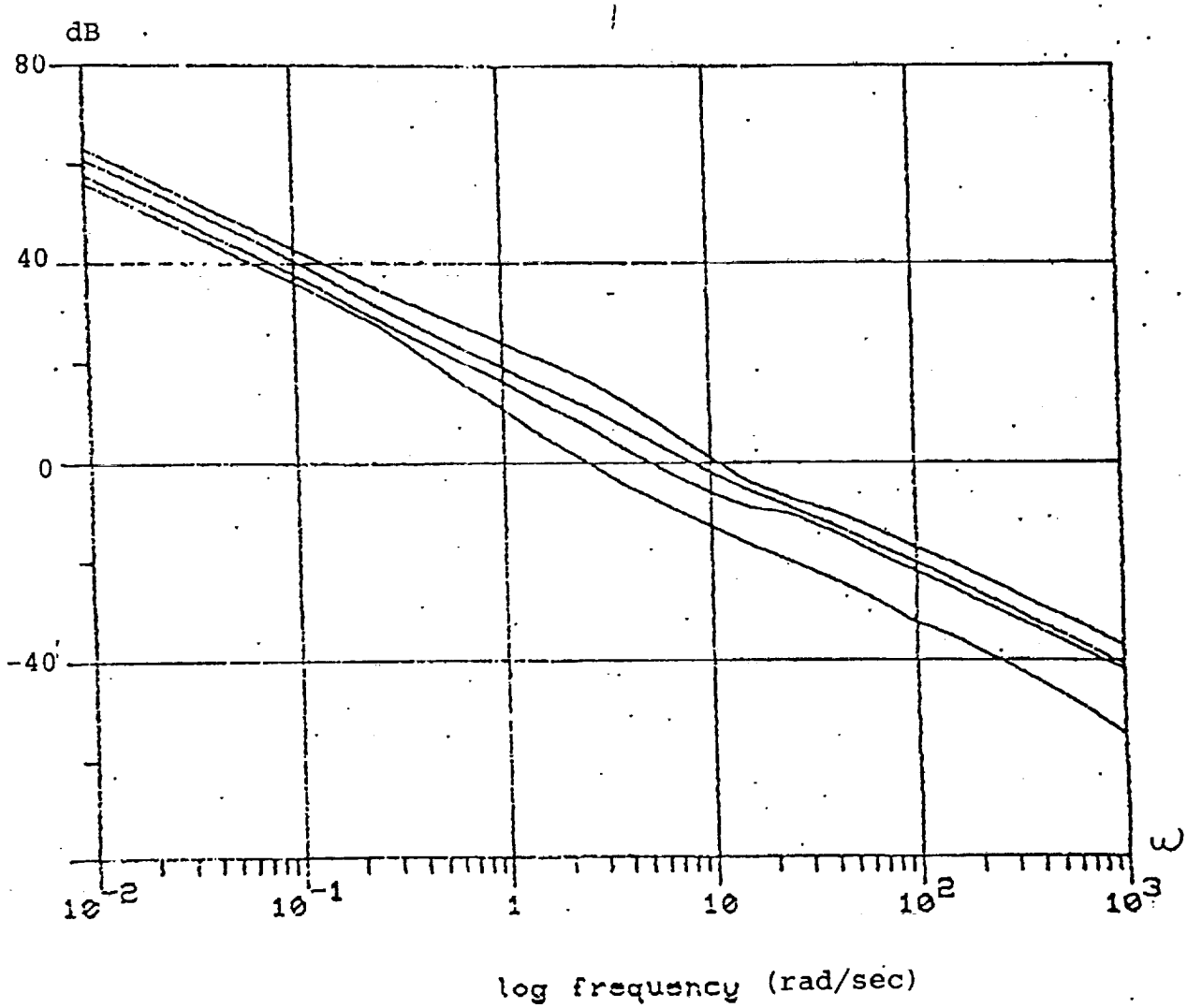

Fig4.14: Loop Transfer Recovery: $q=10^5$. Singular Values vs Frequency.

function $\underline{G}_f(j\omega)$ is recovered from below. This means that the LQG loop transfer function $\underline{G}\,\underline{K}(j\omega)$ remains below $\underline{G}_f(j\omega)$ and as q is increased, it comes closer and closer to $\underline{G}_f$.

As we keep increasing q, it is seen that no great problems are created by the presence of the non-minimum phase zeros. Finally, at the value $q=10^5$ (Fig. 4.14) the recovery is really quite satisfactory. Comparing the two transfer functions in Figs. 4.8 and 4.14 we see that they differ most in the frequency region where the non-minimum phase zeros are. This slight bump in the singular value shapes is the only price we had to pay for the non-minimum phase zeros.

It now only remains to check again that the robustness requirement is met:

$$\text{For all } \omega: \quad \sigma_{min}[\underline{I}+(\underline{G}\,\underline{K}(j\omega))^{-1}] > \sigma_{max}(\Delta\underline{G}_{\mu 1}(j\omega))$$

This is illustrated in Figs. 4.15 and 4.16. The designed minimum singular value of the inverse return difference function stays above the maximum singular value of the appropriate multiplicative error.

To summarize, the design parameters have the following values:

$$\underline{R} = \underline{I}$$

$$\underline{Q} = \underline{H}^T\underline{H} \quad \text{with } \underline{H} = 10^5\underline{C}$$

$$\underline{N} = 5\times10^{-3}\,\underline{I}$$

$$\underline{\Gamma} = \begin{bmatrix} \underline{G}(0)^{-1} \\ \\ \underline{0} \end{bmatrix}$$

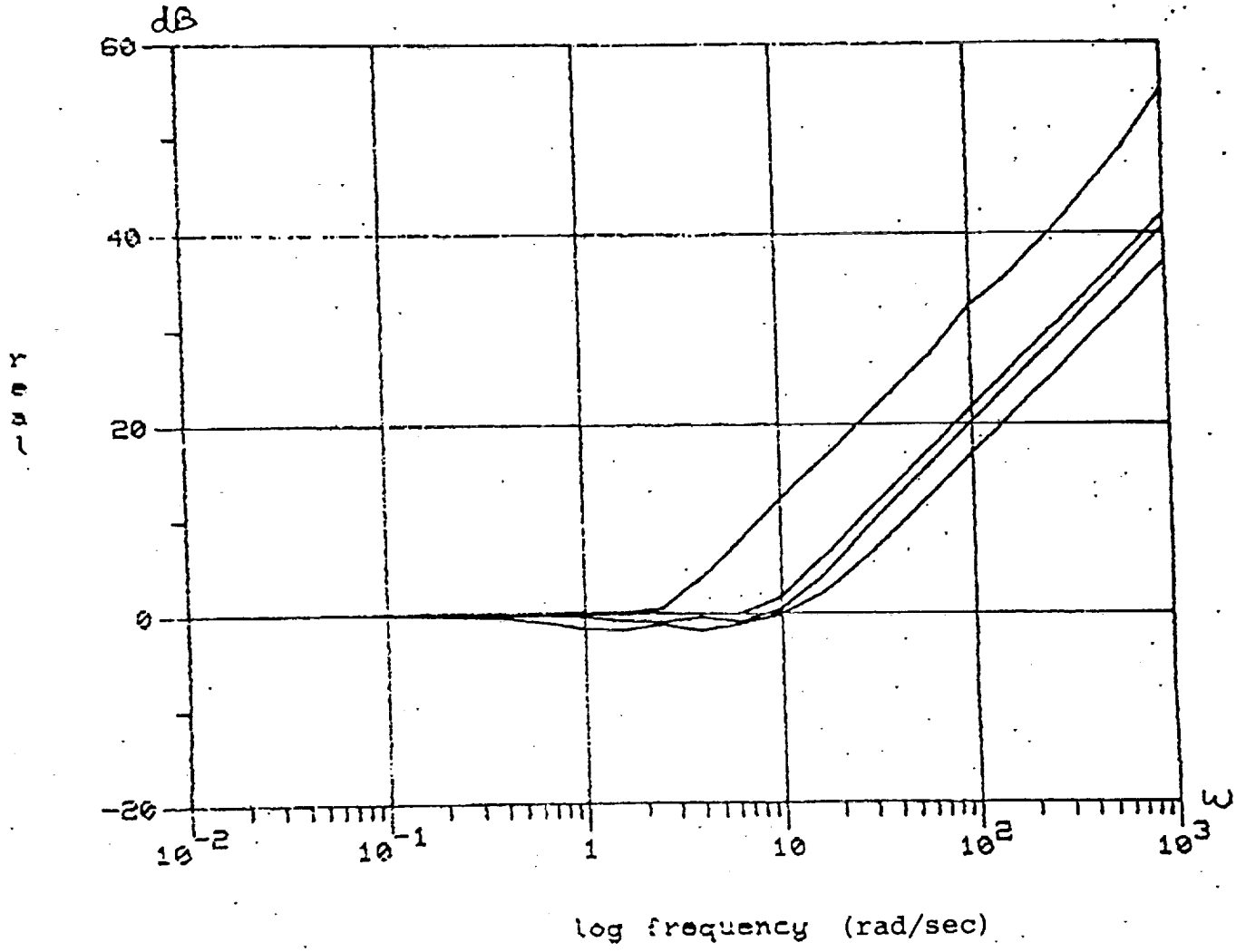

Fig4.15: Inverse Return Difference Singular Value Plot for Recovered Transfer Function.

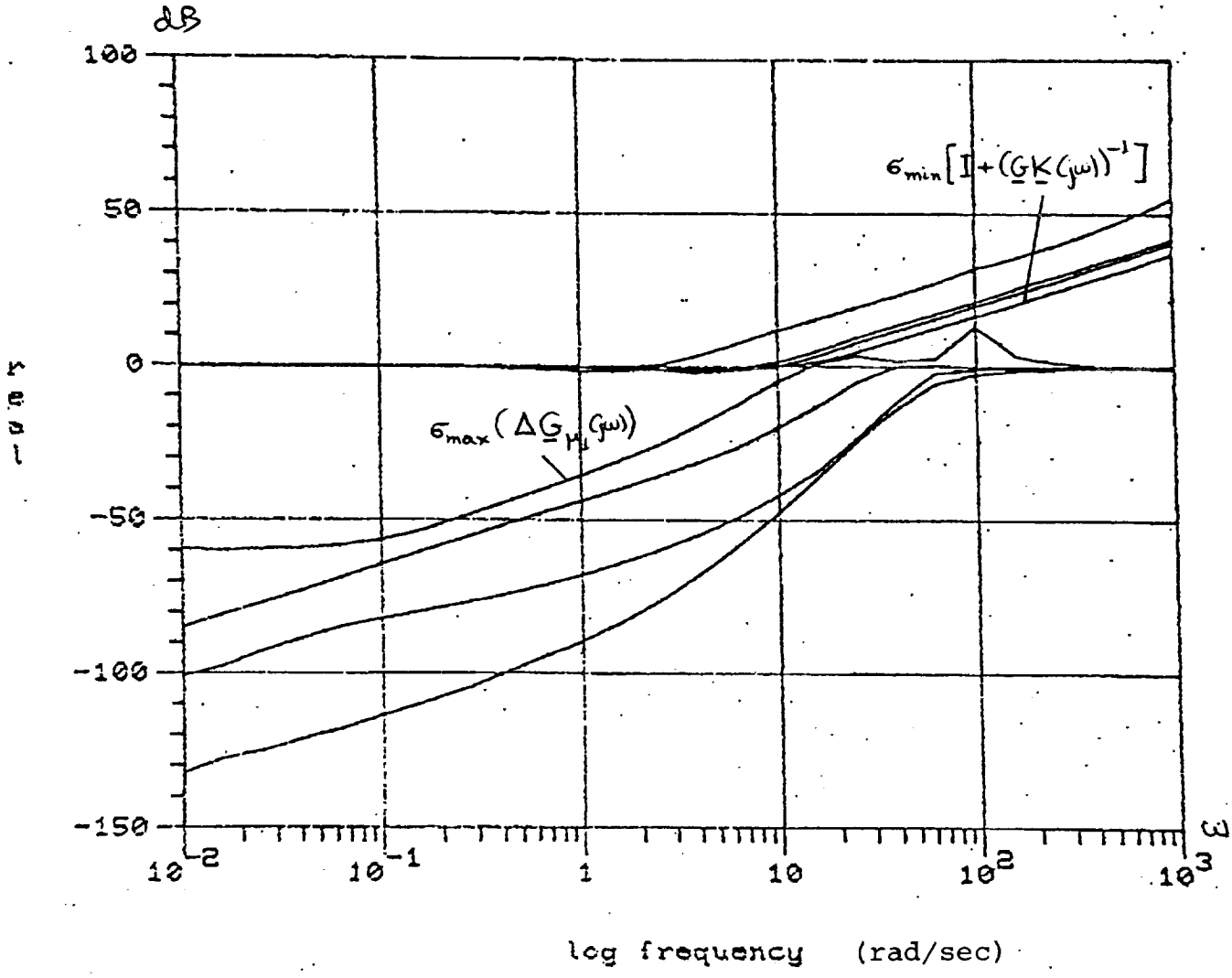

Fig4.16: Robustness Requirement Plot:
Inverse Return Difference Function
of Recovered Design staying over the
Multiplicative Error.

4.6: Evaluation of Actual Closed-Loop Design

The final control configuration includes the LQG Controller followed by the integrators in the input channels of the plant, followed by the full linear plant dynamics, as shown in Fig. 4.17.

We know that this overall system is asymptotically stable, since the robustness requirement is met with the reduced model in place of the full model. As a check, the closed-loop eigenvalues are calculated. They are listed in Table 4.1. It is thus verified that the closed-loop system is stable. All forty four eigenvalues are in the open left-hand plane. A number of them are in the region of the design bandwidth, from 10 to 20 rad/sec.

It is obvious from Fig. 4.17 that the second control specification, that of integral action, is satisfied. The feedback loop includes the integrators in the forward loop, so that the error between the reference signals and the outputs passes through them. Fig. 4.18 plots the singular values of the overall loop transfer function, $\underline{\tilde{G}}(j\omega)\underline{K}(j\omega)$, where $\underline{K}(j\omega)$ is the overall compensator, as in Fig. 4.17. All singular values roll-off at the rate of 20dB/decade at low frequencies, due to the integrators.

The final control specification is that of a satisfactory bandwidth. The crossover behavior of the overall loop transfer function (Fig. 4.18) is very close to that of the loop transfer function with the reduced model in place, as Fig. 4.19 shows. It plots the minimum and maximum singular values of the 'true' and approximate loop transfer functions. It superimposes Fig. 4.19 with Fig. 4.14. The minimum and maximum crossovers of the two transfer functions are at 2.5 and about 12 rad/sec. respectively. The bandwidth of the final design is satisfactory

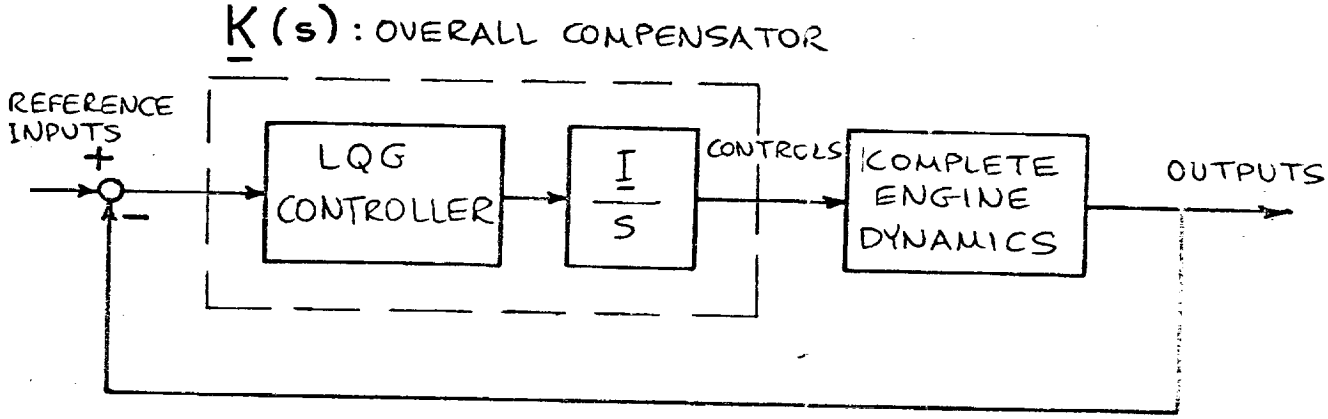

Fig4.17: The Control Setup on the Full Linear Model.

TABLE 4.1

Closed-loop Eigenvalues.

$-0.4748 \pm j1.83E-3$, $-0.649 \pm j6.17E-4$, $-1.482 \pm j1.4$,
-2.122 , -2.127 , $-4.37 \pm j4.08$, $-5.34 \pm j87.6$,
$-5.716 \pm j7.71$, $-8.31 \pm j25.85$, $-8.585 \pm j7.09$,
$-11.775 \pm j1.946$, -13.577 , -16.442 , $-17.92 \pm j4.82$,
$-18.079 \pm j6.275$, -19.853 , $-21.38 \pm j0.8423$,
$-21.95 \pm j0.56$, $-24.556 \pm j35.05$, -41.626 , -50.0 ,
$-50.21 \pm j28.256$, -93.83 , -177.24 , -577.02 ,
-764.24 , -777.35 , -7710.2 , -25075.

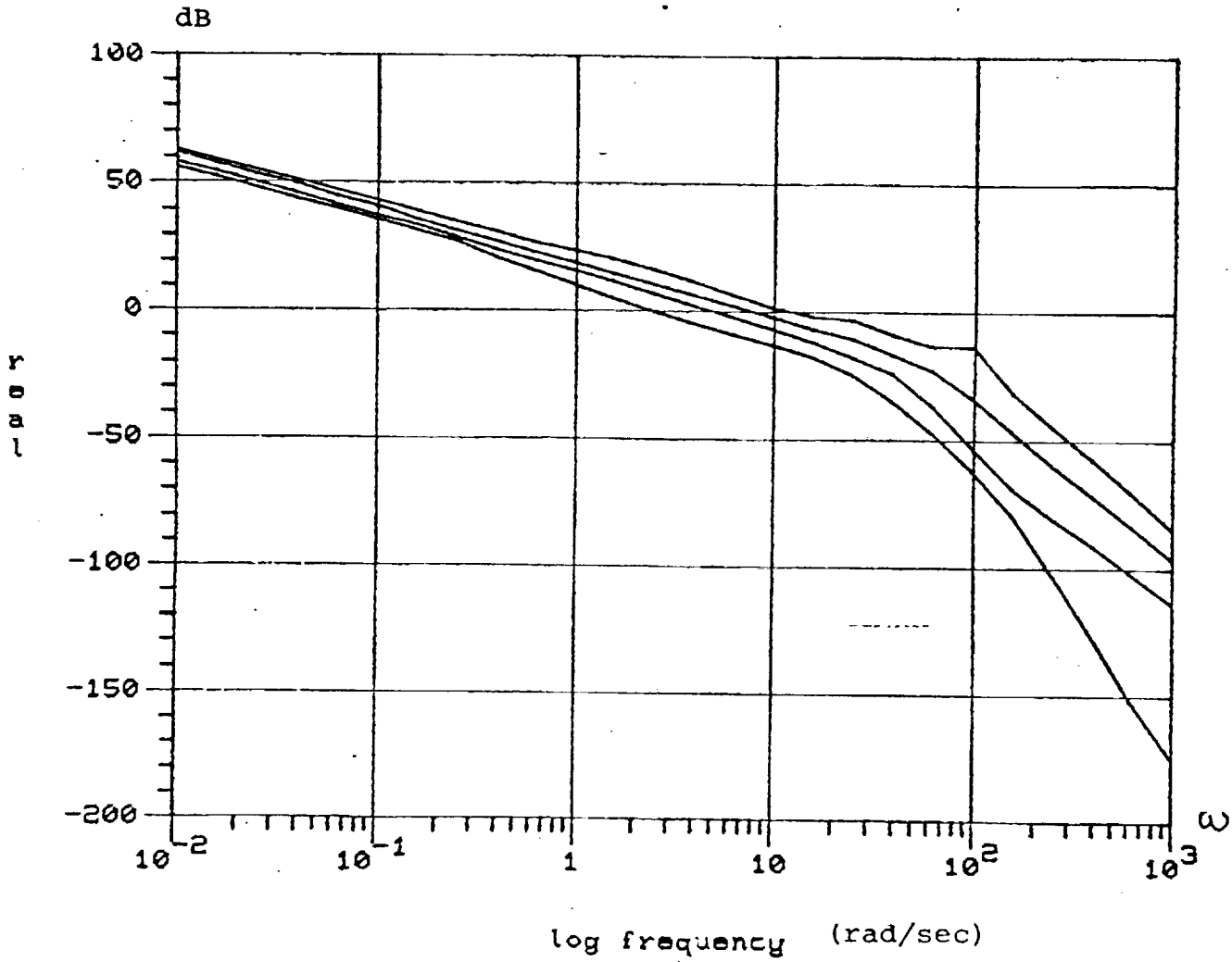

Fig4.18: Loop Transfer Function Singular Value Plot for LQG compensator with the Full Linear Model.

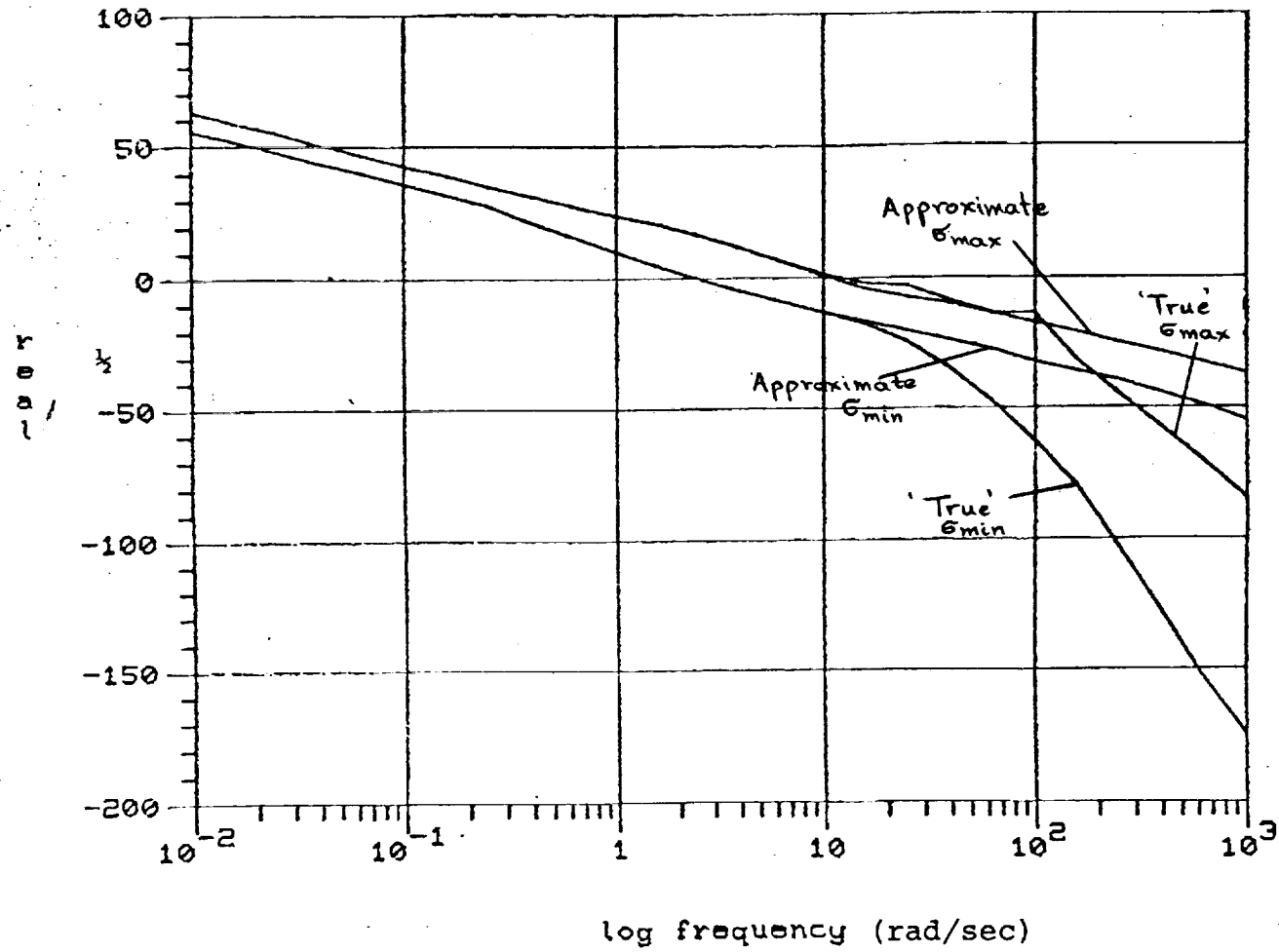

Fig4.19: Maximum and Minimum Singular Values of 'True' and 'Approximate' Loop Transfer Functions.

An additional perspective is provided by Fig. 4.20. It plots the singular values of the closed-loop transfer function $(\underline{I}+\underline{\tilde{G}}(j\omega)(\underline{K}(j\omega))^{-1}\underline{\tilde{G}}(j\omega)\underline{K}(j\omega)$, from the reference inputs to the engine outputs. The noticeable feature of this plot is that all loops remain flat over a broader range of frequencies than the open-loop singular values of the plant itself (compare with Fig. 3.8). Control has opened up the bandwidth of the singular value loops and thus has sped up the responses. Fig. 4.21 plots the unit step responses from each reference input to the corresponding output. These time responses satisfy the requirement of section 2.4. At the two second point, the responses have reached more than 90% of their final values (the responses with the approximate model in the place of the 'true' one are very close to those in Fig. 4.21).

For comparison, the step responses of the open-loop full engine dynamics are also plotted, in dashed lines, in Fig. 4.21. It is obvious that the greatest improvement is in the response of the $T_{4.5}$ output (which was slow due to its slow sensor). For N_1 and N_2, the optimal step responses are slightly less damped than they were, while the response of P_3 is slowed down a little. Fig. 4.21 also plots the responses of the other outputs to the steps in each input. Those outputs not plotted respond by less than 10% of the step magnitude.

4.7 Chapter Summary

Loop-shaping ideas in the LQG setting were used to design a satisfactory controller for the F100 engine.

These loop-shaping ideas, based on the Kalman equalities, were developed in Section 2. They are basically due to Stein et.al., although some new variations were necessary for out setting. Thus, singular value pullings at low and high

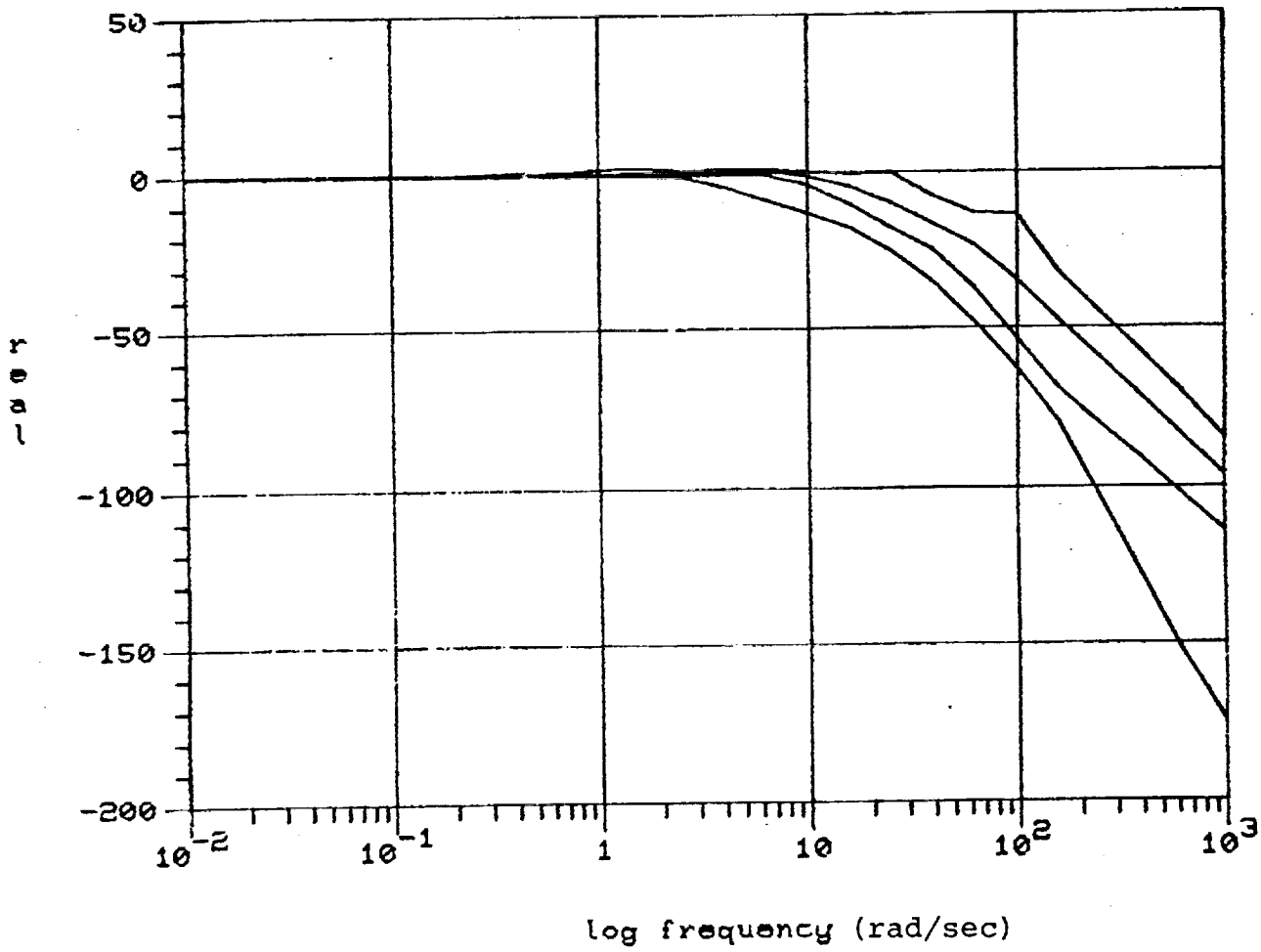

Fig4.20: Closed-loop Transfer Function Singular Values.

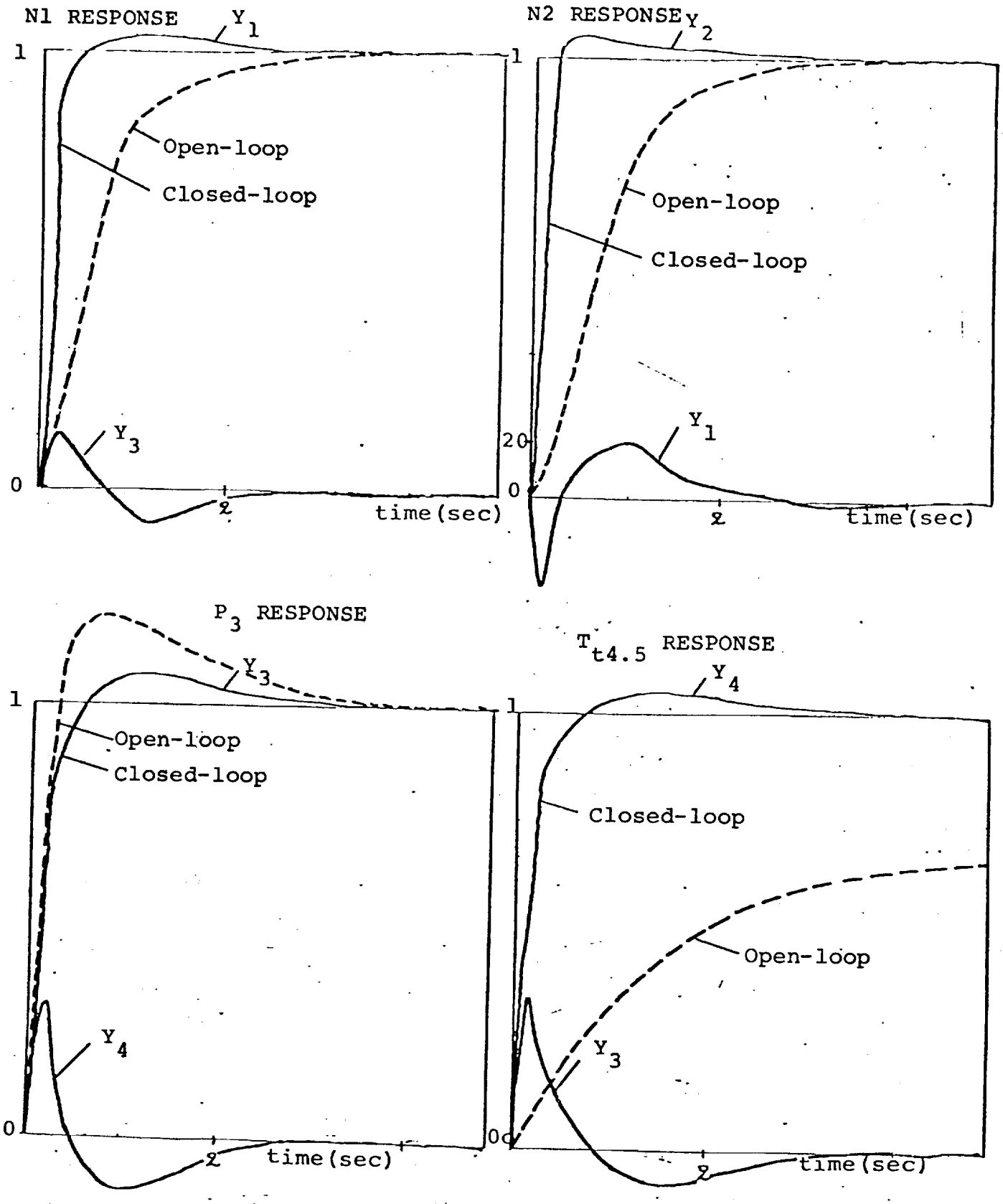

Fig4.21: Comparison of Open-loop (dashed lines) and Closed-loop (solid lines) responses of the four output variables to individual commanded steps (normalized).

frequencies were accomplished in the presence of integral control by appropriate choices of the Kalman filter parameters.

The resulting Kalman filter loop transfer function was then recovered for the overall LQG controller using standard recovery techniques. It was seen that recovery was not hindered by the presence of non-minimum phase zeros.

Finally, it was shown that the designed LQG controller gives a satisfactory stable loop when the full linear model replaces the approximate reduced one.

5. SUMMARY AND DIRECTIONS FOR FURTHER RESEARCH

5.1 Summary

This thesis presented a multivariable control design example which comprises the following parts:

1) Significant actuator and sensor dynamics were added to the full linear model of the F100 engine. Additional dynamics, integrators in the input channels, were added so as to get loop-shapes that the LQG procedure cannot produce by itself.

2) The resultant augmented linear system is taken as the 'true' model. Model reduction is now done in order to reduce the order of the dynamic controller, for simplicity of design. The reduction method follows the robustness perspective. Modal analysis and singular value characterizations of error are the main components of the proposed technique. The result is a 'robust' reduced model that yields an overall stable configuration when replaced by the true model in the feedback loop.

3) The controller was designed based on the LQG methodology in its modern frequency-domain version of Stein, Doyle et.al. Reliable and simple loop-shaping techniques were employed to yield a controller that satisfies the desired bandwidth requirements.

5.2 Some conclusions and directions for further research

The robustness viewpoint to model reduction is a simple enough idea but a useful one, if model approximation is to be viewed in a feedback setting. The development of the reduction method in this work benefitted from the additive decomposition of the system transfer function (the modal decomposition). In the

case when there is no such decomposition (if, for example, the eigenvalues of the model are not distinct), the method does not work. Some extension of the robustness perspective through similar decompositions is therefore necessary. The extension to non-distinct eigenvalues is an example.

Another direction that this thesis supports is that of frequency-domain relations for LQG (state-space) based designs. The Kalman equalities are the most familiar and most useful starting point to date. It is hoped that more work will reveal other frequency-domain properties of LQG designs and will help bridge the gap between practitioners of these two relatively distinct techniques.

The usefulness of singular value characterizations for multivariable systems was demonstrated in this thesis. Both the model reduction stage and the design stage depended on these characterizations. Insomuch as they extend the familiar Bode plots, singular values are a frequency-domain tool. And yet singular value properties of state-space systems are easily handled, as the loop-shaping tools of Chapter 4 showed. We believe that singular values should play a central role in multivariable control design.

APPENDIX A

TABLE A.1

Augmented Linear System (Plant+Sensors+Actuators).

A Matrix

Number of rows = 23
Number of columns = 23

-1.0000E+01	0.0000E+00	0.0000E+00	0.0000E+00	0.0000E+00	0.0000E+00	1st Row
0.0000E+00	0.0000E+00	0.0000E+00	0.0000E+00	0.0000E+00	0.0000E+00	
0.0000E+00	0.0000E+00	0.0000E+00	0.0000E+00	0.0000E+00	0.0000E+00	
0.0000E+00	0.0000E+00	0.0000E+00	0.0000E+00	0.0000E+00		
0.0000E+00	0.0000E+00	1.0000E+00	0.0000E+00	0.0000E+00	0.0000E+00	2nd Row
0.0000E+00	0.0000E+00	0.0000E+00	0.0000E+00	0.0000E+00	0.0000E+00	
0.0000E+00	0.0000E+00	0.0000E+00	0.0000E+00	0.0000E+00	0.0000E+00	
0.0000E+00	0.0000E+00	0.0000E+00	0.0000E+00	0.0000E+00		
0.0000E+00	-1.4205E+03	-4.2113E+01	0.0000E+00	0.0000E+00	0.0000E+00	
0.0000E+00	0.0000E+00	0.0000E+00	0.0000E+00	0.0000E+00	0.0000E+00	
0.0000E+00	0.0000E+00	0.0000E+00	0.0000E+00	0.0000E+00	0.0000E+00	
0.0000E+00	0.0000E+00	0.0000E+00	0.0000E+00	0.0000E+00		
0.0000E+00	0.0000E+00	0.0000E+00	-1.2000E+01	0.0000E+00	0.0000E+00	
0.0000E+00	0.0000E+00	0.0000E+00	0.0000E+00	0.0000E+00	0.0000E+00	
0.0000E+00	0.0000E+00	0.0000E+00	0.0000E+00	0.0000E+00	0.0000E+00	
0.0000E+00	0.0000E+00	0.0000E+00	0.0000E+00	0.0000E+00		
0.0000E+00	0.0000E+00	0.0000E+00	0.0000E+00	-4.0000E+01	0.0000E+00	
0.0000E+00	0.0000E+00	0.0000E+00	0.0000E+00	0.0000E+00	0.0000E+00	
0.0000E+00	0.0000E+00	0.0000E+00	0.0000E+00	0.0000E+00	0.0000E+00	
0.0000E+00	0.0000E+00	0.0000E+00	0.0000E+00	0.0000E+00		
-4.5700E-02	-4.5160E+02	0.0000E+00	-1.0580E+02	-1.5060E+00	-4.3280E+00	
1.7140E-01	5.3760E+00	4.0160E+02	-7.2460E+02	-1.9330E+00	1.0200E+00	
-9.8200E-01	9.9900E-01	1.5210E+00	-4.0620E+00	9.5670E+00	1.0080E+01	
-6.0170E-01	-1.3120E-01	9.6020E-02	0.0000E+00	0.0000E+00		
1.1140E-01	-5.4610E+02	0.0000E+00	-6.5750E+00	-1.0780E+02	-4.4020E-01	
-5.6430E+00	1.2750E+02	-2.3350E+02	-4.3430E+02	2.6590E+01	2.0400E+00	
-2.5920E+00	1.1320E+01	1.0900E+01	-4.0710E+00	-5.7390E-02	-6.0630E-01	
-7.4880E-02	-5.9360E-01	-9.6020E-02	0.0000E+00	0.0000E+00		
2.1530E-01	1.3620E+03	0.0000E+00	1.3460E+01	2.0140E+01	1.0380E+00	
6.0730E+00	-1.6500E+02	-4.4830E+00	1.0490E+03	-8.2450E+01	-5.3140E+00	
5.0970E+00	-9.3890E-03	1.3520E-01	5.6380E+00	2.2460E-02	1.7970E-01	
2.4070E-02	1.1000E+00	2.7430E-02	0.0000E+00	0.0000E+00		
3.2620E-01	2.0800E+02	0.0000E+00	-2.8880E+00	-1.6530E+00	5.3040E-01	
-1.0860E-01	1.3130E+02	-5.7830E+02	1.0200E+02	-9.2400E+00	-1.1460E+00	
-2.4080E+00	-3.0810E+00	-4.5290E+00	5.7070E+00	-2.3460E-01	-2.1110E+00	
-2.4600E-01	-4.6860E-01	-3.2230E-01	0.0000E+00	0.0000E+00		
9.9480E-03	-9.8390E+01	0.0000E+00	5.0690E-01	-1.9400E-01	8.4760E-03	
-1.5630E-02	5.6020E-02	1.5730E+00	-1.0050E+01	1.9520E-01	-8.8040E-03	
-2.1100E-02	2.0900E-03	-5.2560E-02	-4.0770E-02	-9.1820E-03	-8.1780E-02	
3.4280E-02	4.9950E-03	-1.2560E-02	0.0000E+00	0.0000E+00		
2.7280E-02	7.1620E+01	0.0000E+00	9.6080E+00	-3.1600E-01	8.3500E-01	

A Matrix (Continued)

```
-1.2490E-02 -3.5670E-02 -6.0740E-01  3.7650E+01 -1.9790E+01 -1.8130E-01
-2.9620E-02 -1.9530E-02 -1.6220E-01 -6.4390E-03 -2.3460E-02 -2.2010E-01
-2.5140E-02 -3.7490E-03 -3.3610E-02  0.0000E+00  0.0000E+00

 1.7160E-02  7.1710E+01  0.0000E+00  8.5710E+00  7.9890E-01  6.7680E-01
-1.2640E-02 -9.6830E-02 -3.5670E-01  8.0240E+01 -8.2390E-02 -2.0470E+01
-3.9280E-02  1.8780E-02 -2.1290E-01 -9.3370E-03 -3.1440E-02 -2.9190E-01
-3.3700E-02  8.8730E-02 -4.4580E-02  0.0000E+00  0.0000E+00

-7.7410E-02 -1.4120E+02  0.0000E+00 -8.2150E-01  3.9740E+01 -9.6960E-02
 8.6660E-01  1.6870E+01  1.0510E+00 -1.0230E+02  2.9660E+01  5.9430E-01
-1.9970E+01  2.2530E-02  1.7910E-01  8.3710E-03  2.6450E-02  2.5600E-01
 2.8350E-02 -3.7490E-02  3.6350E-02  0.0000E+00  0.0000E+00

 3.8550E-02 -7.7100E+00  0.0000E+00 -4.3710E-02 -1.0240E-01 -8.7850E-03
-1.6360E-02  1.8470E-01  2.1690E-01 -8.4200E+00  7.0030E-01  5.6660E-02
 6.6230E+00 -4.9990E+01  6.7600E-02  3.9460E+01  4.9910E-03  8.9830E-02
 5.3490E-03  0.0000E+00  1.3720E-02  0.0000E+00  0.0000E+00

 5.7070E-04 -1.1440E-01  0.0000E+00 -6.3590E-04 -1.4320E-03 -1.2980E-04
-2.4300E-04  2.7180E-03  3.2140E-03 -1.2460E-01  1.0390E-02  8.3950E-04
 9.8120E-02 -6.6660E-01 -6.6570E-01  5.8470E-01  6.6540E-05  1.3470E-03
 7.1310E-05  0.0000E+00  2.0570E-04  0.0000E+00  0.0000E+00

 5.7270E+00 -1.7450E+03  0.0000E+00 -8.9400E+00 -1.7960E+01 -1.2070E+00
-6.7170E+00  2.6260E+01  1.2490E+01 -1.2690E+03  1.0300E+02  7.4800E+00
 3.6840E+01  2.8540E-01  2.3320E+00 -4.7650E+01  3.4060E-01  3.0650E+00
 3.6240E-01 -4.3430E-01  4.6810E-01  0.0000E+00  0.0000E+00

 1.3920E-01 -2.4300E+01  0.0000E+00 -2.7360E-01 -3.4030E-01 -2.7300E-02
-4.5390E-01 -5.2720E+01  1.9880E+02 -2.8090E+01  2.2430E+00  1.7940E-01
 9.7500E+00 -9.6270E+00 -9.5570E+00  3.8480E+01 -5.0010E+01  1.0110E-01
 1.2030E-02 -4.6860E-02  1.7150E-02  0.0000E+00  0.0000E+00

 6.1720E-03 -1.0820E+00  0.0000E+00 -1.1830E-02 -1.4520E-02 -1.2060E-03
-2.0170E-02 -2.3430E+00  8.8350E+00 -1.2480E+00  9.9750E-02  8.0590E-03
 4.3330E-01 -4.2780E-01 -4.2450E-01  1.7100E+00 -2.0000E+00 -1.9960E+00
 5.3490E-04 -1.9990E-03  7.5440E-04  0.0000E+00  0.0000E+00

 6.7770E-02  1.6600E+01  0.0000E+00  3.9800E-01  2.3110E-02 -1.6130E-01
-2.4690E-01 -2.4050E+01  2.3380E+01  1.4630E+02  1.6380E+00  1.3850E-01
 4.4860E+00 -4.4140E+00 -4.3540E+00  1.7660E+01 -3.1130E+00 -3.0180E+00
-1.9770E+01 -4.9990E-02  1.5090E-02  0.0000E+00  0.0000E+00

 1.8800E-03  9.1470E+00  0.0000E+00 -8.2410E-01  8.9840E-02 -1.2440E-02
 3.0200E-02  1.1980E-01 -4.8210E-02  5.6750E+00 -4.5250E-01  1.9810E+01
 1.2490E-01 -1.1270E-03 -6.7600E-03  1.8350E-02 -9.9810E-04 -1.3470E-02
-1.0700E-03 -2.0000E+01 -2.0570E-03  0.0000E+00  0.0000E+00

 1.6770E-01  4.3580E+02  0.0000E+00 -8.9940E+01  4.9000E+00 -1.6530E+00
 1.8310E+00 -3.8220E+00  1.1340E+02  3.4140E+02 -2.7340E+01 -2.0400E+00
-6.1660E-01  5.0040E-01 -1.4370E-01 -2.4160E+00 -1.0730E-01 -1.0780E+00
 3.0630E+01  1.9890E+01 -5.0160E+01  0.0000E+00  0.0000E+00

 0.0000E+00  0.0000E+00  0.0000E+00  0.0000E+00  0.0000E+00  0.0000E+00
 0.0000E+00  0.0000E+00  0.0000E+00  0.0000E+00  0.0000E+00  0.0000E+00
 0.0000E+00  0.0000E+00  0.0000E+00  0.0000E+00  0.0000E+00  0.0000E+00
 0.0000E+00  0.0000E+00  0.0000E+00  0.0000E+00  1.0000E+00

 0.0000E+00  0.0000E+00  0.0000E+00  0.0000E+00  0.0000E+00  0.0000E+00
 0.0000E+00  0.0000E+00  0.0000E+00  0.0000E+00  0.0000E+00  0.0000E+00
 0.0000E+00  0.0000E+00  0.0000E+00  0.0000E+00  1.0000E+00
 0.0000E+00  0.0000E+00  0.0000E+00 -3.0600E-01 -1.8630E+00
```

B Matrix

Number of rows = 23
Number of columns = 4

1.6000E+04	0.0000E+00	0.0000E+00	0.0000E+00
0.0000E+00	0.0000E+00	0.0000E+00	0.0000E+00
0.0000E+00	5.1138E+02	0.0000E+00	0.0000E+00
0.0000E+00	0.0000E+00	5.7600E+01	0.0000E+00
0.0000E+00	0.0000E+00	0.0000E+00	1.6000E+02
0.0000E+00	0.0000E+00	0.0000E+00	0.0000E+00
0.0000E+00	0.0000E+00	0.0000E+00	0.0000E+00
0.0000E+00	0.0000E+00	0.0000E+00	0.0000E+00
0.0000E+00	0.0000E+00	0.0000E+00	0.0000E+00
0.0000E+00	0.0000E+00	0.0000E+00	0.0000E+00
0.0000E+00	0.0000E+00	0.0000E+00	0.0000E+00
0.0000E+00	0.0000E+00	0.0000E+00	0.0000E+00
0.0000E+00	0.0000E+00	0.0000E+00	0.0000E+00
0.0000E+00	0.0000E+00	0.0000E+00	0.0000E+00
0.0000E+00	0.0000E+00	0.0000E+00	0.0000E+00
0.0000E+00	0.0000E+00	0.0000E+00	0.0000E+00
0.0000E+00	0.0000E+00	0.0000E+00	0.0000E+00
0.0000E+00	0.0000E+00	0.0000E+00	0.0000E+00
0.0000E+00	0.0000E+00	0.0000E+00	0.0000E+00
0.0000E+00	0.0000E+00	0.0000E+00	0.0000E+00
0.0000E+00	0.0000E+00	0.0000E+00	0.0000E+00
0.0000E+00	0.0000E+00	0.0000E+00	0.0000E+00
0.0000E+00	0.0000E+00	0.0000E+00	0.0000E+00

C Matrix

Number of rows = 4
Number of columns = 23

0.0000E+00	0.0000E+00	0.0000E+00	0.0000E+00	0.0000E+00	1.0000E-02
0.0000E+00	0.0000E+00	0.0000E+00	0.0000E+00	0.0000E+00	0.0000E+00
0.0000E+00	0.0000E+00	0.0000E+00	0.0000E+00	0.0000E+00	0.0000E+00
0.0000E+00	0.0000E+00	0.0000E+00	0.0000E+00	0.0000E+00	
0.0000E+00	0.0000E+00	0.0000E+00	0.0000E+00	0.0000E+00	0.0000E+00
1.0000E-02	0.0000E+00	0.0000E+00	0.0000E+00	0.0000E+00	0.0000E+00
0.0000E+00	0.0000E+00	0.0000E+00	0.0000E+00	0.0000E+00	0.0000E+00
0.0000E+00	0.0000E+00	0.0000E+00	0.0000E+00	0.0000E+00	
0.0000E+00	0.0000E+00	0.0000E+00	0.0000E+00	0.0000E+00	0.0000E+00
0.0000E+00	1.0000E-01	0.0000E+00	0.0000E+00	0.0000E+00	0.0000E+00
0.0000E+00	0.0000E+00	0.0000E+00	0.0000E+00	0.0000E+00	0.0000E+00
0.0000E+00	0.0000E+00	0.0000E+00	0.0000E+00	0.0000E+00	
0.0000E+00	0.0000E+00	0.0000E+00	0.0000E+00	0.0000E+00	0.0000E+00
0.0000E+00	0.0000E+00	0.0000E+00	0.0000E+00	0.0000E+00	0.0000E+00
0.0000E+00	0.0000E+00	0.0000E+00	0.0000E+00	0.0000E+00	0.0000E+00
0.0000E+00	0.0000E+00	0.0000E+00	3.0501E-01	6.4500E-01	

TABLE A.2: Reduced Linear Model (13th-order).

A Matrix

Number of rows = 13
Number of columns = 13

-1.8204E-01	0.0000E+00	0.0000E+00	0.0000E+00	0.0000E+00	0.0000E+00	1st Row
0.0000E+00	0.0000E+00	0.0000E+00	0.0000E+00	0.0000E+00	0.0000E+00	
0.0000E+00						
0.0000E+00	-6.4773E-01	0.0000E+00	0.0000E+00	0.0000E+00	0.0000E+00	2nd Row
0.0000E+00	0.0000E+00	0.0000E+00	0.0000E+00	0.0000E+00	0.0000E+00	
0.0000E+00						
0.0000E+00	0.0000E+00	-1.6810E+00	0.0000E+00	0.0000E+00	0.0000E+00	
0.0000E+00	0.0000E+00	0.0000E+00	0.0000E+00	0.0000E+00	0.0000E+00	
0.0000E+00						
0.0000E+00	0.0000E+00	0.0000E+00	-1.9057E+00	0.0000E+00	0.0000E+00	
0.0000E+00	0.0000E+00	0.0000E+00	0.0000E+00	0.0000E+00	0.0000E+00	
0.0000E+00						
0.0000E+00	0.0000E+00	0.0000E+00	0.0000E+00	-2.6184E+00	0.0000E+00	
0.0000E+00	0.0000E+00	0.0000E+00	0.0000E+00	0.0000E+00	0.0000E+00	
0.0000E+00						
0.0000E+00	0.0000E+00	0.0000E+00	0.0000E+00	0.0000E+00	-6.7148E+00	
1.3120E+00	0.0000E+00	0.0000E+00	0.0000E+00	0.0000E+00	0.0000E+00	
0.0000E+00						
0.0000E+00	0.0000E+00	0.0000E+00	0.0000E+00	0.0000E+00	-1.3120E+00	
-6.7148E+00	0.0000E+00	0.0000E+00	0.0000E+00	0.0000E+00	0.0000E+00	
0.0000E+00						
0.0000E+00	0.0000E+00	0.0000E+00	0.0000E+00	0.0000E+00	0.0000E+00	
0.0000E+00	-1.0000E+01	0.0000E+00	0.0000E+00	0.0000E+00	0.0000E+00	
0.0000E+00						
0.0000E+00	0.0000E+00	0.0000E+00	0.0000E+00	0.0000E+00	0.0000E+00	
0.0000E+00	0.0000E+00	-1.2000E+01	0.0000E+00	0.0000E+00	0.0000E+00	
0.0000E+00						
0.0000E+00	0.0000E+00	0.0000E+00	0.0000E+00	0.0000E+00	0.0000E+00	
0.0000E+00	0.0000E+00	0.0000E+00	-1.7805E+01	4.7811E+00	0.0000E+00	
0.0000E+00						
0.0000E+00	0.0000E+00	0.0000E+00	0.0000E+00	0.0000E+00	0.0000E+00	
0.0000E+00	0.0000E+00	0.0000E+00	-4.7811E+00	-1.7805E+01	0.0000E+00	
0.0000E+00						
0.0000E+00	0.0000E+00	0.0000E+00	0.0000E+00	0.0000E+00	0.0000E+00	
0.0000E+00	0.0000E+00	0.0000E+00	0.0000E+00	0.0000E+00	-2.1327E+01	
8.2083E-01						
0.0000E+00	0.0000E+00	0.0000E+00	0.0000E+00	0.0000E+00	0.0000E+00	
0.0000E+00	0.0000E+00	0.0000E+00	0.0000E+00	0.0000E+00	-8.2083E-01	
-2.1327E+01						

B Matrix

Number of rows = 13
Number of columns = 4

-1.0208E+02	-5.4804E+01	6.1782E+00	-6.0380E+00
-9.5696E+01	-5.3693E+01	6.0663E+00	-4.0074E+00
-5.2944E+02	-3.4591E+02	4.5373E+01	-5.5671E+00
4.1156E+02	2.7677E+02	-3.6298E+01	-4.0825E+00
1.8033E+03	1.2088E+03	-1.1150E+02	-3.6040E+02
-7.1127E+03	3.7908E+03	2.9841E+02	-3.7316E+02
3.4852E+03	-7.0229E+03	2.3309E+03	-5.5582E+02
-1.7929E+04	-4.5900E-13	1.3229E-13	-1.1499E-14
2.5552E-03	8.6478E-04	-2.6201E+03	-5.4893E-04
-3.3495E+03	-1.4558E+03	1.9954E+03	-1.7168E+03
-7.8277E+03	-9.0622E+03	2.8374E+03	-3.9883E+02
-2.1596E+03	2.7043E+03	-1.4267E+03	-2.9133E+03
4.3323E+02	5.1529E+02	8.7011E+02	1.0469E+03

C Matrix

Number of rows = 4
Number of columns = 13

-1.2191E-16	-5.7540E-03	1.6744E-15	6.2025E-03	7.4149E-03	-8.6084E-03
-2.3112E-03	4.1692E-03	-3.3729E-03	1.0773E-03	-2.5420E-04	5.8003E-04
-2.9312E-04					
-4.1063E-17	-7.9997E-03	7.5435E-16	3.1829E-03	6.5244E-03	1.4814E-03
1.6061E-03	3.7509E-04	3.4668E-03	1.7975E-03	1.1369E-03	4.4066E-04
-3.9096E-04					
9.4307E-18	-2.0845E-03	4.6635E-17	4.2193E-04	2.1854E-03	5.7540E-05
2.7827E-03	7.2614E-05	3.9814E-03	-1.6006E-04	1.0811E-03	-8.4891E-04
-9.0062E-05					
-1.8456E-01	1.2719E-03	-3.9839E-01	-3.0070E-01	-1.8362E-02	1.2475E-02
1.0197E-02	-6.4502E-05	1.8712E-02	6.7780E-03	6.4378E-03	1.7616E-03
-1.9437E-03					

D Matrix

Number of rows = 4
Number of columns = 4

1.9803E-01	1.0703E-01	-7.1554E-03	7.0440E-02
4.5757E-01	3.5007E-01	-2.1356E-03	2.9165E-01
-1.0649E-01	9.6939E-01	4.2396E-02	5.2261E-02
1.5824E+00	1.5492E+00	2.5866E-02	7.4509E-01

TABLE A.3: LQG Compensator State Space Matrices

A Matrix

Number of rows = 17
Number of columns = 17

-1.3632E+05 -7.5630E+04 2.2566E+02 -5.7732E+04 1.4188E+04 -1.3732E+02
2.9522E+04 2.2056E+04 1.2365E+03 -5.5235E+02 -6.4918E+02 -1.0012E+02
-1.1099E+03 -4.1890E+02 -3.8405E+02 -1.1366E+02 1.2281E+02 } 1st Row

-7.5623E+04 -1.6445E+05 -4.9085E+03 -4.4085E+04 9.3288E+03 -5.2391E+02
1.8644E+04 1.4256E+04 1.2757E+03 -8.1959E+02 -4.6670E+02 1.3299E+02
-8.1161E+02 -2.5579E+02 -2.6031E+02 -4.2803E+01 7.2448E+01 } 2nd Row

2.2424E+02 -4.9042E+03 -9.9955E+02 -8.8700E+00 -1.1534E+02 -4.3050E+02
2.1826E+02 7.1362E+02 5.6552E+02 -7.1399E+02 -3.1958E+02 3.3595E+02
-4.8829E+02 6.3872E+01 -8.0414E+01 6.3980E+01 -1.0151E+01

-5.7731E+04 -4.4088E+04 -8.0692E+00 -3.4686E+04 -6.9495E+03 -6.6257E+02
-1.4373E+04 -1.0526E+04 -1.7018E+02 4.0031E+02 4.3397E+02 -2.5734E+00
4.8376E+02 1.9114E+01 1.3757E+02 -1.1728E+00 -9.0167E+00

-9.2057E+01 -5.0610E+01 6.0754E+00 -1.6494E+00 -1.0732E+00 -2.3439E-02
-1.9236E+00 -1.4270E+00 -5.9019E-02 3.9496E-02 3.4010E-02 1.2390E-02
7.1729E-02 4.1734E-02 2.8490E-02 1.5460E-02 -1.0921E-02

-8.8063E+01 -5.2915E+01 5.8652E+00 -5.1611E-01 -4.2337E-01 -6.9782E-01
-9.1387E-01 -6.5859E-01 3.9314E-03 2.0771E-02 1.4125E-02 1.0318E-02
3.7255E-02 3.0463E-02 1.5851E-02 1.2763E-02 -7.1378E-03

-5.1940E+02 -3.9698E+02 4.2530E+01 -1.4781E+00 3.3553E+00 -5.5676E-01
5.5617E+00 5.7829E+00 8.0354E-01 -3.1919E-01 -2.6871E-01 1.1101E-01
-3.8591E-01 2.2938E-02 -1.0274E-01 5.0363E-02 8.4200E-03

4.0638E+02 3.2401E+02 -3.3766E+01 -6.9409E+00 -3.7545E+00 5.4857E-01
-8.1042E+00 -8.3046E+00 -8.1926E-01 2.8406E-01 2.5115E-01 -8.3591E-02
3.6736E-01 -2.5381E-03 1.0488E-01 -3.6827E-02 -1.3330E-02

1.6947E+03 1.3956E+03 -9.6929E+01 -4.6426E+02 -3.6100E+01 6.4883E+00
-7.7923E+01 -6.0891E+01 -1.0862E+01 1.1466E-02 7.7967E-01 1.7665E-01
8.3639E-01 -2.2825E-01 3.9490E-01 -1.5818E-01 -7.4370E-02

-5.2441E+03 9.0638E+03 4.6316E+02 7.1343E+02 -2.7113E+02 -7.5675E+00
-5.8525E+02 -4.3161E+02 -1.2331E+01 -6.7694E+00 1.9083E+01 7.9465E+00
3.0079E+01 9.5994E+00 1.1251E+01 4.7697E-01 -3.3014E+00

-9.4847E+00 -1.3632E+04 2.1333E+03 -2.6270E+03 4.3911E+02 -1.4663E+00
9.4784E+02 7.2468E+02 4.7071E+01 -5.1861E+01 -4.5821E+01 8.8299E+00
-6.7128E+01 -1.5144E+01 -2.0188E+01 -9.1174E-01 4.6400E+00

-1.5217E+04 5.7869E+03 1.6839E+02 1.6055E+03 -3.2351E+02 -9.2738E+00
-6.9831E+02 -5.2234E+02 -2.0396E+01 1.9606E+01 2.6011E+01 -8.2733E+00
4.4894E+01 1.2515E+01 1.4882E+01 9.4008E-01 -3.9381E+00

4.3914E+02 -8.2358E+02 -2.6491E+03 2.2897E+02 -4.8446E+01 1.2413E+01
-1.0457E+02 -9.5622E+01 -2.3956E+01 3.2187E+01 8.1309E+00 -1.2931E+01
2.2327E+00 5.8052E-01 2.3388E+00 2.3616E-01 1.0236E-01

-3.6952E+03 -1.1292E+03 2.0110E+03 -1.9613E+03 6.1153E+00 -2.1103E+00
1.3200E+01 1.8370E+01 8.0766E+00 -1.9658E+01 -5.3224E+00 7.9071E+00
-9.4695E+00 -1.8411E+01 3.2273E+00 -5.0786E-02 -5.2813E-02

-8.6633E+03 -1.0529E+04 2.7902E+03 -8.6861E+02 1.2696E+02 -5.5182E+00
2.7405E+02 2.1281E+02 1.8878E+01 -1.7196E+01 -1.0776E+01 4.1636E+00
-1.8320E+01 -8.2865E+00 -2.3053E+01 -1.8940E-01 1.0921E+00

-1.5789E+03 3.8311E+03 -1.3851E+03 -2.6682E+03 -1.3942E+02 1.1326E+01
-3.0094E+02 -2.3337E+02 -2.3491E+01 1.2188E+01 8.2556E+00 -2.4832E+00
1.3745E+01 2.6563E+00 4.2253E+00 -2.1070E+01 -1.3037E-01

4.1864E+02 7.7193E+02 8.7530E+02 1.0766E+03 2.5042E+01 -6.4319E+00
5.4054E+01 4.5676E+01 9.5065E+00 -6.8668E+00 -1.5876E+00 2.8038E+00
-2.5992E+00 1.4328E-01 -4.1816E-01 -8.5972E-01 -2.1373E+01

B Matrix

Number of rows = 17
Number of columns = 4

2.9025E-01	2.2167E-01	1.9718E+00	1.1708E+00
-2.5731E+00	1.3526E+00	-4.5641E+00	-2.3102E+00
-1.6851E+01	5.7610E+00	-6.4092E+00	9.7720E-01
1.9137E+00	-9.3996E+00	1.1545E-01	2.8721E+00
-2.8712E+00	-2.8681E+00	4.7417E+00	-4.8285E+00
-2.0115E+00	-6.6049E+00	5.4710E+00	-2.2939E+00
-2.1435E+01	-6.4094E+01	4.9137E+01	1.8180E+01
1.4548E+01	6.5703E+01	-4.1550E+01	-2.0343E+01
-1.2484E+02	9.2165E+02	-1.9911E+02	-1.9560E+02
-1.9698E+03	1.0886E+03	-3.2674E+03	-1.4691E+03
-2.2252E+03	1.0439E+03	2.8846E+03	2.3792E+03
-3.5270E+02	-4.0717E+02	-2.9824E+03	-1.7528E+03
3.1750E+03	-1.1183E+03	1.3224E+03	-2.6249E+02
-2.0066E+03	1.3562E+03	-6.5809E+02	3.3134E+01
-9.9716E+02	4.4736E-01	5.2329E+02	6.8790E+02
4.9721E+02	1.0384E+03	-3.8514E+02	-7.5540E+02
-6.4361E+02	-2.3463E+02	-3.2579E+02	1.3568E+02

C Matrix

Number of rows = 4
Number of columns = 17

1.3632E+05	7.5626E+04	-2.2577E+02	5.7731E+04	-1.4188E+04	1.3733E+02
-2.9522E+04	-2.2056E+04	-1.2365E+03	5.5233E+02	6.4916E+02	1.0012E+02
1.1099E+03	4.1889E+02	3.8404E+02	1.1366E+02	-1.2280E+02	
7.5626E+04	1.6446E+05	4.9087E+03	4.4087E+04	-9.3293E+03	5.2390E+02
-1.8645E+04	-1.4256E+04	-1.2757E+03	8.1960E+02	4.6672E+02	-1.3298E+02
8.1166E+02	2.5580E+02	2.6033E+02	4.2804E+01	-7.2453E+01	
-2.2577E+02	4.9087E+03	9.9969E+02	7.9836E+00	1.1552E+02	4.3043E+02
-2.1787E+02	-7.1323E+02	-5.6540E+02	7.1382E+02	3.1954E+02	-3.3588E+02
4.8823E+02	-6.3872E+01	8.0403E+01	-6.3980E+01	1.0149E+01	
5.7731E+04	4.4087E+04	7.9836E+00	3.4686E+04	6.9500E+03	6.6250E+02
1.4374E+04	1.0527E+04	1.7028E+02	-4.0031E+02	-4.3398E+02	2.5691E+00
-4.8377E+02	-1.9119E+01	-1.3758E+02	1.1709E+00	9.0192E+00	

APPENDIX B

PROOF OF THE INVERSE KALMAN EQUALITIES

(EQUATIONS (4.12),(4.14))

To prove (4.12)

ASSUMPTIONS: $\underline{B}$ full rank, $\underline{R}>0$, $\underline{Q} \geq 0$. Since $\underline{B}$ has full rank, it has a left inverse $\underline{B}_L^{-1}$ such that: $\underline{B}_L^{-1}\,\underline{B} = \underline{I}$.

Taking transposes:

$$(\underline{B}^T)\,(\underline{B}_L^{-1})^T = \underline{I}$$

so $\underline{B}^T$ has a right inverse $(\underline{B}^T)_R^{-1} = (\underline{B}_L^{-1})^T$. Now start with the algebraic Riccati equation:

$$\underline{A}^T\underline{P} + \underline{P}\,\underline{A} + \underline{Q} - \underline{P}\,\underline{B}\,\underline{R}^{-1}\underline{B}^T\underline{P} = 0$$

Add and subtract $(j\omega\underline{P})$:

$$-(-j\omega\underline{I}-\underline{A}^T)\underline{P} - \underline{P}(j\omega\underline{I}-\underline{A}) + \underline{Q} - \underline{P}\,\underline{B}\,\underline{R}^{-1}\underline{B}^T\underline{P} = 0$$

Pre-multiply by $\underline{R}\,\underline{B}_L^{-1}\underline{P}^{-1}$; Post-multiply by $\underline{P}^{-1}(\underline{B}^T)_R^{-1}\,\underline{R}$

$$-\underline{R}\,\underline{B}_L^{-1}\underline{P}^{-1}(-j\,\underline{I}-\underline{A}^T)(\underline{B}^T)_R^{-1}\,\underline{R} - \underline{R}\,\underline{B}_L^{-1}(j\,\underline{I}-\underline{A})\underline{P}^{-1}(\underline{B}^T)_R^{-1}\,\underline{R} -$$

$$+\,\underline{R}\,\underline{B}_L^{-1}\underline{P}^{-1}\underline{Q}\,\underline{P}^{-1}(\underline{B}^T)_R^{-1}\,\underline{R} - \underline{R} = 0$$

Identifying:

$$[\underline{G}_c^{-1}(j\omega)]^* = \underline{R}\,\underline{B}_L^{-1}\underline{P}^{-1}(-j\omega\underline{I} - \underline{A}^T)(\underline{B}^T)_R^{-1}$$

$$\underline{G}_c^{-1}(j\omega) = \underline{B}_L^{-1}(j\,\underline{I}-\underline{A})\underline{P}^{-1}(\underline{B}^T)_R\,\underline{R}$$

and adding on both sides the term $(\underline{G}_c^{-1})^*\,\underline{R}\,\underline{G}_c^{-1}$ we obtain (4.12).

Equation (4.14) is the exact dual of (4.12) and is proved in the same way.

PROOF OF ROBUSTNESS PROPERTIES (2) AND (4).

For $\underline{R} = \rho\underline{I}$ we get, from (4.12):

$$[\underline{I}+\underline{G}_c^{-1}(j\omega)]^*[\underline{I}+\underline{G}_c^{-1}(j\omega)] \geq (\underline{G}_c^{-1}(j\omega))^*(\underline{G}_c^{-1}(j\omega))$$

since $\quad ((\underline{K}_c)^{-1})^T \underline{Q}(\underline{K}_c)^{-1} \geq 0.$

From this it follows that:

$$\sigma_i[\underline{I}+\underline{G}_c^{-1}(j\omega)] \geq \sigma_i(\underline{G}_c^{-1}(j\omega)) =$$

$$= \sigma_i[\underline{I}+\underline{G}_c^{-1}(j\omega)-\underline{I}] \geq$$

$$\geq 1 - \sigma_i[\underline{I}+\underline{G}_c^{-1}(j\omega)]$$

and for i=n the result follows from the identity: $\sigma_{i+j-1}(\underline{A}+\underline{B}) \leq \sigma_i(\underline{A}) + \sigma_j(\underline{B})$ [12], for the case i=1, j=1.

REFERENCES

[1] M.K. Sain, J.L. Peczkowski, J.L. Melsa, eds: Alternatives for Linear Multivariable Control, National Engineering Consortium, 1978.

[2] S. Chan: Small-signal Control of Multiterminal DC/AC Power Systems, MIT, LIDS-TH-1121, August 1981.

[3] R.L. DeHoff, W. Hall: F100 Multivariable Control Synthesis Program, AFAPL-TR-77-35, 1976.

[4] S.L. Dixon: Fluid Mechanics and Thermodynamics of Turbomachinery, 2nd Ed., Pergamon, 1978.

[5] J. Hickin, N.K. Sinha: Model Reduction for Linear Multivariable Systems, IEEE Tr. on Automatic Control, AC-25, Dec. 80, pp. 1121-1128.

[6] M.S. Idelchik: An Application of Modern Control Theory to a High-bypass Variable Compressor Geometry Jet Engine, S.M. Thesis, MIT, 1981.

[7] T. Kailath: Linear Systems, Prentice-Hall, 1980.

[8] J.L. Kerrebrock: Aircraft Engines and Gas Turbines, MIT Press, 1977.

[9] H. Kwakernaak: Optimal Low-Sensitivity Linear Feedback Systems, Automatica, 5, 1969, pp279-286.

[10] H. Kwakernaak, R. Sivan: Linear Optimal Control Systems, Wiley, 1972.

[11] H. Kwakernaak, R. Sivan: The Maximally Achievable Accuracy of Linear Optimal Regulators and Linear Optimal Filters, IEEE Trans. on Auto. Control, AC-17, pp. 79-85, February 1972.

[12] A.J. Laub: Robust Stability of Linear Systems: Some Computational Consideratic MIT, LIDS-R-904, 1979.

[13] N.A. Lehtomaki: Practical Robustness Measures in Multivariable Control Systems Analysis, Ph.D. Thesis, MIT, 1981.

[14] N.A. Lehtomaki, et.al: Robustness Tests Utilizing the Structure of Modelling Error, MIT, LIDS-P-1151, Oct. 1981.

[15] N.A. Lehtomaki, N. Sandell, M. Athans: Robustness Results in LQG-Based Multivariable Control Design, IEEE Trans. on Auto. Control, AC-26, Feb. 1981, pp. 75-92.

[16] R.J. Miller, R.D. Hackney: F100 Multivariable Control System Engine Models/ Design Criteria, AFAPL-TR-76-74, 1976.

[17] M.G. Safonov: Robustness and Stability Aspects of Stochastic Multivariable Feedback System Design, Ph.D. Thesis, MIT, 1979.

[18] P. Sannuti, P.V. Kokotovic: Near-optimum Design of Linear Systems by a Singular Perturbation Method, IEEE Trans. on Auto. Control, AC-14, Feb. 1969, pp. 15-21.

[19] G. Stein: LQG-Based Multivariable Design: Frequency Domain Interpretation, AGARD-LS-117.

[20] G. Stein, J. Doyle: Multivariable Feedback Design: Concepts for a Classical Modern Synthesis, IEEE Trans. on Auto. Control, AC-26, Feb. 1981, pp. 4-16.

[21] G. Stein, N. Sandell: Classical and Modern Methods for Control System Design, Notes, MIT, 1979.

[22] J.R. Szuch, et.al: F100 Multivariable Control Synthesis Program-Evaluation of a Multivariable Control Using a Real-Time Engine Simulation, NASA Technical Paper 1056, 1977.

[23] M.Vidyasagar: Algebraic System Theory, Notes, MIT, Spring 1983.